UNIVERSITY OF CALIFORNIA,
IRVINE

Mitochondrial Akt Signaling and Embryonic Stem Cell Differentiation

DISSERTATION

submitted in partial satisfaction of the requirements
for the degree of

DOCTOR OF PHILOSOPHY

in Biomedical Science

by

Hsiao-Chen Lee

Dissertation Committee:
Professor Ping H. Wang, Chair
Associate Professor Edwin S Monuki
Professor Jefferson Y. Chan
Professor Bogi Andersen
Assistant Professor Matthew A. Inlay

2018

DEDICATION

To

My Mom and Dad,

Sister Hsiao-Tzu Li,

Brother Shiao-Tee Lee, Sister in Law Yen-Hua Chen, Niece Jin-Han Lee

moreover, friends

In recognition of their worth and support

TABLE OF CONTENTS

LIST OF FIGURES

Page

LIST OF TABLES

Page

ACKNOWLEDGMENTS

I am especially indebted to Professor Ping H. Wang, the chairman of my committee, who established the collaborative graduate student program between the University of California, Irvine and Kaohsiung Medical University, Taiwan. With his support and guidance, I had the opportunity to study at UC, Irvine, and finish the training and dissertation. This work would not have been possible without the financial support from Kaohsiung medical university, Kaohsiung Medical University Hospital, and Dr. Wang.

I would especially like to thank Professor Bogi Andersen, Bob Ziguang Lin in Andersen's lab, and Dr. Brian Pedersen, the rheumatologist in UCSD, helped establishing a scRNA-seq platform and analyze the data. Also, thank Dr. Melanie Oakes, and UCI Genomics High-Throughput Facility (GHTF) provide technical and knowledge support. I would also like to thank each of the members of my Dissertation Committee, who provided extensive personal and professional guidance and taught me a great deal about scientific research, and precious suggestions to refine this dissertation.

I am grateful to all of those with whom I have had the pleasure to work during this and other related projects. I would also like to thank Dr. Yumay Chen and Dr. Hank Yu-Han Chen, who demonstrated the skills required for this project and a lot of precious suggestions; Albert Paul Ta, who helped me fix grammar; and Christina Tu, who taught me the skills and knowledge about stem cell. Also, a special thanks to Professor YaLing Hsu in

the graduate institute of medicine, Kaohsiung Medical University, Taiwan. With her kindly help, I could have this incredible chance to study at UC, Irvine.

I would like to thank the members of my family, especially my dearest Mom, Pastor Daniel Ling-Kang Chiu and Adela Chiu, whose love and unlimited support are with me in whatever I pursue. Also, I wish to thank friends, who gave me many wishes; and brothers and sisters in Jesus, who pray for me. Also, I would like to thank Emma Chen and Jou-En, my best friend in Irvine, and friends in 1.5G EFCI living spring fellowship. Without your pray and accompany, I could not work out through these difficult time. Most importantly, I would like to dedicate the dissertation to the God in heaven for the wonders that He created.

CURRICULUM VITAE

Hsiao-Chen Lee

1992-2000	Doctor of Medicine, School of Medicine, Kaohsiung Medical University, Kaohsiung, Taiwan
1999-2000	Internship, Kaohsiung Medical University Hospital, Kaohsiung, Taiwan
2000-2004	General Surgery Residency, Kaohsiung Medical University Hospital, Kaohsiung, Taiwan
2004-2006	Plastic Surgery Residency, Kaohsiung Medical University Hospital, Kaohsiung, Taiwan
2006-2009	Attending of Plastic Surgery, Division of Plastic Surgery, Department of Surgery, Kaohsiung Medical University Hospital, Kaohsiung, Taiwan
2007-2009	M.S. in Biomedical Engineering, School of Engineering, National Cheng Kung University, Tainan, Taiwan
2009-2012	Attending of Plastic Surgery, Division of Plastic Surgery, Department of Surgery, Chia-Yi Christian Hospital, Chia-Yi City, Taiwan
2012-	Attending of Plastic Surgery, Division of Plastic Surgery, Department of Surgery, Kaohsiung Medical University Hospital, Kaohsiung, Taiwan
2013	Lecturer at Tatung Institute Commerce and Technology, Chia-Yi, Taiwan
2014-2018	Ph.D. in Biomedical Science, University of California, Irvine

BOARD CERTIFICATION

2004	Active member of Taiwan Surgical Association ID#4680
2004	Member of Taiwan Society for Burn Injury and Wound Healing ID#0849
2006	Active member of Taiwan Society of Plastic Surgery ID#000432
2007	Member of Taiwan Society for Surgery of the Hand ID#0641
2016	International Member of American Society of Plastic Surgery ID# 134012

FIELD OF STUDY

Stem Cell Biology, Mitochondria, Cellular Metabolism

PUBLICATIONS

IF Sun, SS Lee, TM Lin, HC Lee, CS Lai, SD Lin. "Our experience of continuous renal replacement therapy in burned patients with acute renal failure." The Journal of Taiwan Society of Plastic Surgery, 2005; 14(1):49-57

HC Lee, TM Lin, SS Lee, CS Lai, SD Lin. "Refinement of Continuous Intra-Arterial Infusion Therapy to Hydrofluoric Acid Dermal Burns." The Journal of Taiwan Society of Plastic Surgery, 2006; 15(4):338-348

KP Chang, HC Lee, CS Lai, SD Lin. "Use of Single Saphenous Interposition Vein Graft for Primary Arterial Circuit and Secondary Recipient Site in Head and Neck Reconstruction: A Case Report." Head & Neck, 2007; 29(4):412-415

HC Lee, CC Lin, SS Yu, BW Chang, HC Chang "Using impedance sensing system to evaluate the effect of wound healing behavior on cells treated by vitamin C. Biomedical engineering: applications, basis, and communications." 2009, 21(6):445-448

Master Thesis:
"Using Impedance Sensing System to Evaluate the Wound Healing Behavior of Cells Treated by Vitamin C" (2009)

KP Chang, HC Lee, SS Lee, SH Huang, CS Lai, SD Lin. "MicroRNA Signatures in Ischemia-Reperfusion Injury." Annals of Plastic Surgery 2012; 69(6):668-671

ACADEMIC MEETING

HC Lee, TM Lin, JY Lee, IF Sun, YF Chye, SD Lin, CS Lai. "Pressurized liquid ammonia-induced chemical burn – Case Report." Annual Meeting of Taiwan Surgical Association, 2004, Poster

HC Lee, SS Lee, SD Lin, CS Lai. "Nasal dorsum flap for nasal tip reconstruction." Annual Meeting of Taiwan Surgical Association, 2005, Interaction Poster

HC Lee, TM Lin, SS Lee, CS Lai, SD Lin. "Guillain-Barré Syndrome Following Facial Bone Fracture." Annual Meeting of Taiwan Surgical Association, 2006, Oral

YH Lin, HC Lee, YF Chye, SS Lee, SD Lin, CS Lai. "Lipoblastoma of hand – case report and literature review." Annual Meeting of Taiwan Surgical Association, 2006, Poster

HC Lee, SD Lin, CS Lai. "Subungual Verruca with Squamous Cell Carcinoma – Case Report and Literature Review." Annual Meeting of Taiwan Surgical Association, 2007, Poster

HC Lee, SS Yu, BW Chang, HC Chang. “Impedimetric sensing of cell attachment on interdigitated microelectrodes.” 6th Asian Conference on Electrochemistry, 2008, Oral Award

HC Lee, YM Su, CH Chang-Chien. “Unusual imaging findings of Kimura Disease in upper extremity – case report and literature review” Annual Meeting of Taiwan Society of Plastic Surgery, 2012, Poster

HC Lee, YC Cheng, DK Lu, SS Lee, SD Lin, CS Lai. “Refinement of Nasal Dorsum Flap for Nasal Tip Reconstruction.” 17th IPRAS, 2013, oral

HC Lee, YM Su, CH Chang-Chien. “Immediate breast reconstruction in breast cancer patient with siliconoma.” 17th IPRAS, 2013, oral/e-poster

HC Lee, YM Su, CH Chang-Chien. “Immediate breast reconstruction in breast cancer patient with siliconoma and pectoralis major muscle fibrosis – case report and literature review.” Annual Meeting of Taiwan Surgery Association, 2013, Poster

HC Lee, YM Su, CL Fang, CH Chang-Chien “Kimura’s Disease in upper extremity – case report and literature review in image finding.” Annual Meeting of Taiwan Society for Surgery of the Hand, 2013, Oral

HC Lee, YM Su, CL Fang, CH Chang-Chien. “Association of nipple hypertrophy, galactorrhea, and herbs – case report and literature review.”Annual Meeting of Taiwan Surgery Society, 2014, Poster

ABSTRACT OF THE DISSERTATION

Mitochondria Akt1 Signaling and Embryonic Stem Cell Differentiation

By

Hsiao-Chen Lee

Doctor of Philosophy in Biomedical Science

University of California, Irvine, 2018

Professor Ping H. Wang, Chair

The ability of self-renewal and the unlimited potential to differentiate into three germ layers make pluripotent stem cells a key player in regenerative medicine and disease modeling. Recent studies have shown that several signaling pathways and the bioenergetic function of mitochondria play critical roles in the regulation of stem cell differentiation and somatic cell reprogramming. Phosphatidylinositol-3 kinase/Akt signaling (PI3K/Akt) has been previously reported to be critical for maintaining the pluripotency of embryonic stem cells (ESC) via interaction with other signaling pathways, such as LIF/JAK/STAT. It has been shown that Akt translocates into mitochondria after growth factor or cytokine stimulation in differentiated cells. Herein, we demonstrated the translocation of Akt into mitochondria also occurs in human embryonic stem cells (hESCs) after serum stimulation. Intriguingly, our previous data showed that activation of mitochondrial Akt signaling enhanced somatic cell reprogramming. However, the effect of mitochondrial Akt signaling on stem cell differentiation has not yet been investigated.

Testing the effect of temporarily inhibiting mitochondrial Akt1 signaling in hESCs, I transduced cells with the His-tagged mitochondrial-targeting dominant negative Akt1/GFP adenoviral vector (Ad-mdnAkt1/GFP) or the GFP adenoviral vector (Ad-GFP) and differentiated spontaneously *in vitro* in differentiation medium. Evaluating transduction rate by fluorescence microscopy and flow cytometry and was determined to be over 60% in both groups. Immunoblotting was used to verify mutant Akt1 expression, and respiratory function of cells was evaluated by an extracellular flux analyzer. Spontaneous differentiation *in vitro* was characterized with H&E staining and showed that Ad-mdnAkt1/GFP treated cells formed more organized colonies than Ad-GFP treated cells. In line with this, bulk RNA analyzed by human cell lineage identification qPCR array showed that marker genes of mesoderm and endoderm were up-regulated and marker genes of ectoderm were down-regulated in Ad-mdnAkt1/GFP treated cells. Further Identification of unique development by single-cell RNA sequencing revealed inhibition of hematological and immune cells differentiation and promotion of lung and kidney development, middle ear morphogenesis and smooth muscle cell differentiation in Ad-mdnAkt1/GFP treated cells.

CHAPTER 1

Introduction

Stem cells are defined by two essential characteristics of self-renewal (i.e., prolonged undifferentiated proliferation) and developmental potency (i.e., the capacity to differentiate into more than one cell type). According to the differentiation potential, stem cells can be classified into three categories: pluripotent, multipotent and unipotent [1-3]. Pluripotent stem cells (PSC), such as embryonic stem cells (ESC) and induced pluripotent stem cells (iPSC), can give rise to all tissues of the body. Multipotent stem cells, also known as somatic or adult stem cells, can form the cells of the original tissues to ensure tissue homeostasis and repair of damaged tissue, but will not become an unrelated lineage under normal physiologic circumstances. Unipotent stem cells can differentiate into only a single cell type. For example, spermatogonial stem cells, which give rise to sperm.

The first pluripotent cells were derived from mouse testicular teratoma by L.C. Stevens in 1958 [2,4]. Later, mouse pluripotent stem cells were isolated from the inner mass of pre-implantation mouse blastocysts and were named embryonic stem cells (ESC) [5,6]. These cells can be cultured *in vitro* as unlimited, non-transformed cell lines. To distinguish PSCs from different origins, those derived from embryos were called “embryonic stem cells” (ESC) while those from teratocarcinoma cells called “embryonal carcinoma cells” (EC) [5]. Until the 1990s, papers on deriving ESC from primate [7,8] and human [9] embryos were primarily published by James Thomson. Three male human ES cell lines (H1, H13, and H14)

and two female ES cell lines (H7 and H9) were isolated. The morphology of these human embryonic stem cells (hESC) has a distinctly high nucleus to cytoplasm ratio and prominent nucleoli. These hESCs maintained the ability to differentiate into all three germ layers, including ectoderm (neural epithelium, stratified squamous epithelium), mesoderm (cartilage, bone, smooth muscle, striated muscle) and endoderm (gut epithelium) after remaining undifferentiated culture *in vitro* for several months [9]. A recent advancement has allowed for the induction of terminally differentiated somatic cells into ESC-like stem cells by ectopic expression of transcription factors, such as OCT4 (octamer-binding transcription factor4), SOX2 (SRY (sex-determining region Y)-box 2), KLF-4 (Kruppel-like factor 4), and c-Myc. Yamanaka et al. first reported the induced pluripotent stem cells (iPSC) generated from mice. In 2006 [10], and then in the next year, iPSCs generated from human were published by Yamanaka *et al.* and Thomson *et al*. [11,12]. The iPSCs provides an alternative source of PSCs in regenerative medicine and cell therapy [10-12].

To give stem cells the promising application, understanding the mechanism regulating their self-renewal, pluripotency and differentiation is important. Recent studies support that mitochondria, the sites of cellular respiration and energy production, and oxidative metabolism, are directly involved in the regulation of stem cell pluripotency [1,13-18] Researchers found that metabolic transition from oxidative phosphorylation (OXPHOS) to glycolysis was necessary and earlier than the induction of pluripotency [19]. The decrease of OXPHOS by inhibiting electron transport chain (ETC) respiratory complexes also enhanced the efficiency and speed of reprogramming [17]. On the other hand, emerging evidence has shown that mitochondrial fusion and fission plays a role in signaling pathways regulating

stem cell proliferation and differentiation. Several studies also reported that the increase in mitochondrial content and a metabolic shift toward OXPHOS were associated with embryonic stem cell differentiation. For example, proper cardiomyocyte differentiation from pluripotent stem cells required an increase in OXPHOS capacity [1,17].

Other important factors that influence stem cell fate are cell signaling pathways, such as the Wnt/β-catenin signaling pathway [20,21], LIF/JAK/STAT signaling pathway[22,23], and PI3K/Akt signaling pathway [24-26]. Among these signaling pathways, Phosphatidyl-inositol 3-kinase / Akt (v-akt murine thymoma viral oncogene homolog 1, protein kinase B, PI3K/Akt) signaling pathway plays an important role in maintaining pluripotency and self-renewal of ES cells through the crosstalk with other signaling pathways [27]. PI3K/Akt signaling regulates diverse processes within cells, including growth (viability, proliferation, and differentiation) and survival (apoptosis inhibition), glucose metabolism, immune response, and cell-cell communication[28,29]. Recent studies demonstrated that when cells are stimulated with insulin-like growth factor-1 or insulin, Akt will be phosphorylated to form its active state, and then translocated into mitochondria within several minutes [29-31]. So the level of mitochondrial Akt, localized in the matrix and the inner and outer membranes of mitochondria, is dynamically regulated [28,29].

In 2000, Yali *et al.* reported that FGF signaling through the PI3K/Akt pathway is required for early epithelial differentiation [32]. In 2003, Takahashi *et al.* reported that activation of PI3K/Akt signaling is required for the proliferative and tumorigenic activities of the embryonic stem cells [33]. In 2006, Watanabe *et al.* further showed that active form Akt

could help mouse and primate embryonic stem cells maintain their pluripotency [34]. However, the human embryonic stem cell (hESC) differentiation will be influenced by mitochondrial Akt1 signaling or not is still unknown. Herein, exploring the effect of mitochondrial Akt1 signaling and stem cell differentiation can help us understanding the crosstalk between mitochondria and stem cell fate.

1.1. Hypothesis and Specific Aims

Hypothesis

Herein, we hypothesized that inhibiting mitochondrial Akt1 signaling during initial stages of embryonic development could modulate the transcriptional programming underlining embryonic stem cell differentiation. To address the hypothesis, I set the following specific aims.

Specific Aims

Aim 1: Determine whether inhibition of mitochondria Akt signaling alters gene expression profile in hESC during differentiation

Aim 2: Establish single-cell RNA-seq in hESC with 10X Genomics platform

Aim 3: Analyze the effect of mitochondria Akt on hESC differentiation into the specific lineage and cell types

CHAPTER 2

Mitochondria, Akt1 signaling and Stem Cells

2.1. Mitochondria and Stem Cell Fate

The mitochondria are double-membraned organelles found in eukaryotes and contain their genome. Mitochondria are believed to be evolved from bacteria because their genomes are highly similar, which is the hypothesis of endosymbiosis. The mitochondrial circular genomic DNA resides in the matrix and consists of 37 genes, 13 of which encode for proteins integrated into the mitochondrial inner membrane, while others encode for mitochondrial tRNAs and rRNAs [35]. Mitochondria are estimated to have a proteome of ~1000-1500 proteins [36], and the majority of which are encoded by the cell nucleus. They are a highly specialized organelle that regulates various cellular functions. The most well-known function of mitochondria is its role in energy production through a series of coupled biochemical reactions, which compose the tricarboxylic acid (TCA) cycle. Other important functions mediated by mitochondria include reactive oxygen species, mediating apoptosis, calcium signaling, and mitophagy.

The roles of mitochondria in stem cells were noticed recently. Studies have shown that ESCs contain fewer mitochondria with immature cristae structure. Upon differentiation, however, the number of mitochondria increases and they become larger and develop distinct cristae. This increase was demonstrated by a measured increase in mitochondrial DNA copy number upon ESC differentiation. The distribution of

mitochondria in stem cells was shown to be perinuclear but became homogenously distributed post differentiation. The interpretations of the morphological differences between differentiated and undifferentiated cells have yet to be established (**Figure 1**).

In addition to the differences in morphology, ESCs are also metabolically different from their differentiated counterparts. ESCs reside in the hypoxic environment during embryo development; it is, therefore, logical, that embryonic cells rely on anaerobic metabolism to generate energy [37,38]. Upon differentiation, however, a metabolic shift was observed [39-41]. The development of mature mitochondrial cristae potentially fulfills the higher demand for mitochondrial respiration in differentiated cells, which facilitates the metabolic shift from glycolysis to oxidative phosphorylation (OXPHOS). The inhibition of mitochondrial OXPHOS complex III increased Nanog expression and reduced gene profile associated with differentiation in hESCs [59]. Collectively, these results suggest that mitochondria-mediated metabolism plays a role during embryo development and stem cell fate decision.

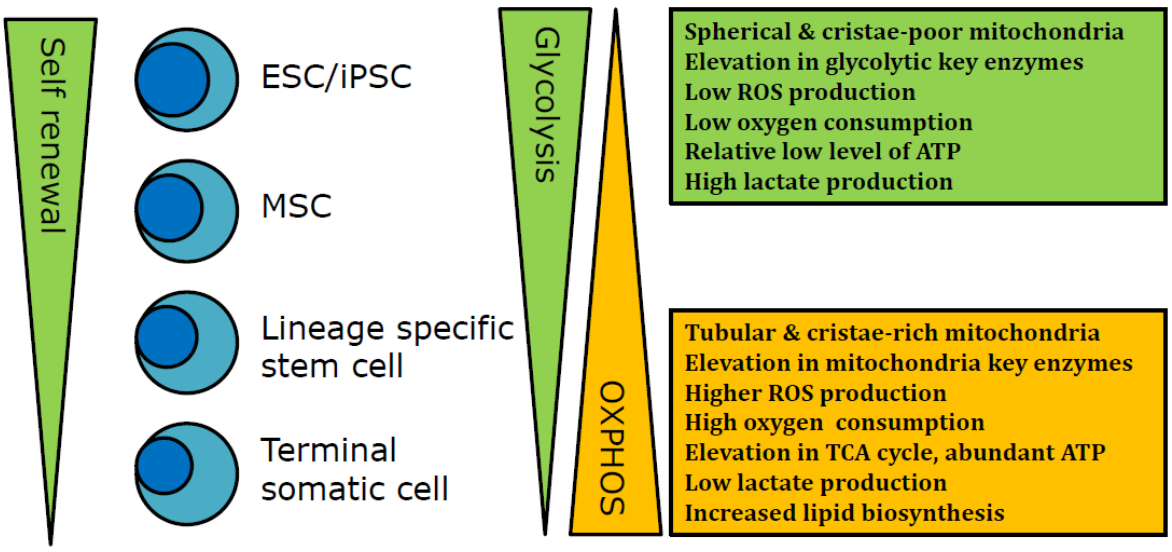

Figure 1. Metabolism and Stem Cell Fate. ESC: embryonic stem cell; iPSC: induced pluripotent stem cell; MSC: mesenchymal stem cell; OXPHOS: oxidative phosphorylation; ROS: reactive oxygen species; ATP: adenosine triphosphate; TCA cycle: tricarboxylic acid cycle [14]. (Modified from *Int J Mol Sci* . 2016; 17:253)

2.2. Akt Signaling and Stem Cell Fate

The phosphoinositide 3-kinase/Akt (PI3K/Akt) signaling pathway modulates several cellular functions, including promoting survival, proliferation, and growth, inhibiting apoptosis and modulating glucose metabolism. The two major proteins involved are PI3K (phosphoinositide 3-kinase) and Akt [42-44].

Akt (protein kinase B)

Akt also referred to as protein kinase B (PKB), cellular Akt (c-Akt) or related to protein kinase A and C (RAC) protein kinase, is a 57 kD cytoplasmic serine/threonine protein kinase[45,46] [47]. Akt1 (PKBα), Akt2 (PKBβ) and Akt3 (PKBγ) are the three Akt isoforms expressed in mammalian cells and encoded by different genes. These isoforms consist of similar structures, which are a pleckstrin homology (PH) domain at N-terminal region (amino terminus); a connecting hinge region; and a kinase domain at C-terminal region. Akt2 has 81%, and Akt3 has 83% homology of the amino acid sequence as Akt1 [47]. Akt1 is ubiquitously and highly expressed in all tissue. Instead, Akt2 is expressed in skeletal muscle, liver and adipose tissue, which are insulin-sensitive tissues. Akt3 is highly expressed in the brain and testis and, to a lesser extent, in the intestine and muscle tissues. [42,43,48] Several reports unveiled the functional differences between Akt isoforms. For example, overexpression of Akt2 can reverse insulin-mediated glucose intake in $Akt2^{-/-}$ adipocytes. In human cancer, Akt2 and Akt3 are pathologically increased. In contrast, over-expression of Akt1 failed to generate cancer-related phenotypes, such as increasing cell motility, invasion, and metastatic potential [43].

Activation of PI3K/Akt signaling

Akt remains in an inactive conformation in the cytoplasm until activated by hormones, growth factors or stimuli, such as insulin, platelet-derived growth factor (PDGF), epidermal growth factor (EGF) or basic fibroblast growth factor (bFGF) [46,48]. Growth factors bind to receptor tyrosine kinases (RTK), leading to receptor dimerization and cross-phosphorylation of tyrosine residues in the intracellular domains. Following this, the plasma will recruit Class IA PI3K through the phosphorylation-dependent interaction between the Src homology 2 (SH2) domains in their regulatory subunit p85 and the phospho-tyrosine residues on the receptor. This interaction stabilizes the catalytic subunit, p110 of PI3K, and allows for full activation of PI3K. Activated PI3K phosphorylates phosphatidylinositol-3,4-bisphosphate (PI-3,4-P2 or PIP2) to generate phosphatidylinositol-3,4,5-trisphosphate (PIP3) as a secondary messenger [43]. Akt interacts with PIP3 through binding of its PH domain and subsequently translocates to the plasma membrane. PIP3 also binds phosphoinositide-dependent kinase 1 (PDK1), which phosphorylates Akt kinase domain on Thr308 and results in partial activation of Akt. Full activation of Akt needs further phosphorylation of Ser473 by multiple proteins, including phosphoinositide-dependent kinase 2 (PDK2), integrin-linked kinase (ILK) [47], the mechanistic target of rapamycin complex (mTORC) and DNA-dependent protein kinase (DNA-PK) [49]. Once Akt is activated, Akt dissociates from the plasma membrane and is phosphorylated targets in the cytoplasm and nucleus to modulate its biological function, such as promoting cell survival by inhibiting apoptosis. Noteworthily, the localization of Akt in mitochondria and accumulation of active Akt in mitochondria was also observed and reported by Bijur et al. in 2003 [29].

Akt signaling influences stem cell fate

Several signaling pathways have been demonstrated to play important roles in stem cell fate, including the Wnt/β-catenin signaling pathway [20,21], LIF/JAK/STAT signaling pathway[22,23], bone morphogenic protein (BMP) signaling pathway [50,51], transforming growth factor-beta (TGF-β) signaling pathway [52], FGF signaling pathway and PI3K/Akt signaling pathway [24-26]. Among these signaling pathways, PI3K/Akt signaling plays an important role in maintaining pluripotency and self-renewal of ES cells and its components crosstalk to LIF/JAK/STAT signaling, Wnt/β-catenin signaling and TGF-β signaling [27]. In 2000, Yali et al. reported that early epithelial differentiation requires FGF signaling through the PI-3-K/Akt pathway [53].

Takahashi *et al.* reported the importance of PI3K pathway activated by growth factors and cytokines, including insulin and LIF, in proliferation, survival, tumorigenicity, and maintenance of pluripotency to mouse ESC (mESC) [54]. Ling *et al.* also demonstrated that the PI3K signaling pathway, independent of canonical Wnt signaling, is sufficient to maintain self-renew and survival in mESCs. They found ES cells actively expressing 3-phosphoinositide-dependent protein kinase-1 (PDK1) or Akt maintained pluripotency and LIF-independent Oct4 expression, lost both when treated with Akt inhibitors.[55] Interestingly, other studies showed that Akt is phosphorylated throughout murine preimplantation development and PI3K/Akt pathway plays a critical role in preimplantation embryo survival [56,57]. Riley *et al.* reported that inhibition of Akt activity had significant effects on the normal physiology of the murine blastocyst and trophoblasts, specifically resulted in a reduction in insulin-stimulated glucose uptake and delayed in

blastocyst hatching [57]. Lonai *et al.* demonstrated that fibroblast growth factor (FGF) signaling through PI3K/Akt pathway is necessary for murine embryoid body (EB) differentiation. Short-term inhibition of Akt activation by wortmannin (inhibiting Akt activation for 10 minutes) did not affect murine EB differentiation, but long-term inhibition by Ly294002 (PI3K inhibitor) inhibited the differentiation of murine ESCs into murine EB by the third day of culture [58]. Paling *et al.* also demonstrated that inhibition of PI3K via dominant negative Δp85 or Ly294002 led to a reduction in the ability of LIF to maintain self-renewal and concomitantly promotion of mouse ES cell differentiation [55,59].

In hESC, Ho *et al.* reported that ELABELA (ELA), an endogenous peptide hormone produced by human ESCs, supports self-renew and prevents apoptosis upon cellular stress through activating PI3K/Akt signaling pathway. On the other hand, ELA primes hESCs for endodermal differentiation through TGF-β signaling [24]. Intriguingly, Armstrong *et al.* demonstrated the down-regulation of PI3K/Akt, MAPK/ERK and NFκβ pathways during hESC differentiation [60]. Other researchers reported that the expression of Akt2 increased drastically during the differentiation of adipose tissue and skeletal muscle [47]. Taken together, the PI3K/Akt signaling pathway plays an important role in maintaining pluripotency and differentiation.

2.3. Mitochondrial Akt Signaling

Akt was previously reported to localize in the cytosol and nucleus to play its vital role in many cellular processes such as apoptosis, proliferation, and survival. In 2003, Akt was found to reside in the matrix and inner and outer membranes of mitochondria and was not merely attached to the outer surface of mitochondria in SH-SY5Y human neuroblastoma cells by Bijur and Jope for the first time [29]. It was shown that Akt translocated to the mitochondria within a few minutes and reached peak level around 15 minutes after stimulation with growth factor, insulin or stress. Furthermore, β-subunit of ATP synthase, Complex V of mitochondria electron transport chain, and glycogen synthase kinase-3β (GSK3β) were phosphorylated following translocation of Akt to mitochondria. [29,61] Another report mentioned that heat shock protein 90 (HSP90) is responsible for Akt accumulation in the mitochondria in unstimulated cells [62]. However, the role of Akt in mitochondria of ESC has not been previously investigated.

2.4. Akt Translocated Into Mitochondria After Serum Stimulation In hESC

To confirm that serum stimulation influences the translocation of Akt into mitochondria in hESCs, the cells were starved then treated with serum and the purified cytosolic, and mitochondria fractions were immunoblotted for phosphorylated (S473) and total (E45) Akt.

Materials and Methods

Serum starvation and stimulation in hESC

Feeder-free undifferentiated hESCs (H9, Passage 62-66) were grown on Matrigel (BD Biosciences) coated plate in mTeSR™1 (STEMCELL Technologies) and were passaged every 4-7 days with ReLeSR™ (STEMCELL Technologies) [63,64]. For serum starvation, hESC were cultured up to 80% confluency and pretreated with fresh full mTeSR™1 medium 6 hours. After washing with 1X Phosphate-buffered saline (PBS, Sigma), hESCs were incubated in mTeSR™1 basal medium for 8 hours at 37°C, 5% CO_2.

Serum-starving hESCs were washed with 1X PBS twice, then incubated with mTeSR™1 basal medium (no serum) or full mTeSR™1 medium (serum stimulation) at 37° C, 5% CO_2 for 15 minutes [29]. Cells were harvested by scraper after ice-cold PBS washed three times. The graphs represent the results from three independent experiments analyzed with densitometry. Six 10-cm dishes were collected in each group (with or without serum stimulation).

Subfractionation of mitochondria and cytosol

Cells were harvested by scraper after ice-cold 1X PBS washed three times then spun down at 200 g at 4°C for 10 minutes. Cell pellets were suspended in ice-cold lysis buffer (Mitochondria Isolation Kit for human cell, Miltenyi Biotec, cat. no. 130-094-532) with protease inhibitor (Sigma FAST™ protease inhibitor, cat. no. S8820), 1.0 mM phenylmethylsulfonyl fluoride (PMSF), 20 mM NaF, 2 mM Na_3VO_4, 1.0 mM dithiothreitol (DTT). After incubating on ice for 10 minutes, the cells were homogenized with ten strokes of loose pestle and 35 strokes of the tight pestle. The cell debris was removed by centrifugation at 1,000g for 10 minutes twice. 1.0 ml of supernatant was mixed with 9.0 ml 1X separation buffer and 50 µl Anti-TOM22 MicroBeams well, then incubated for 1 hour in the cold room (4°C) with gentle shaking. An LS column (MACS Separation Columns, Cat. No. 130-042-401) was placed in the MidiMACS Separation Unit and rinsed with 3 ml of 1X separation buffer. After labeling mitochondria, the mitochondrial suspension was loaded into the reservoir of the LS column and ran through. The column was washed three times with 1X separation buffer. The magnetically labeled mitochondria were flushed out immediately. The mitochondria suspension was centrifuged at 13,000g for 2 minutes at 4°C, and the resulting mitochondrial fractions which were washed with mitochondria isolation buffer (20 mM HEPES-KOH, pH 7.2, 10 mM KCl, 1.5 mM MgCl2, 1.0 mM sodium EDTA, 1.0 mM sodium EGTA, 1.0 mM dithiothreitol (DTT) and 250 mM sucrose), supplemented with 1X protease inhibitor (Sigma FAST™ protease inhibitor, S8820), 1 mM phenylmethylsulfonyl fluoride (PMSF), 20 mM NaF, and 2 mM Na_3VO_4 and centrifuged at 13,000g for 2 minutes at 4°C. Total cells were lysed in lysis buffer (10 mM Tris pH 7.5, 150 mM NaCl, 1% Nonidet P-40 (NP-40), 0.5% Na deoxycholate, 0.1% SDS, 1 mM EGTA)

supplemented with 1X protease inhibitor (Sigma FAST™ protease inhibitor, S8820), 1 mM PMSF, 20 mM NaF, and 2 mM Na_3VO_4. The protein concentration of mitochondria was determined by the Bradford method.

Electrophoresis and western blots

Equal amounts (10 μg) of proteins from each sample (total cell lysate, cytosolic fraction and mitochondria lysate) were separated by 10% SDS-polyacrylamide gel electrophoresis (SDS-PAGE) and transferred to PVDF membranes (Millipore), and incubated with the blocking buffer (5% BSA/TBS-T (20mM Tris–HCl (pH7.5), 137 mM NaCl, and 0.1% Tween 20) for 1 hour at room temperature. The PVDF membranes were probed with primary antibodies (p-Akt (Ser473, D9E), Cell signaling, 4060L; α-actinin, Santa Cruz sc-15335; VDAC1, Millipore AB10527; total Akt (E45), Abcam, ab32038) at 1:1000 dilution in 5% BSA/TBS-T overnight at 4℃, washed three times with 1XTBS-T, then incubated with horseradish peroxidase (HRP)-conjugated secondary antibodies (Cell signaling, 7074S) at 1:2,000 (all other primary antibodies) or 1:10,000 (for p-Akt antibody) dilution in 5% BSA/TBS-T for 1 hour at room temperature. After TBS-T wash, the membranes were incubated in SuperSignal West Femto Maximum Sensitivity Substrate (Thermo Scientific, 34096) or SuperSignal West Pico Chemiluminescent Substrate (Thermo Scientific, 34578) for 5 minutes. Then the bounded proteins were detected with chemiluminescence system (SYNGENE G: BOX).

The intensity of p-Akt, total Akt and VDAC1 were calculated by Image J. Total Akt, and p-Akt were normalized by VDAC1. Statistical significance was evaluated by the Student's t-test with excel and set at $p < 0.05$.

Results and Discussion

Translocation of phospho-Akt into mitochondria after serum stimulation

Low amount of phospho-Akt (p-Akt) was detected in total cell lysate and cytosolic fraction lysate but not a mitochondrial fraction (**Figure 2**). Phospho-Akt (p-Akt) increased after 15-minute serum stimulation in all lysates, especially in the cytosolic fraction. Total Akt (E45) was detected in all samples. Noteworthy, total Akt but no p-Akt in mitochondrial fraction was detected in serum starving cell, while total Akt was increased in mitochondrial fraction but slightly decreased in cytosolic fraction after serum stimulation. Comparing to serum-starved cells, p-Akt and total Akt in mitochondria significantly increased ($p<0.01$) after serum stimulation (**Table 1**). The increasing ratio of total Akt was 1.4 and p-Akt was 16.1 (**Figure 3**). Also, the elevation of p-Akt over total Akt in mitochondria was 12-fold and highly significant ($p<0.001$), which is compatible with previously published data [29]. Taken together; it suggested that Akt locates in mitochondria as an inactive form and translocates from the cytosol into mitochondria as an active form after serum stimulation in hESCs, same as in other differentiated or somatic cells.

Table 1. Fold change of Akt in mitochondria with or without serum stimulation

	p-Akt/VDAC		Akt/VDAC		pAkt/Akt	
Serum stimulation	-	+	-	+	-	+
Folds	1	16.1	1	1.4	1	12.1
SEM	0.34	0.46	0.10	0.03	0.27	0.25
p-value	<0.0001		0.0063		<0.0001	

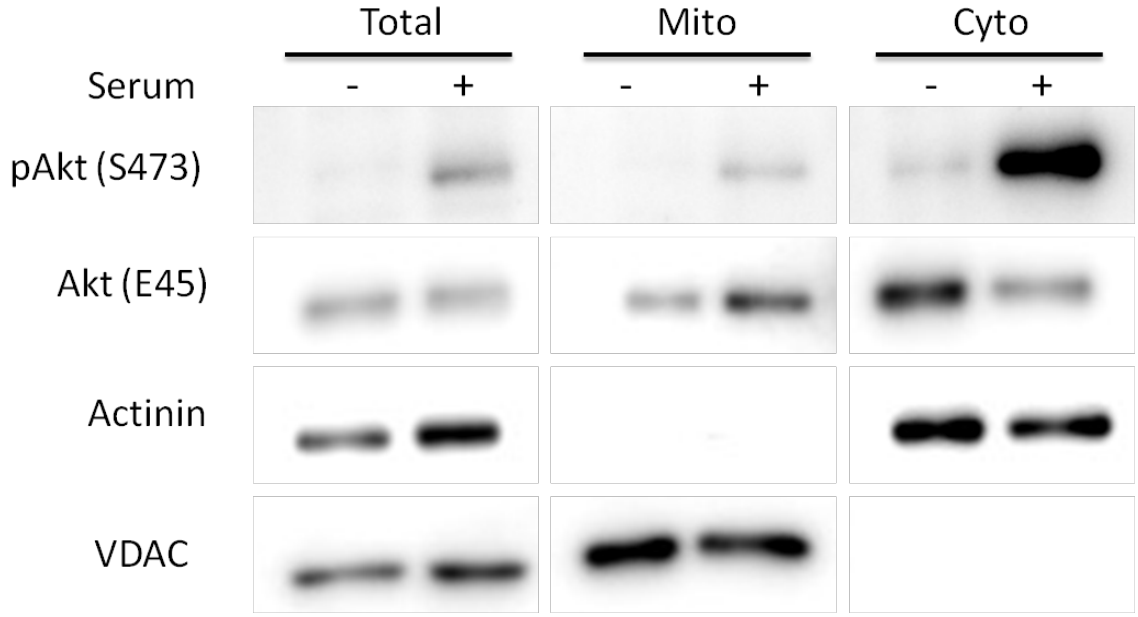

Figure 2. Translocation of phospho-Akt (p-Akt) into mitochondria after serum stimulation in hESCs. Total cell lysate, mitochondrial fraction and cytosolic fraction lysate of hESCs (H9) with and without serum stimulation were collected. Protein was separated by 10% SDS-PAGE. The cytosolic and mitochondrial subfractionation were immunoblotted for the compartment-specific proteins α-actinin and VDAC (or porin), respectively. With serum stimulation, all samples showed higher p-Akt (S473), especially the cytosolic fraction. Total Akt (E45) increased in mitochondrial fraction but decreased in the cytosolic fraction. The immunoblots demonstrated that p-Akt translocated into mitochondria after serum stimulation.

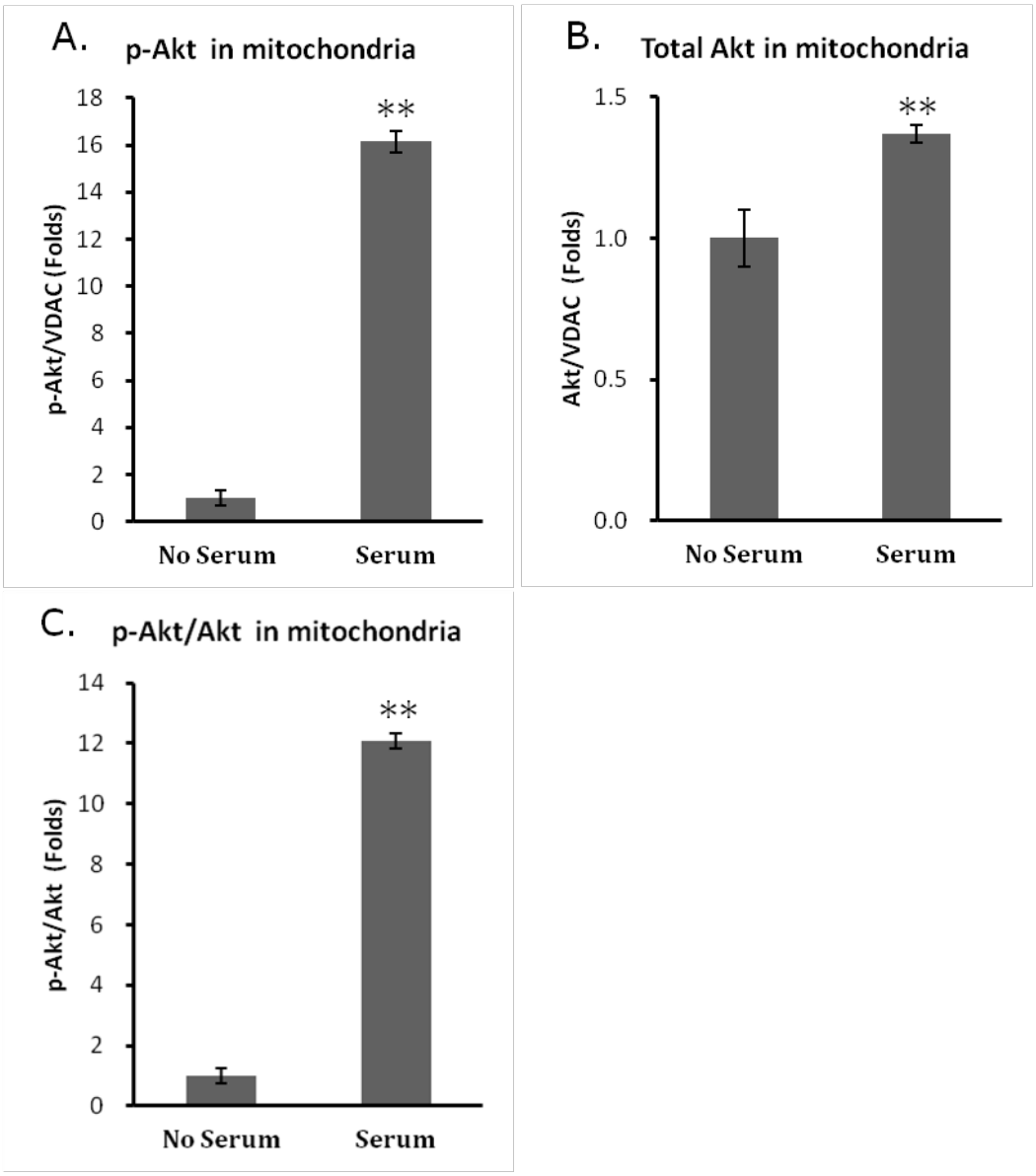

Figure 3. Quantification of p-Akt in mitochondria after serum stimulation in H9 cells.
Mitochondria fraction from three individual samples of hESCs (H9) in each group was immunoblotted for total Akt (E45), p-Ser473-Akt, and VDAC. Protein bands were analyzed by Image J. Increasing of p-Akt (A), total Akt (B), and p-Akt over total Akt (C) were highly significant after serum stimulation (** $p < 0.01$). Taken together, it showed that the increase of p-Akt in mitochondria is translocated from the cytosol, as well as activation of Akt in the mitochondria.

2.5. Mitochondrial Akt1 Signaling Enhanced Reprogramming

To study the effect of mitochondria Akt1 signaling on stem cell fate, two constructs were mitochondria-targeting dominant negative Akt1 (Mito-dnAkt1) and a constitutive active Akt1 (Mito-caAkt1) construct carried by adenoviral vector or lentiviral vector. Expression of Mito-dnAkt1 protein and Mito-caAkt1 protein in mitochondria were verified by western blot [31,42,48,65]. Our preliminary data showed that Sox2 and Oct4 protein expression were higher when transduction of Mito-Akt1 vector in hESCs (H1). In contrast, Mito-dnAkt1 transduced hESCs lost pluripotency markers, such as Oct4, stage-specific embryonic antigen-4 (SSEA-4) and alkaline phosphatase (AP). These results suggested that mitochondrial Akt1 signaling played a role in stem cell pluripotency and differentiation.

Throughout the past decade, induction of pluripotency stem cells from somatic cells with defined factors, also known as Yamanaka factors, became an important tool in regenerative medicine, disease modeling, and stem cell biology research [10-12]. We hypothesized that mitochondrial Akt1 signaling might enhance induced pluripotency stem cell (iPSC) reprogramming. With the same constructs mentioned, we found that adding the Mito-Akt1 adenoviral vector in the protocol of mouse & human fibroblasts reprogramming generated significantly higher alkaline phosphatase (AP)-positive colonies than control viral vector only. Also, the number of mouse pluripotency marker, SSEA-1, positive iPS cells significantly increased after adding Mito-Akt1 but significantly decreased after Mito-dnAkt1 were added [65]. These provide evidence that mitochondrial Akt1 signaling enhanced iPSC reprogramming and reduced the iPSC production efficiency when it was inhibited.

Herein, the effect of inhibiting mitochondrial Akt1 signaling during initial stages of embryonic development was tested in this dissertation.

Chapter 3

The Effect of Mitochondrial Akt1 Signaling on Stem Cell Differentiation

3.1 Introduction

In order to dissect the effect of inhibiting mitochondrial Akt1 signaling on stem cell differentiation, we generated a mitochondrial-targeting dominant negative Akt1 expressing adenoviral vector. With this adenoviral vector, we designed a protocol to differentiate hESCs *in vitro* in three conditions: without adenoviral vector (C group), adenoviral vector only (GFP group) and an adenoviral vector carrying mdnAkt1 construct (mDN group) to verify our hypothesis (**Table 2**).

Table 2. Design of experiment group

Group	Adenoviral Vector
Control (C)	No
GFP (G)	GFP (Ad-GFP)
mDN	Mitochondria-targeting dominant negative Akt1 and GFP (Ad-mdnAkt1/GFP)

3.2 Materials and Methods

Cell line and cell culture

Feeder-Free undifferentiated hESCs (H1 & H9, Passage 38-44) were maintained on matrigel-coated plate in mTeSR™1 (STEMCELL Technologies) and were passaged every 4-7 days with ReLeSR™ (STEMCELL Technologies) [63,64]. For spontaneous differentiation *in vitro*, hESCs were cultured in differentiation medium, which contained Dulbecco's modified Eagle's medium/F12 (DMEM/F12, Sigma, D8437) supplemented with 10% fetal bovine serum (FBS, Omega Scientific, FB-12), 1 mM sodium pyruvate (Gibco, 11360-070), 0.1 mM nonessential amino acid (NEAA, Gibco), 2 mM L-glutamin (Gibco) and 55 μM 2-mercaptoethanol (Gibco) [66].

HEK 293 cell line cultured in DMEM/F12 supplemented with 10% FBS, 1 mM sodium pyruvate, 0.1 mM NEAA and 2 mM L-glutamin. Neonatal human dermal fibroblast (nHDF, passage 4-7) cultured in DMEM/F12 supplemented with 10% FBS, 2 mM L-glutamin.

Mitochondrial-Targeting Akt1 Construct

To study the effect of mitochondrial Akt1 signaling, we generated a new adenoviral vector carrying a his-tagged mitochondria-targeting dominant negative Akt1 and green fluorescent protein (GFP) construct (Ad-mdnAkt1/GFP) (AdEasy Adenoviral Vector Systems, Agilent Technologies). This construct consisted of two separated sequences: mdnAkt1 and GFP, each driven by their CMV promoters [42]. The sequence of mdnAkt1 contains three modifications to endogenous Akt1. The first modification is a mitochondrial targeting

sequence (MSVLTPLLLRGLTGSARRLPVPRAKIHSL) at the amino terminus of the Akt1 sequence. The second one is a mutation from Lys179 (K) to methionine179 (M) on kinase domain[26]. The final modification is his-tag was fused at the carboxyl terminus of the Akt1 sequence, which can be used to detect protein expression (**Figure 4**). Control adenoviral vector carries GFP protein only (Ad-GFP). The transgene expression was examined by western blot with the anti-His antibody (Cell signaling, D3I10) (**Figure 8**(C)).

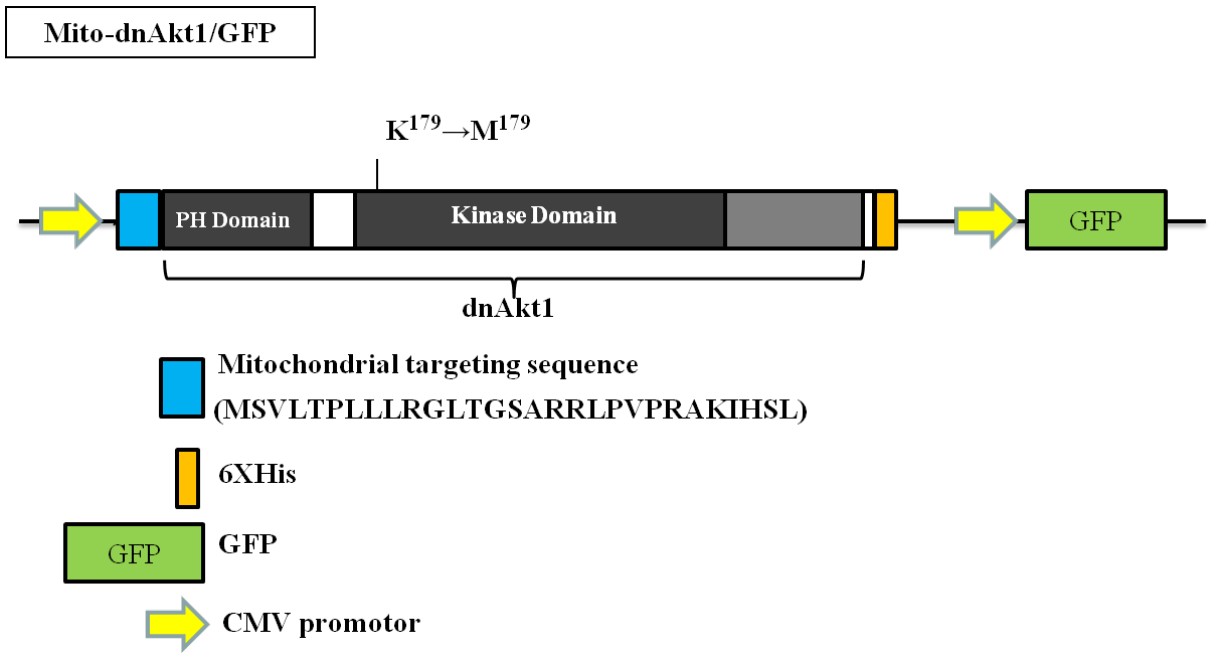

Figure 4. His-tagged Mitochondria-targeting dominant negative/GFP construct Mito-dnAkt1, and GFP gene is driven by CMV promoter (yellow arrow) individually. Mitochondrial targeting sequence is highlighted as the blue box, and 6X his-tag is highlighted as a brown-yellow box. Functionally important amino acid residues in the pleckstrin homology (PH) and kinase domains are noted. The 6X His epitope tag is on the carboxyl terminus of constructs; the mitochondrial sequence is on the amino terminus.

Viral vector amplification and titer

The two adenoviral vectors, Ad-GFP and Ad-mdnAkt1/GFP, was amplified in HEK 293 cells. To collect viral vector, transfected HEK 293 cells was broken by freeze-thaw cycle three times, then was spun down at 16,000g for 30 minutes at 4°C. Collecting supernatant, then the supernatant was spun at 16,000g for 30 minutes at 4°C. The viral vectors-contained supernatant was collected.

The viral concentration (or viral titer) was verified by viral plaque assay.[67,68] The day before the assay, HEK 293 cells were seeded on two 6-well vessels at 90 - 100% confluence. A ten-fold serial dilution of viral vector solution was performed in DMEM/F12 medium. The 500 ul serial dilutions were added in each well and incubated at 37°C, 5% CO_2 for 1 hour. The full medium with 0.3% agarose was pre-warmed in 42°C water bath, then added 2 ml per well as agarose overlay and cooling at room temperature for 20 minutes. After the addition of overlay, the HEK 293 cells were incubated at 37°C, 5% CO_2 for ten days. HEK 293 cells were fixed by adding 1 ml of 10% formalin (Protocol, 245-684) for overnight. GFP expressed viral colonies were counted under a fluorescence microscope to calculate plaque forming units (pfu) and multiplicity of infection (MOI). At least two technical repeats were done for each viral vector.

Transduction of human fibroblasts by adenoviral vector

Human fibroblasts were trypsinized to single cells and incubated with an equal viral titer of Ad-GFP and Ad-mdnAkt1/GFP in full medium at 37°C, 5% CO_2 for 1 hour. Then the cells were plated out. GFP expression was observed under EVOS microscope 48-72 hours after transduction.

Transduction of hESC by adenoviral vector

Based on the above two new adenoviral vectors, we designed three experiment groups: Control (no viral vector), GFP (Ad-GFP viral vector) and mDN (Ad-mdnAkt1/GFP viral vector) (**Table 2**).

To harvest single cells of hESCs, hESCs were cultured until reached 60 – 80% confluence, changed fresh mTeSR™1 medium 6 hours ahead and added rock inhibitor (Thiazovivin, final concentration 2 μM, STEMCELL Technologies) one hour before harvest. Cells were detached by Accutase® (STEMCELL Technologies) as the manufacturer's manual. The collected cell pellet was re-suspended in mTeSRTM1 supplemented with rock inhibitor; then cell number was counted. For each experiment group, the single cell suspension was incubated with one MOI viral vector or no viral vector at 37°C, 5% CO_2 for 1 hour. Then cells were plated back to the matrigel-coated well in the density of $1x10^6$ cells / well of 6-well vessel[66,69]. On the next day, the mTeSR™1 medium was replaced by 4 ml/well differentiation medium (DMEM/F12 with 10% FBS) for spontaneous differentiation *in vitro*. The differentiation medium was changed every 2 – 3 days (**Figure 5**).

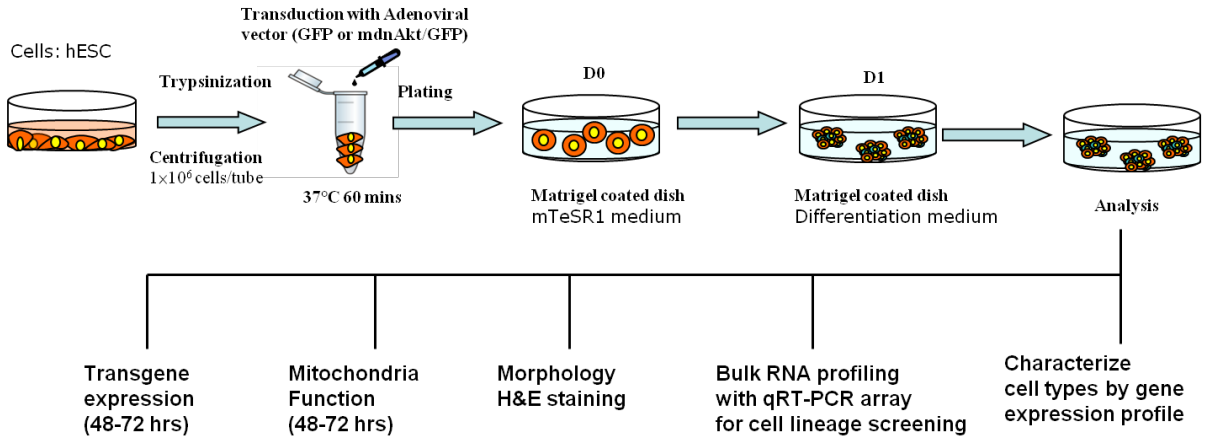

Figure 5. Experimental protocol for the analysis of human embryonic stem cell differentiation (hESC)

Evaluation of transduction efficiency by fluorescence microscopy

GFP expression was assessed with Eclipse Ti fluorescence microscope (Nikon) or EVOS microscope (**Figure 8** (A)). Twenty-four hours after transduction, GFP started to express and reached peak signal around 48 to 72 hours. GFP signal decreased drastically after five days of transduction. Only a few cells expressed GFP up to 2 weeks, particularly in mDN group.

Evaluation of transduction efficiency by flow cytometry

Transduction rate was quantified by flow cytometry 48-72 hours post-transduction (**Figure 8**(B)). Cells were detached by Accutase and re-suspended in 2% FBS in 1X PBS for GFP expression analysis with BD LSR II Flow Cytometry Analyzer. Four individual samples in each group were counted. FACS data were analyzed with Flow Jo V10. GFP positive cells were presented as mean ± SD %. Median intensity was presented as mean ± SD.

Transgene expression examined by western blot

Cells were harvested by scraper after ice-cold PBS washed three times and suspended in ice-cold mitochondrial isolation buffer supplemented with a protease inhibitor, 1 mM PMSF, 20 mM NaF, and 2 mM Na_3VO_4. After incubating on ice for 30 minutes, these cells were homogenized by using a Dounce homogenizer with 10 strokes of loose pestle and 35 strokes of the tight pestle. The cell debris was removed by centrifugation at 1,000g for 10 minutes twice at 4°C and mitochondria contained supernatant was centrifuged at 10,000g for 30 minutes at 4°C. The supernatant was collected as cytosolic fraction. The mitochondria pellet was re-suspended in mitochondria isolation buffer and spun down at 10,000g for 30 minutes at 4°C.

The protein concentration of mitochondrial and cytosolic fractions was determined by the Bradford method (Bio-Rad, protein assay dye reagent concentrate, 5000006). Proteins extracted from the cytosolic and mitochondrial fractions were separated by 10% SDS-polyacrylamide gel electrophoresis (SDS-PAGE) and transferred onto PVDM. The mdnAkt1 protein translated from transgene was identified with the N-Akt1 antibody (1:1000, Cell Signaling, 2938s) and anti-His antibody (1:1000, Cell Signaling, D3I10). Mitochondria fraction was verified with MnSOD antibody (1:1000, Millipore, 06-984) and VDAC antibody (1:2000, Calb-chem). Cytosolic fraction was verified with Alpha-tubulin (1:1000, Santa Cruz, sc-15335).

Analysis of cell respiration by extracellular flux analyzer

Mitochondria respiration of hESC (H1) in three experiment group was evaluated and analyzed by mitochondrial stress test using Seahorse Bioscience XF24 Extracellular Flux Analyzer (Seahorse Bioscience, North Billerica, MA) and following the manufacturer's protocol [70]. Cells post 48 hours transduction were detached with Accutase, plated in the density of 8.0 $x10^4$ cells per well in Matrigel-coated 24-well Seahorse XF-24 assay plate and grown at 37°C, 5% CO_2 overnight before analysis. Before analysis, cells were washed once with freshly prepared KHB buffer (111 mM NaCl, 4.7 mM KCl, 2 mM MgSO4, 1.2 mM Na2HPO4, 2.5 mM glucose and 0.5 mM carnitine; pH 7.4) and incubated in KHB buffer at 37°C in a non-CO2 incubator for 1 hr. Three baseline measurements of oxygen consumption rate (OCR) were taken before sequential injection of following mitochondrial inhibitors and final concentration: oligomycin (1 g/ml), carbonilcyanide p-triflouromethoxyphenylhydrazone (FCCP) (3 μM) and rotenone (0.1 μM). Three measurements were taken after the addition of each inhibitor. OCR and ECAR values were automatically calculated and recorded by the Seahorse XF-24 software. The basal respiration was calculated by averaging the three measurements of OCR before injection of oligomycin substrate OCR after injection of rotenone. ATP-linked respiration was calculated by averaging the three measurements of OCR difference before and after injection of oligomycin. Non-mitochondrial oxygen consumption was calculated by average the three measurements of OCR after rotenone injection. Data were presented as mean ± SEM unless noted otherwise. Student's t-test evaluated statistical significance as $p < 0.05$.

Evaluating spontaneous differentiation *in vitro* by hematoxylin and eosin (H&E) staining

After four weeks of spontaneous differentiation *in vitro*, cells were washed with 1X PBS twice then fixed in 4% paraformaldehyde (Electron Microscopy Sciences, RT 15710) for 1 hour. After washing with 1X PBS twice, cells were stained with H&E. Whole well scanning for each group was recorded by Eclipse Ti fluorescence microscope (Nikon).

Cell lineage screening with a qRT-PCR array

For feasible cell lineage or cell type identification, total RNA of differentiated cells 21st -day post-transduction was isolated with TRIzol® LS Reagent (Life Technologies, 10296-028). Thermo Scientific™ NanoDrop 2000 and 2000c are used to quantify and assess the purity of RNA. RNA was reverse transcribed into complementary DNA (cDNA) by using RT^2 First Strand Kit (Qiagen), then the cDNA mixed with RT^2 SYBR Green Fluor qPCR Mastermix (Qiagen) was loaded in Human Cell Lineage Identification RT^2 Profiler PCR Array (Qiagen). All procedures were done as manufacture protocol. The quantitative reverse transcription polymerase chain reaction (qRT-PCR) was performed and analyzed by the Applied Biosystems ViiA 7 Real-Time PCR System (ThermoFisher Scientific). Quality evaluation and data analysis were done with Qiagen software (http://www.qiagen.com/geneglobe).

3.3 Results and Discussion

Mitochondrial Akt1 gene expression in human fibroblast and hESC

To verify the consistency between adenoviral vectors, viral titer, and transgene expression, human fibroblasts were incubated with the equal MOI of Ad-GFP or Ad-mdnAkt1/GFP viral vector at 37°C for 24 hours. Seventy-two hours after transduction, GFP expression, representatives of transgene expression, was observed in more than 80% of Ad-GFP or Ad-mdnAkt1/GFP transduced fibroblasts (**Figure 6**). Hence, the transduction efficiencies of these two viral vectors in human fibroblasts were the same in differentiated cells.

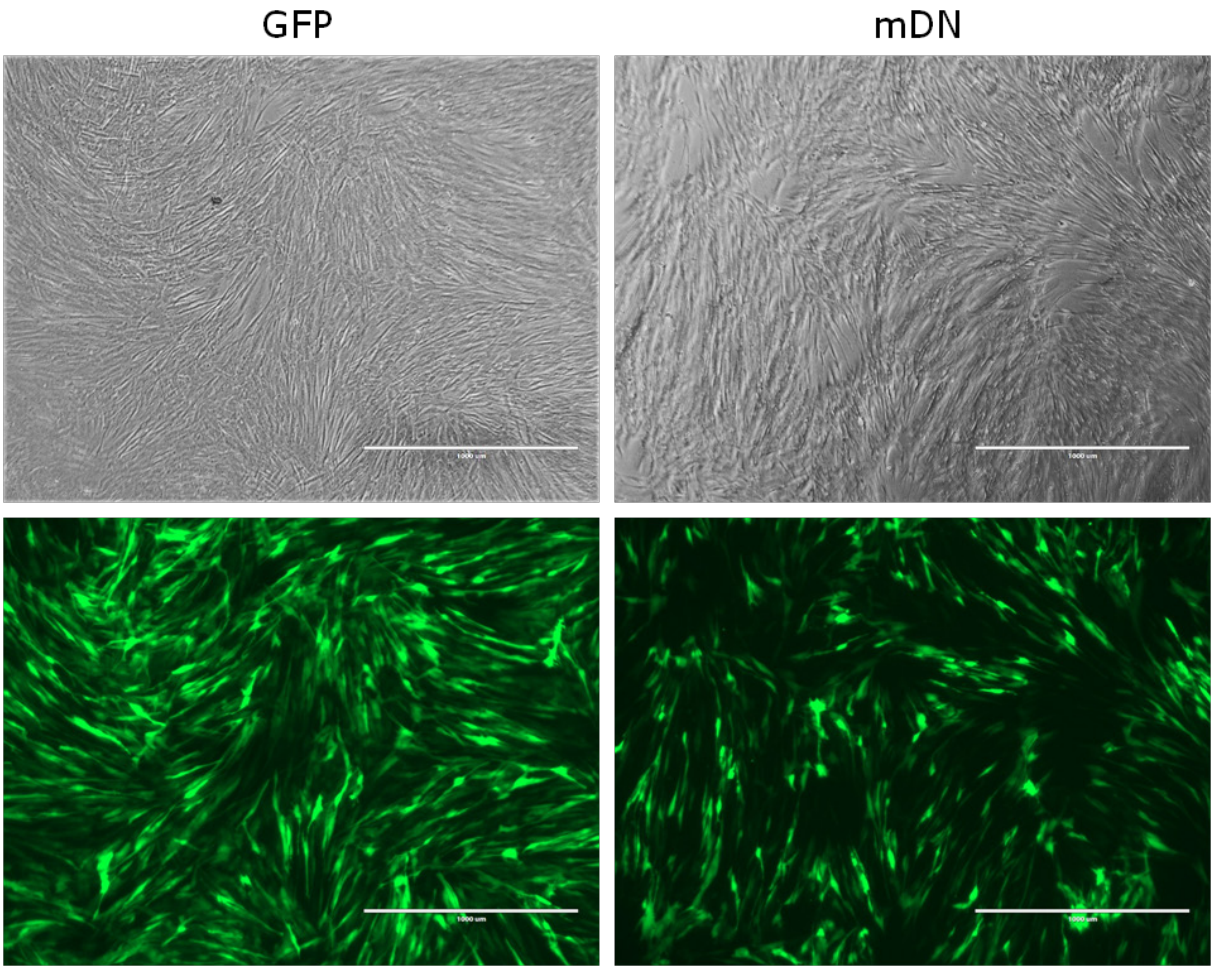

Figure 6. Human fibroblasts transduced with Ad-GFP and Ad-mdnAkt1/GFP. Incubated human fibroblasts with an equal viral titer. Transduction efficiencies were evaluated 72 hours after viral vector incubation. GFP expression in Ad-GFP (GFP) or Ad-mdnAkt1/GFP (mDN) transduced cells is around 80~90%.

Based on this preliminary data, the equal viral titer was mixed in the mTeSR1 medium for Ad-GFP and Ad-mdnAkt1/GFP transduction in hESC. Unlike human fibroblasts, poor GFP expression rate (lower than 10%) was found when hESCs were maintained in the mTeSR1 medium. (Data was not shown here) Previous studies also reported a wide range of transduction rates in hESC with the adenovirus vector. For instance, hESC transduced with MOI of 500 obtained transduction rate of 11% [66] or MOI of 50,000 obtained transduction rate of 59% [71]. Kawabata *et al.* found that some types of stem cells cannot be efficiently transduced with an adenovirus vector containing the cytomegalovirus (CMV) promoter due to lack of coxsackievirus and adenovirus receptor (CAR) [69]. In mES cells, elongation factor 1α (EF-1α) and CA (β-actin promoter/CMV enhancer) promoters were shown to be highly active, while the CMV promoter was inactive [72]. In other words, the adenovirus vector with CMV promoter had higher transduction rates in differentiated cells.

For increasing the transduction rate, two modifications of the initial transduction protocol were applied, including incubation of viral vectors with single cell suspension for one hour and replacement of mTeSR1 medium to differentiation medium (DMEM/F12 supplemented with 10% FBS) 24 hours after transduction. Through single cell suspension transduction, adenoviral vector (Ad-GFP & Ad-mdnAkt1/GFP) was transduced into hESC efficiently. When adding equal MOI or no viral vector, transduction efficiency quantified by flow cytometry after 48 hours transduction was 3.76 ± 0.52 % in control group, 66.0 ± 3.44% in GFP group and 90.5 ± 2.56 % in mDN group respectively (**Figure 7**). Median fluorescence intensity was 8720 ± 248 in control group, 40458 ± 8282 in the GFP group and 153574 ± 50957 in mDN group (**Table 3**).

Table 3. Transduction efficiency evaluated by flow cytometry

	Control	GFP	mDN
GFP expression %	3.76	66.0	90.5
SD	0.52	3.44	2.56
Median intensity	8720	40458	153574
SD	248	8282	50957

A.

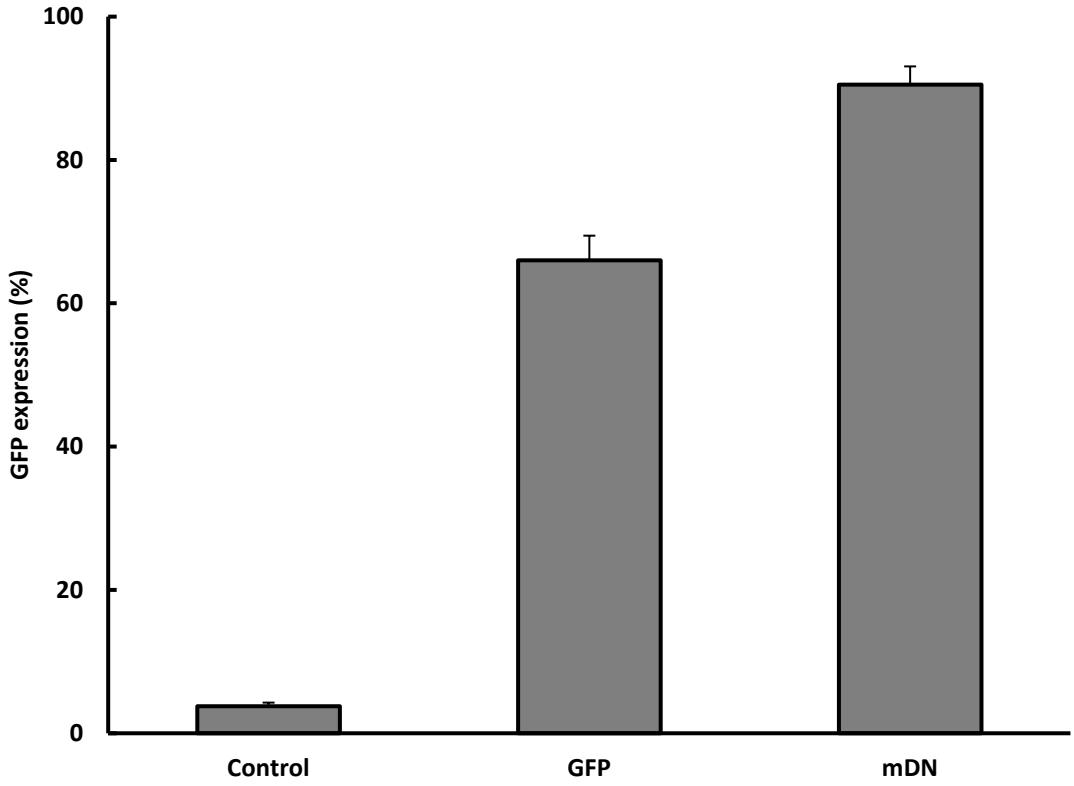

B.

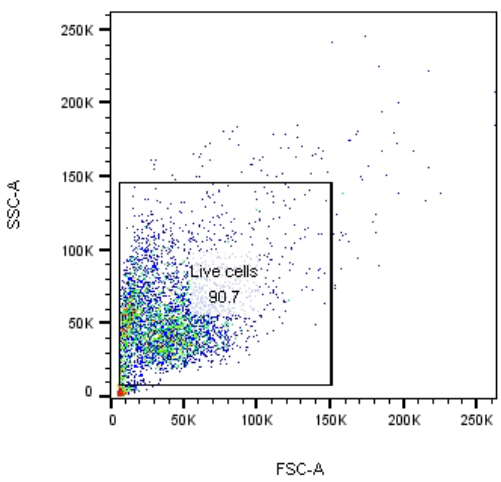

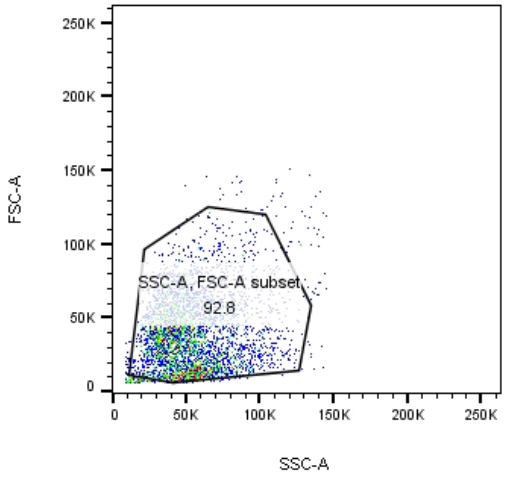

C.

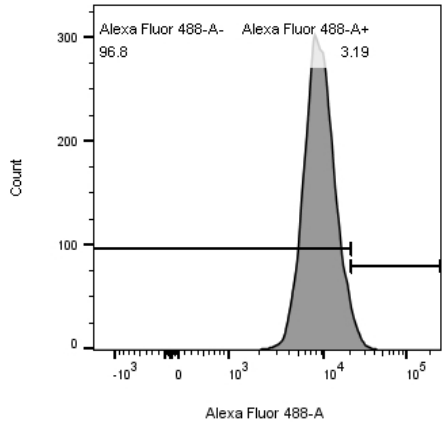

Tx39_WA01_P43_Control_1_001.fcs
SSC-A, FSC-A subset
8693

Alexa Fluor 488-A+: **Median** : *Alexa Fluor 488-A*: 23261
Alexa Fluor 488-A-: **Median** : *Alexa Fluor 488-A*: 8467

Ancestry Subset Statistic For	Median intensity	GFP +
Tx39_WA01_P43_Control_1_001.fcs	8600	3.19
Tx39_WA01_P43_Control_2_003.fcs	8262	2.78
Tx40_WA01_P43_001_Control_1_001.fcs	8814	4.11
Tx40_WA01_P43_001_Control_1_012.fcs	8814	4.11
Tx40_WA01_P43_001_Control_2_003.fcs	9074	4.22
Tx40_WA01_P43_001_Control_2_014.fcs	9074	4.22
Tx40_WA01_P43_002_Control_1_001.fcs	8543	3.40
Tx40_WA01_P43_002_Control_1_020.fcs	8543	3.40
Tx40_WA01_P43_002_Control_2_003.fcs	8736	4.10
Tx40_WA01_P43_002_Control_2_022.fcs	8736	4.10
Mean	*8720*	*3.76*
SD	*248*	*0.52*

D.

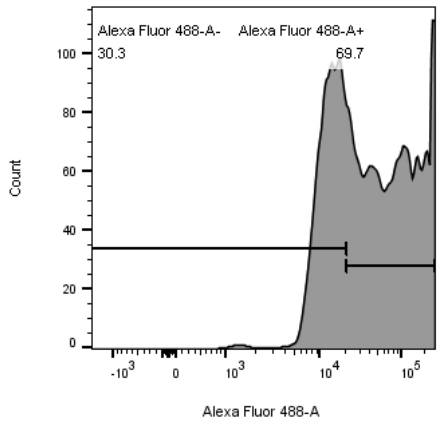

Tx40_WA01_P43_001_GFP_1_002.fcs
SSC-A, FSC-A subset
8284

Alexa Fluor 488-A+: **Median** : *Alexa Fluor 488-A*: 108003
Alexa Fluor 488-A-: **Median** : *Alexa Fluor 488-A*: 12496

Ancestry Subset Statistic For	Median intensity	GFP +
Tx39_WA01_P43_GFP_1_002.fcs	36812	65.1
Tx39_WA01_P43_GFP_2_004.fcs	34003	64.6
Tx40_WA01_P43_001_GFP_1_002.fcs	49559	69.7
Tx40_WA01_P43_001_GFP_1_013.fcs	49559	69.7
Tx40_WA01_P43_001_GFP_2_004.fcs	50286	69.9
Tx40_WA01_P43_001_GFP_2_015.fcs	50286	69.9
Tx40_WA01_P43_002_GFP_1_002.fcs	35167	63.1
Tx40_WA01_P43_002_GFP_1_021.fcs	35167	63.1
Tx40_WA01_P43_002_GFP_2_004.fcs	31869	62.2
Tx40_WA01_P43_002_GFP_2_023.fcs	31869	62.2
Mean	*40458*	*66.0*
SD	*8282*	*3.44*

E.

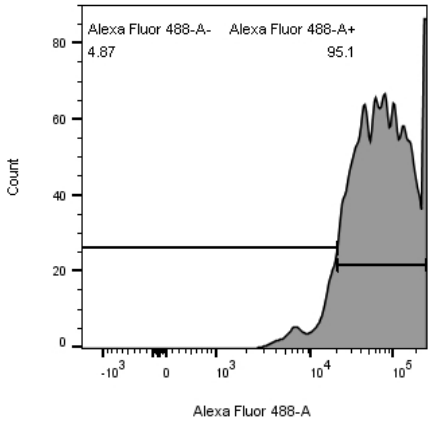

Tx39_WA01_P43_DN_1_005.fcs
SSC-A, FSC-A subset
7969

Alexa Fluor 488-A+: **Median** : *Alexa Fluor 488-A*: 261573
Alexa Fluor 488-A-: **Median** : *Alexa Fluor 488-A*: 13606

Ancestry Subset Statistic For	Median intensity	GFP +
Tx39_WA01_P43_DN_1_005.fcs	234633	95.1
Tx39_WA01_P43_DN_2_007.fcs	261573	95.3
Tx40_WA01_P43_001_DN_1_005.fcs	141885	90.1
Tx40_WA01_P43_001_DN_1_016.fcs	141885	90.1
Tx40_WA01_P43_001_DN_2_007.fcs	135738	89.7
Tx40_WA01_P43_001_DN_2_018.fcs	135738	89.7
Tx40_WA01_P43_002_DN_1_005.fcs	121220	88.5
Tx40_WA01_P43_002_DN_1_024.fcs	121220	88.5
Tx40_WA01_P43_002_DN_2_007.fcs	120922	88.9
Tx40_WA01_P43_002_DN_2_026.fcs	120922	88.9
Mean	*153574*	*90.5*
SD	*50957*	*2.56*

Figure 7. Transduction efficiency calculated by flow cytometry (A) Bar graph; (B) Gating according to cell size and granularity; (C, D, E) Histogram and statistics data calculated by Flow Jo. C: Control; D: Ad-GFP (GFP); E: Ad-mdnAkt1/GFP (DN)

Observing GFP positive cells under a microscope, there were more GFP positive cells and stronger GFP signaling in mDN group (**Figure 8**). In western blot, 6X His-tag antibody detected mutant Akt protein expressed in the mitochondrial fraction of mDN group only. The larger size protein detected by Akt1 antibody was the same size protein detected by 6X His-tag antibody. Both VDAC1 antibody and MnSOD antibody were detected in mitochondria fraction, but alpha-tubulin antibody was not detected in the mitochondrial fraction. The immunoblotting suggested that the mutant Akt size was bigger than indigenous Akt and specifically located in mitochondria (**Figure 8**(B)).

Interestingly, the mutant Akt was also detected by Akt1 antibody in the cytosolic fraction. Both VDAC1 antibody and MnSOD antibody were not detected in the cytosolic fraction; this showed that the cytosolic fraction did not contaminate by mitochondria. There was also a faint band detected by 6X His-tag antibody in the cytosolic fraction, but the size of this faint band was bigger than the one detected in the mitochondrial fraction. Because the adenoviral vector was an over-expressed system for the transgene, the mutant Akt protein was expressed abundantly; there was some mutant Akt protein can be detected before it was translocated into mitochondria. Taken together, this mutant Akt protein was modified or cut when it was translocated into mitochondria to become an active form.

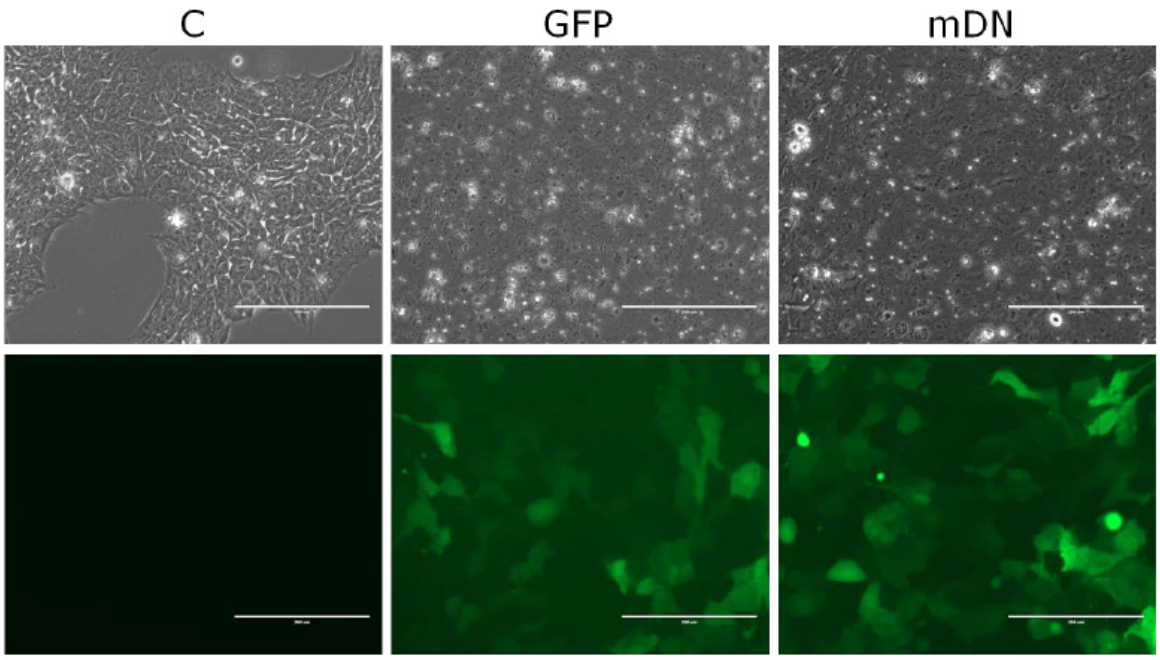

A.

B.

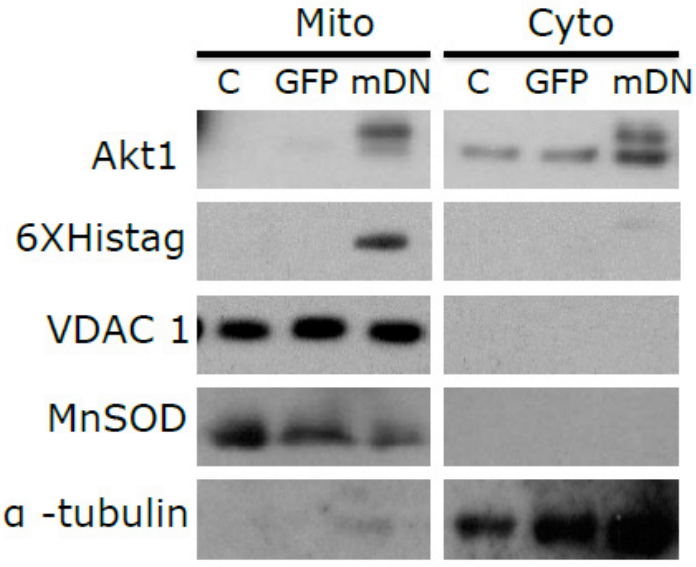

Figure 8. **Transgene expression in hESCs** (A) GFP expression observed under EVOS microscope (scale bar: 200 μm). (B) Immunoblot showed mdnAkt1 protein expressed in mitochondria. C: control, GFP: Ad-GFP, mDN: Ad-mdnAkt1/GFP.

Comparing to transduction of the equal MOI to human fibroblasts, similar GFP signal intensity and GFP positive cell numbers were observed under EVOS microscopy in Ad-GFP or Ad-mdnAkt1/GFP group (**Figure 6**). The result suggested the cells transduced by the same MOI of Ad-GFP and Ad-mdnAkt1/GFP adenoviral vector were able to express transgene equally. However, the same MOI transduced into hESCs expressed GFP differently. The GFP positive cells found in mDN group were more than in the GFP group (**Figure 8**(A)). Analyzing by flow cytometry and Flow Jo v10, cells in mDN group showed a higher percentage of GFP positive cells and stronger median fluorescence intensity. According to published reports, the CMV promoter was relatively inactive in stem cells. Therefore, the higher GFP expression in mDN group suggested that the hESC differentiation was faster when mitochondrial Akt1 signaling was inhibited.

Elevation of mitochondria oxygen consumption rate

Mitochondria stress testing showed that the oxygen consumption rate (OCR) of mitochondrial basal respiration elevated drastically in mDN group, about two-fold over GFP group ($p < 0.001$). (**Figure 9** (A)) At the same time, OCR of non-mitochondria respiration and ECAR increased significantly in mDN group ($p < 0.05$) compared to GFP or control group, but there was no statistical difference between GFP and control group ($p > 0.05$). (**Figure 9** (C, D)) This indicated that inhibition of mitochondrial Akt1 signaling increased oxygen consumption by both mitochondrial and non-mitochondrial respiration.

Noteworthy, the mitochondrial proton leak of mDN group also increased by 1.9 fold compared to GFP ($p < 0.001$). (**Figure 9** (E)) Mechanisms of mitochondrial proton leak, a process that dissipates energy generated through electron transport chain, includes direct movement of protons across the mitochondrial inner membrane, diffusion through or around integral membrane proteins and inducible transport through the adenine nucleotide translocase (ANT) or uncoupling proteins (UCP1, UCPx).[73,74] Previous studies have shown that higher proton leak is linked to higher oxidative phosphorylation rates, resulting in protection by mild uncoupling against excessive reactive oxygen species (ROS) production[75]. The increased of proton leakage after mitochondrial Akt1 signaling inhibition may correspond to elevated mitochondrial respiration and ROS production.

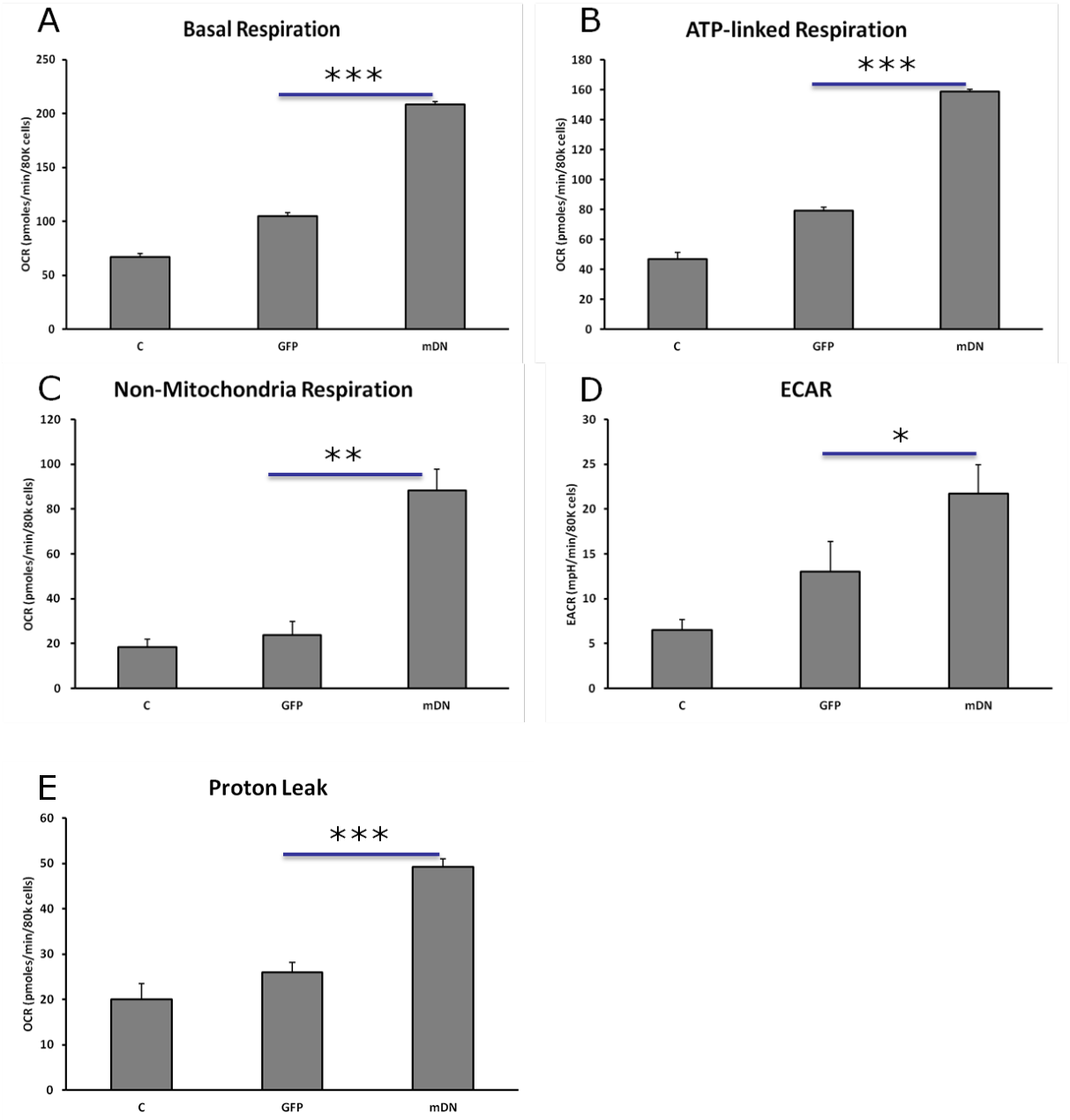

Figure 9. Inhibition of mitochondrial Akt1 singling alters mitochondria function in hESCs Mitochondrial respiration was evaluated by Seahorse Bioscience XF24 Extracellular Flux Analyzer. Oxygen consumption rate (OCR) of mitochondria basal respiration and non-mitochondria respiration were highly significantly elevated in mDN group. ECAR were also increased ($p < 0.05$). Noteworthy, proton leak drastically increased, corresponding to protect cells against excessive ROS production by uncoupling.

Morphological evaluation by H&E staining

Human ESCs transduced with Ad-GFP, or Ad-mdnAkt1/GFP differentiated *in vitro* led to many cell types and organized cell colonies after 28-day differentiation (**Figure 10**). The organized cell colonies of the mDN group were bigger than those of the GFP group. Also, more cell types were observed in the mDN group. The differentiated cells were found earlier in mDN group than in GFP group 7-day after transduction. The most obvious differentiation differences were found 21-day post-transduction (Data were not shown here). In line with this, inhibiting mitochondrial Akt1 signaling for a short duration led to faster differentiation, more cell types, and more organized or mature cells.

A.

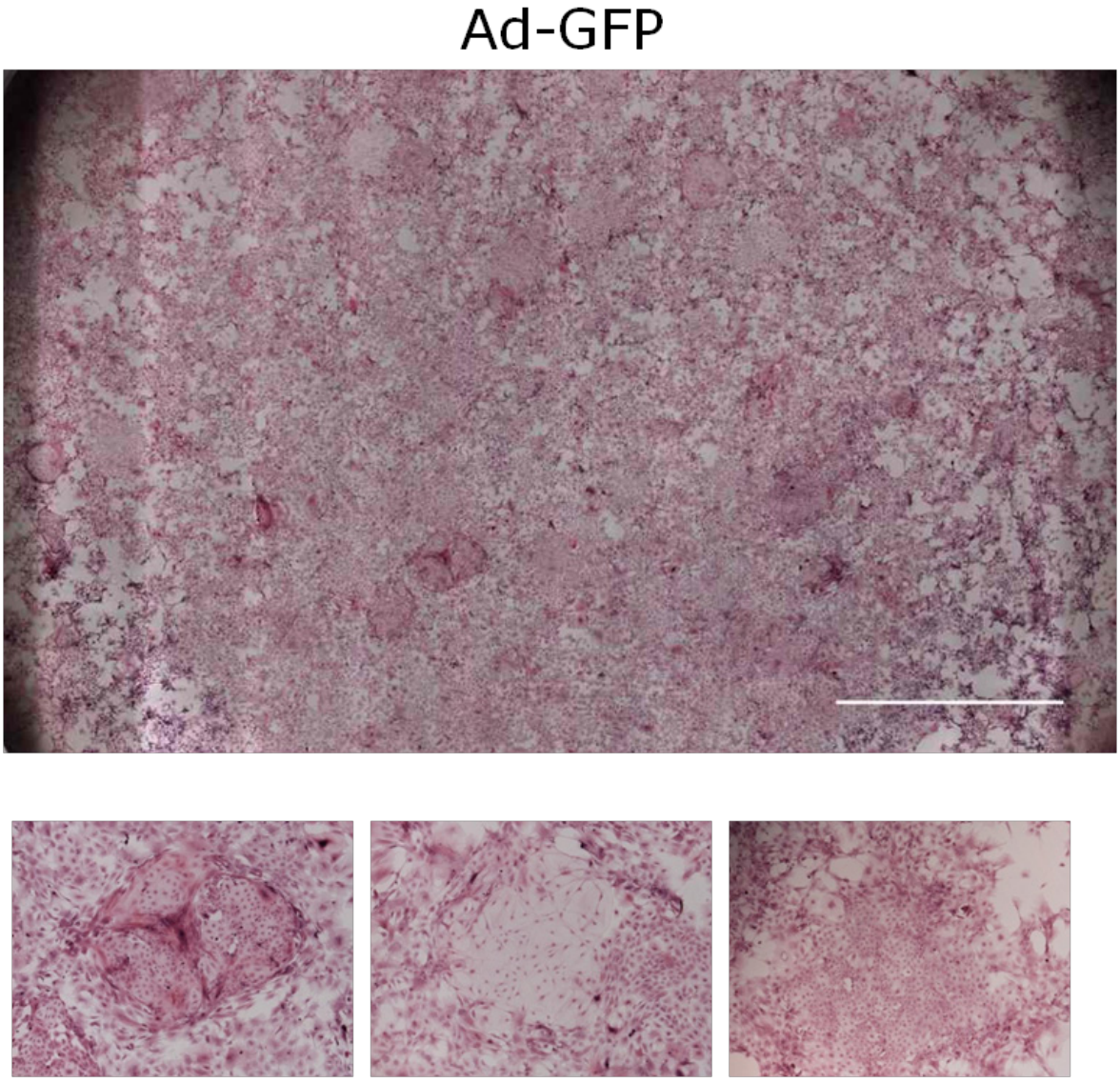

B.

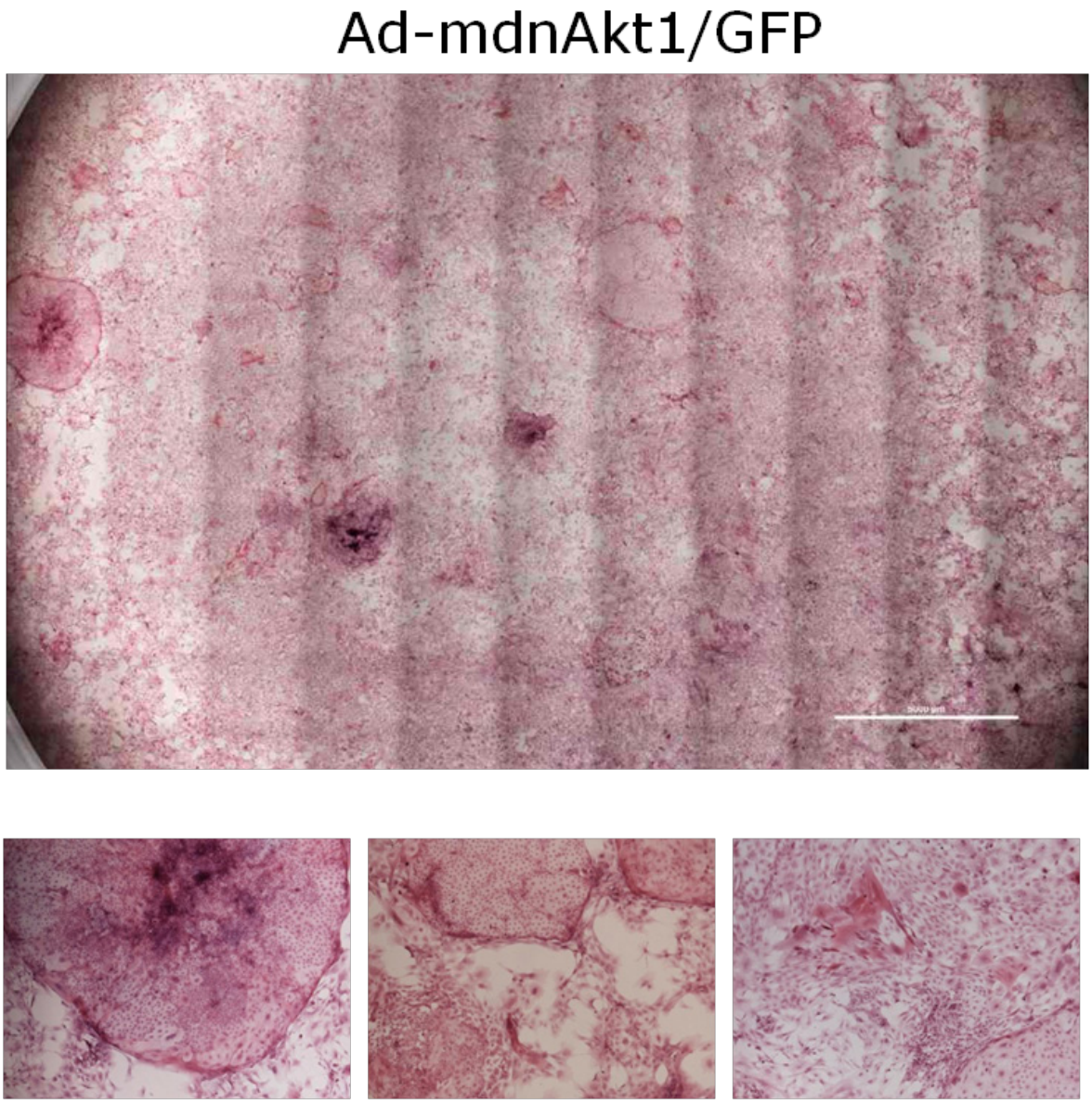

Figure 10. ***In Vitro*** **spontaneous differentiation of hESCs transduced with Ad-GFP or Ad-mdnAkt1/GFP** (A) GFP group (B) mDN group. Transient mitochondrial Akt1 signaling inhibition (B) in early differentiation led to more cell types and more organized cells.

Cell lineage-specific gene expression

Based on the above findings, I decided to explore the cell types on the 21th-day after transduction according to the bulk RNA (also known as total RNA) and human cell lineage identification PCR array. The cutoff value was set as fold change over 1.5 folds and $p < 0.05$. Comparing to the GFP group, some genes were expressed differently in mDN group (**Figure 11** and **Table 4**). In the ectoderm lineage, the following marker genes were significantly up-regulated, including ectoderm (OTX2 and FOXD3), neural progenitor (SOX2 and PROM1), limbal progenitor (MSLN and ENO1), and motor neuron progenitor (FOXG1). No terminal differentiation marker genes from ectoderm lineage were significantly up-regulated. In the endoderm lineage, significantly up-regulated marker genes of lung cell (SFTPD) and hepatic stem cell (MAP3K12) were noted. Noteworthy, DDP4, a hepatic stem cell marker gene, was the only one significantly down-regulated gene in mDN group comparing to the GFP group.

In the mesoderm lineage, mesoderm marker genes (BMP4, IGF2, HAND1, PDGFRA, DCN, and GATA2) and muscle and bone associated terminal differentiated marker genes were up-regulated. Marker genes of skeletal muscle cells (MYH1), smooth muscle cells (MYH11), early cardiomyocytes (HAND2), and cardiomyocytes (RYR2, NPPA, MYL3) were significantly up-regulated. Significantly up-regulated bone associated genes included SMTN (osteoclast), COMP and COL10A1 (chondrocytes). No down-regulated marker genes represent mesoderm lineage was found. Taken together, transient inhibition of mitochondrial Akt1 signaling in the early differentiation stage facilitated ES cells

differentiation dominantly into the mesoderm, muscle, and bone, especially cardiomyocytes. Ectoderm lineage stayed mainly in progenitor status.

In contrast, no difference was found in progenitors from endoderm lineage, and only one of the lung cell marker genes was up-regulated. There even was an opposite expression of hepatic stem cell marker genes. The major limitation of bulk RNA screening is detecting highly expressed genes mainly. To verify if there are any specific cell populations in mDN group, in the next chapter, I used single-cell RNA sequencing (scRNA-seq) to identify the RNA profiles in each cell to annotate cell population in mDN group and GFP group.

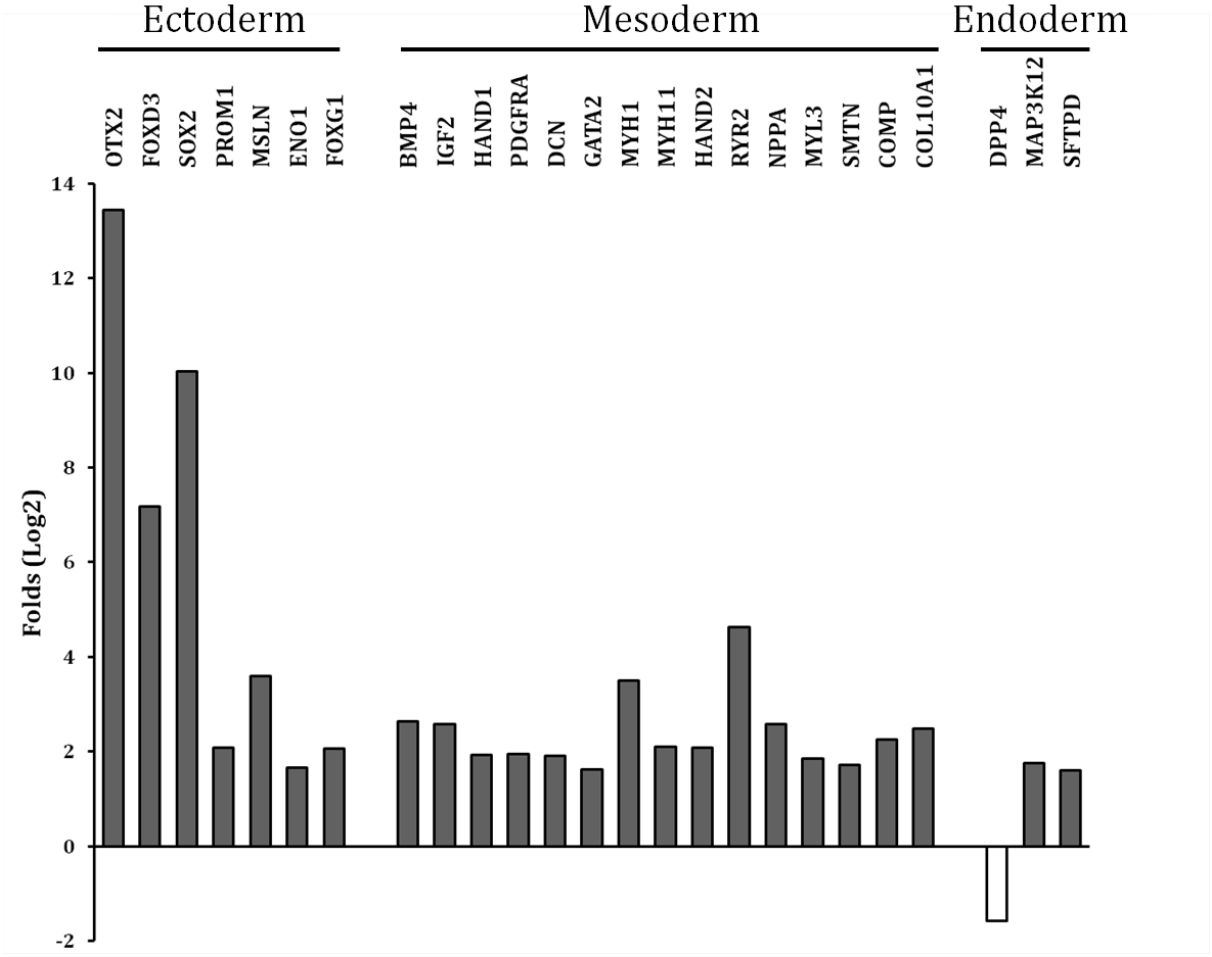

Figure 11. Fold change of lineage marker genes in Ad-mdnAkt-GFP transduced cells. RNA expression of cells transduced by Ad-mdnAkt-GFP and Ad-GFP on 21-day spontaneous differentiation compared by RT^2 Profiler™ PCR Array Human Cell Lineage Identification. Three independent samples were used, and technical triplicate was done in data collection.

Table 4. Lineage maker gene comparison

Lineage	Marker	Gene	Fold Regulation	p-value
Ectoderm	Ectoderm	OTX2	13.43	0.000*
		FOXD3	7.17	0.001*
		FGF5	-3.40	0.108
	Neuroectoderm	GBX2	2.21	0.079
	Neural progenitor	SOX2	10.03	0.000 *
		PROM1	2.08	0.011 *
	Limbal progenitor	MSLN	3.60	0.015 *
		ENO1	1.67	0.000 *
	Motor neuron progenitor	FOXG1	2.06	0.047 *
	Immature Neuron	DCX	1.61	0.169
	Gluotamergic neuron	SLC17A6	2.27	0.171
	Cholinergic neurons	CHAT	-2.85	0.088
	Oligodendorcyte	NKX2-2	-2.96	0.079
	Photoreceptor cells	RCVRN	1.54	0.257
Mesoderm	Mesoderm	BMP4	2.63	0.001*
		IGF2	2.58	0.001*
		HAND1	1.92	0.009*
		PDGFRA	1.94	0.008*
		DCN	1.91	0.001*
		GATA2	1.62	0.010*
		T	2.48	0.098
		MIXL1	2.17	0.147
	Skeletal uscle Cell	MYH1	3.50	0.008*
	Smooth muscle cell	MYH11	2.10	0.002*
	Early cardiomyocytes	HAND2	2.08	0.029*
	Cardiomyocytes	RYR2	4.63	0.000*
		NPPA	2.58	0.009*
		MYL3	1.85	0.014*
		MYH7	1.26	0.015*
	Osteoclast	CTSK	1.48	0.001*
		SMTN	1.71	0.001*
	Condrocyte	COMP	2.24	0.003*
		COL10A1	2.48	0.025*

Cutoff: fold change > 1.5 or < -1.5; * $p < 0.05$

Table 5. Lineage maker gene comparison (Continute)

Lineage	Marker	Gene	Fold Regulation	p-value
Endoderm	Endoderm	GATA1	1.22	0.030*
	Hepatic Stem Cell	DPP4	-1.58	0.005*
		MAP3K12	1.75	0.009*
		APOH	1.68	0.140*
	Hepatocyte	ALB	3.64	0.055
	Pancreatic islet cell	KRT19	1.28	0.005*
	Beta cell	INS	1.26	0.015*
	Lung cell	SFTPD	1.61	0.045*
		SFTPB	1.26	0.015*

Cutoff: fold change > 1.5 or < -1.5; * $p < 0.05$

Chapter 4

Analysis of the Effect of Mitochondrial Akt Signaling on Embryonic Stem Cell Differentiation by Single Cell RNA-seq

4.1 Introduction of Single Cell RNA Sequencing (scRNA-seq)

Application of scRNA-seq

Bulk RNA sequencing is useful to compare transcriptomics of samples from the same tissue from different species or to quantify expression of markers in disease studies. However, measuring gene expression in any cell populations with microarray or RNA sequencing is insufficient to demonstrate the true distribution of gene expression in each cell, especially when studying heterogeneous systems, such as early development or complex tissues; or to provide insights into the stochastic nature of gene expression. [76,77] Therefore, it is crucial to quantify gene expression in individual cells. In 2009, Tang *et al.* published the first protocol for single-cell sequencing and subsequently used this protocol to trace the derivation of mouse embryonic stem cells from the inner cell mass [76,78]. In the past few years, scRNA-seq has been used to unveil new biological questions associated with cell-specific changes in transcriptome, including cell types identification, gene regulatory mechanisms, the dynamics of development processes, heterogeneity of cell responses, and inference of gene regulatory networks across cells [76,77].

4.2 Materials and Methods

Single cell isolation

Washed the cells in 6-well vessels 1X PBS for three times and incubated at 37 ℃ for 15-20 minutes after adding 1 ml / well of collagenase[79]. Following removal of collagenase, 1 ml of Accutase per well was added and then incubated at 37 ℃ for 10 minutes. After collecting detached cells, the residual cells were detached by adding 0.5 ml/well of 0.25% Trypsin at 37℃ for 5 minutes and then neutralizing by the addition of 1 ml full-medium. The cell suspension was spun down at 300 g for 5 minutes and then resuspended with 4-9 ml basal medium.

Dead cells were removed using the dead cell removal kit (Milteneyi) and then resuspended in 0.04% BSA/PBS. Resuspended cells were filtered through a 40 µm nylon cell strainer twice and spun down pass-through suspension at 300 g for 5 minutes. The cell pellet was then resuspended in 0.04% BSA / PBS on ice. Cell number was counted with a hemocytometer twice after trypan blue staining to verify the percentage of cell viability and proper cell density for scRNA-seq. Proper cell density should be more than $1x10^6$ cells /mL. If not, cells were spun down and resuspended in the proper amount of 0.04 % BSA / PBS. Cell number was count at least twice for each sample (**Figure 12**).

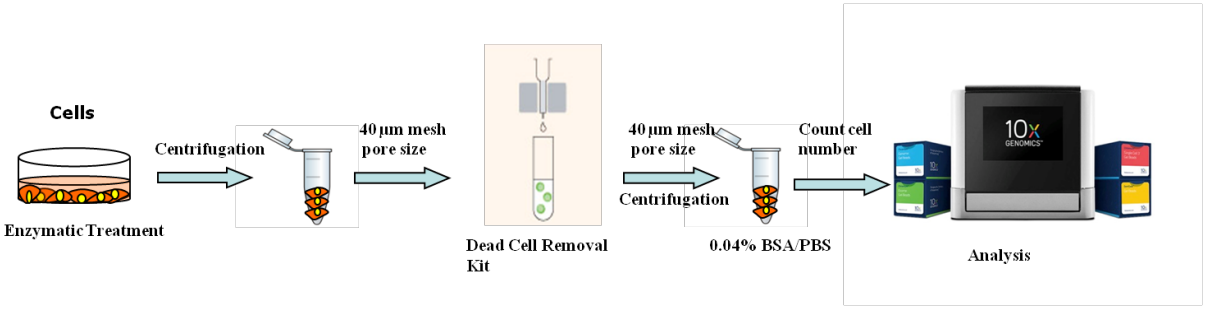

Figure 12. Sample preparation for scRNA-seq.

Single cell capture and cDNA library preparation

Using 10x Genomics chromium platform – GemCode to prepare Single cell cDNA libraries. Single-cell GEMs were generated by Single Cell 3' reagent v2 (**Figure 13**). This system captures one cell in barcoded nanolitre oil droplets and hosts each droplet in a hydrogel carrying barcoded primers. cDNA libraries are generated with specific barcode for each cell and gene [80] (**Figure 14**).

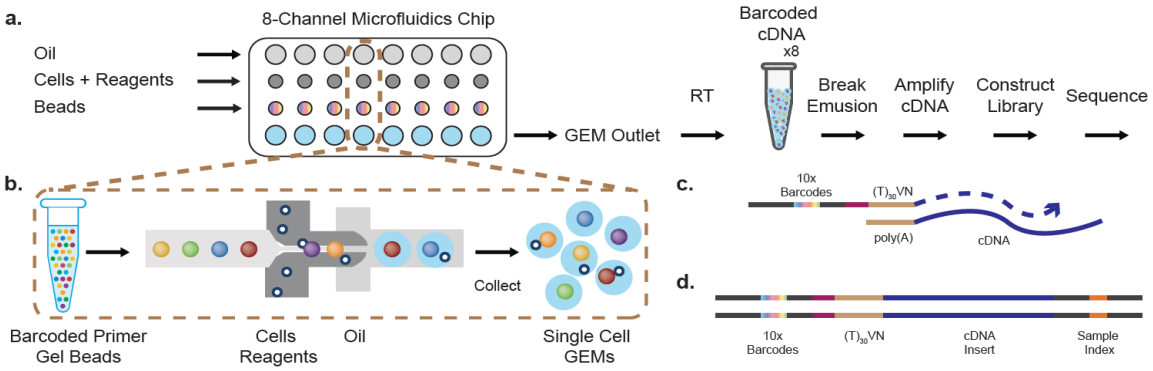

Figure 13. GemCode™ single cell platform from 10x Genomics. (a) After forming Gel bead in Emulsion (GEM), reverse transcription takes place inside each GEM, which is then pooled for cDNA amplification and library construction in bulk. (b) Formation of single-cell GEMs by adding oil, cells with RT reagents, and barcoded primer gel beads in the individual channel of the microfluidic chip. (c) Barcoded oligonucleotides consisted of Illumina adapters, 10x barcodes, UMIs, and oligo dTs, contained inside GEMs. (d) Final library molecules allow pooling and sequencing of multiple libraries [81] (https://www.10xgenomics.com/).

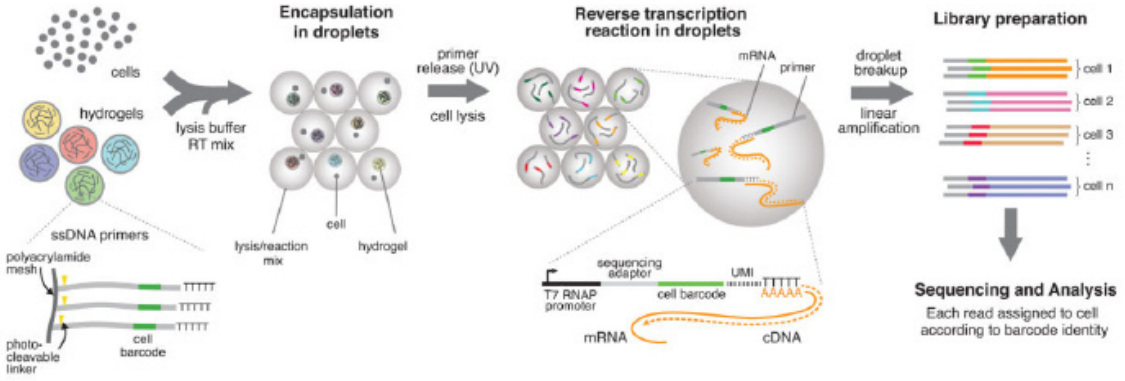

Figure 14. Single cell cDNA library preparation. Cells are captured in nanolitre oil droplet, one cell per droplet, ideally. Then each droplet is hosted in a hydrogel carrying barcode primers to generate cDNA library [80].

RNA sequencing

Sequencing is done by Illumina HiSeq 2500 with a dual mode system for either high output or rapid mode sequencing.

Analysis of single-cell RNA sequencing data

The first step in primary data analysis is to inspect the read quality and trim low-quality bases following by mapping to reference genome, checking mapping quality, and quantifying the expression level of each gene for each cell. The next step is to check cell gene expression qualities and normalization of the gene expression. Finally, apply these data sets to clustering, differential expression analysis or functional annotation [76,77] (**Figure 15**).

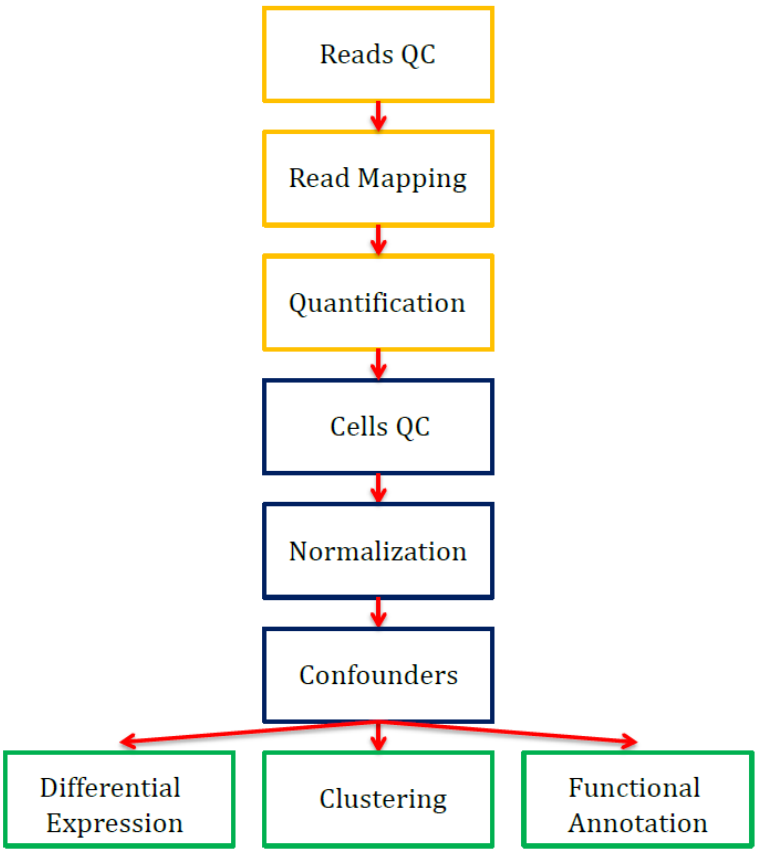

Figure 15. Flowchart of scRNA-seq analysis [77].

Gene-cell matrix generation

The raw base call (BCL) files from the Illumina sequencer were processed with Cell Ranger to generate gene-cell matrices after reading quality control. Cell Ranger is a set of analysis pipelines, including cellranger mkfastq, cellranger count, cellranger aggr and cell ranger reanalyze. In this dissertation, Cell Ranger version 2.0.0 was used for shallow sequencing analysis and Cell Ranger version 2.1.1 was used for deep sequencing analysis. Cellranger mkfastq was applied to demultiplexed BCL files into FASTQ files as primary analysis. A secondary analysis was performed with cellranger count and cellranger aggr. Cellranger count extracted the 10X cellular barcode sequence and unique molecular identifiers (UMI) from FASTQ files and aligned reads via STAR (Spliced Transcripts Alignment to a Reference) to genome and transcriptome simultaneously (**Figure 13**). Human GRCh38 was pre-built as reference and ENSEMBL genomes and gene annotation were used for annotation. 10X cellular barcode was a 16bp unique sequence to each gel beads and told us from which cell the transcript is. UMIs were short (10bp) random barcodes added to transcripts during reverse transcription, and therefore enable accurate transcript counts in each cell. According to 10x cellular barcodes and UMIs, cell barcode filtering and duplicates marking were done, and filtered gene-cell matrices were generated. Pooling of gene-cell matrices from different samples was done by cellranger aggr for batch effect analysis or comparison between different conditions. Therefore, the matrices of deep sequencing data of GFP1 and mDN1 were combined then depth normalization was done.

The quality of the gene-cell matrix was evaluated by ranked barcode plot (**Figure 16** and **Figure 20**). Ranked barcode plot was the sum of UMI counts for each barcode. A drop-

off was located at the selecting barcodes with total UMI counts over 10% of the 99th percentile of the expected recovered cells. A steep drop-off indicated the good separation of the barcodes associated with cells and empty partitions and implied the good quality of gene-cell matrix. Additional criteria of good quality included Q30 bases in RNA read over 70% and read mapped confidently to transcriptome over 30%. All gene-cell matrices from shallow or deep sequencing showed good qualities according to the above criteria [77].

GFP1

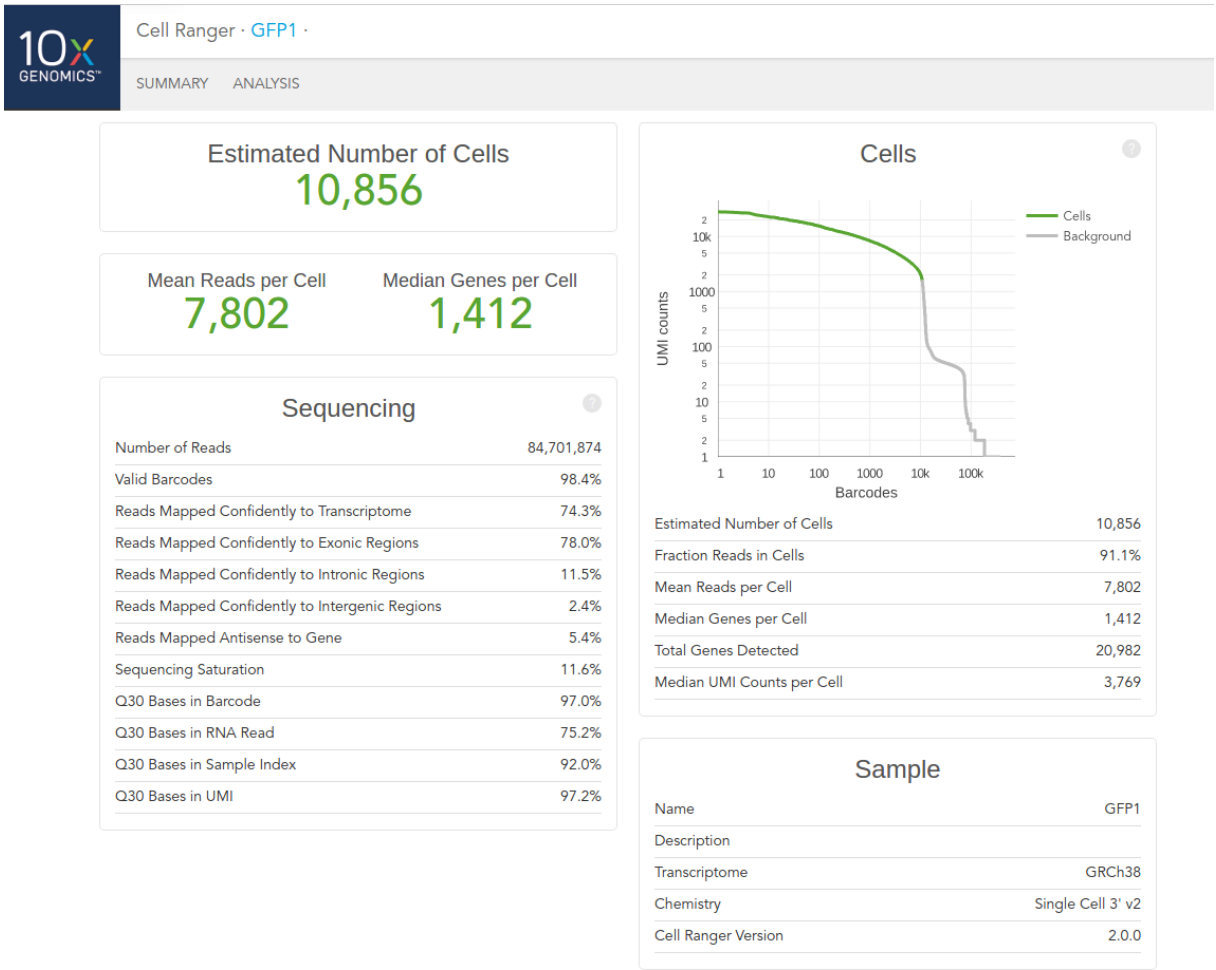

GFP2

Cell Ranger · GFP2 ·

SUMMARY ANALYSIS

Estimated Number of Cells

16,750

Mean Reads per Cell	Median Genes per Cell
5,093	1,034

Sequencing

Number of Reads	85,314,736
Valid Barcodes	98.5%
Reads Mapped Confidently to Transcriptome	74.7%
Reads Mapped Confidently to Exonic Regions	78.3%
Reads Mapped Confidently to Intronic Regions	10.6%
Reads Mapped Confidently to Intergenic Regions	2.3%
Reads Mapped Antisense to Gene	5.5%
Sequencing Saturation	11.3%
Q30 Bases in Barcode	96.9%
Q30 Bases in RNA Read	73.1%
Q30 Bases in Sample Index	92.7%
Q30 Bases in UMI	97.2%

Cells

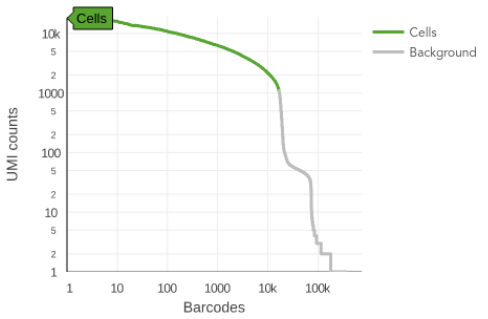

Estimated Number of Cells	16,750
Fraction Reads in Cells	90.8%
Mean Reads per Cell	5,093
Median Genes per Cell	1,034
Total Genes Detected	20,826
Median UMI Counts per Cell	2,493

Sample

Name	GFP2
Description	
Transcriptome	GRCh38
Chemistry	Single Cell 3' v2
Cell Ranger Version	2.0.0

mDN1

Cell Ranger · mDN1 ·

SUMMARY ANALYSIS

Estimated Number of Cells

18,026

Mean Reads per Cell	Median Genes per Cell
5,119	1,002

Sequencing

Number of Reads	92,277,963
Valid Barcodes	98.4%
Reads Mapped Confidently to Transcriptome	72.6%
Reads Mapped Confidently to Exonic Regions	76.3%
Reads Mapped Confidently to Intronic Regions	12.6%
Reads Mapped Confidently to Intergenic Regions	2.5%
Reads Mapped Antisense to Gene	5.1%
Sequencing Saturation	11.2%
Q30 Bases in Barcode	97.0%
Q30 Bases in RNA Read	73.7%
Q30 Bases in Sample Index	91.5%
Q30 Bases in UMI	97.2%

Cells

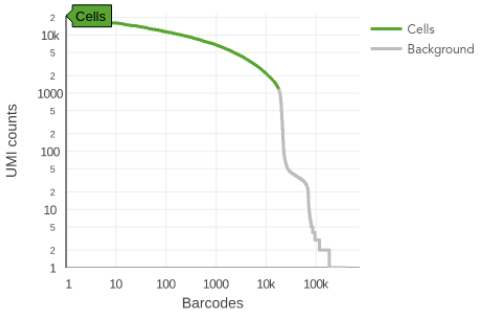

Estimated Number of Cells	18,026
Fraction Reads in Cells	91.8%
Mean Reads per Cell	5,119
Median Genes per Cell	1,002
Total Genes Detected	21,193
Median UMI Counts per Cell	2,337

Sample

Name	mDN1
Description	
Transcriptome	GRCh38
Chemistry	Single Cell 3' v2
Cell Ranger Version	2.0.0

mDN2

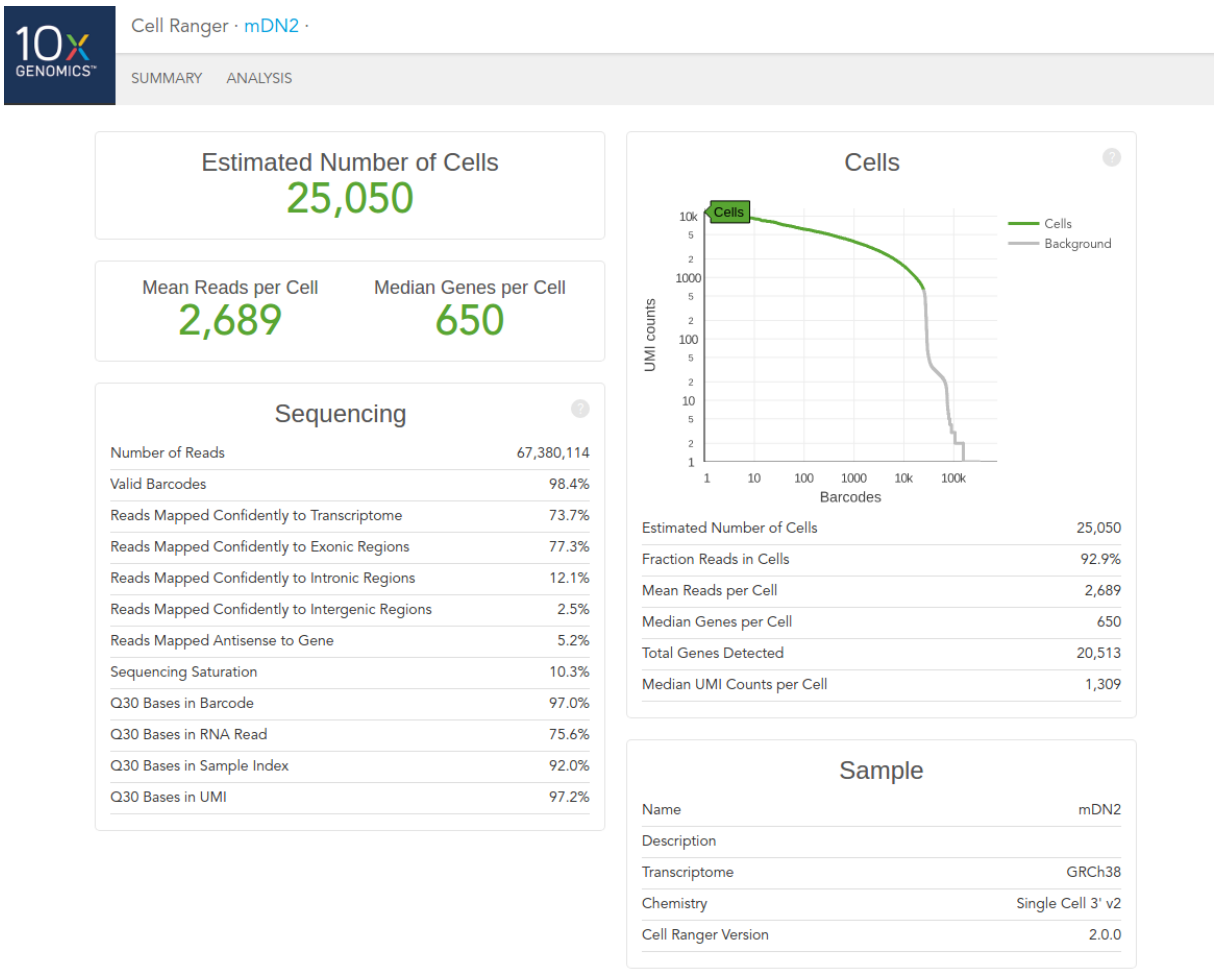

Figure 16. Ranked barcode plot for quality control evaluation in shallow scRNA-seq. The qualities of sequencing in four samples were good. The valid barcodes were over 98%. GFP1 and GFP2 represented two independent samples; each sample represented a pooling of sextuplicate from Ad-GFP transduced hESCs. mDN1 and mDN2 represented two independent samples; each sample represented a pooling of sextuplicate from Ad-mdnAkt1/GFP transduced hESCs.

Downstream analysis - Clustering

To identify subpopulations of cells across multiple data sets and downstream comparative analysis, the R toolkit Seurat version 2.0.1 was applied. Seurat is an R package designed for quality control, analysis, and exploration of scRNA-seq data.[82,83] The cells were filtered out by two strategies to control cell quality for downstream analysis. One strategy is to visualize genes and molecule counts and exclude cells with a clear outlier number of genes detected as potential multiplets. The other one is the percentage of mitochondrial genes presents (**Figure 17**).

In Seurat, t-distributed stochastic neighbor embedding (t-SNE, non-linear dimensional reduction) was plotted to visualize heterogeneity cell types within each group. (**Figure 19**, **Figure 22**) Then the biomarkers that defined clusters via differential expression were output for downstream analysis. At the same, top 20 marker genes in each cluster were used to plot heatmap (**Figure 18**).

GFP1

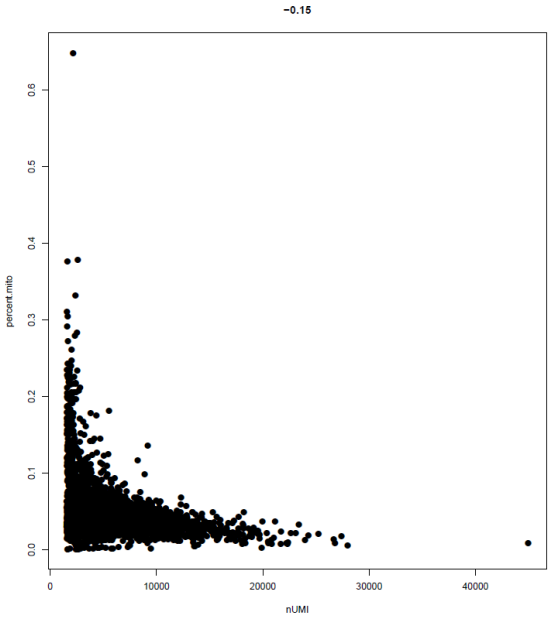
−0.15
percent.mito
nUMI
0.0
0.1
0.2
0.3
0.4
0.5
0.6
0
10000
20000
30000
40000

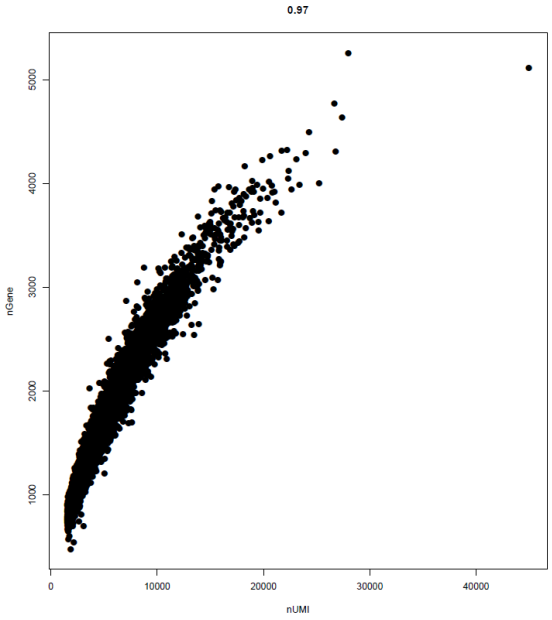
0.97
nGene
nUMI
1000
2000
3000
4000
5000
0
10000
20000
30000
40000

GFP2

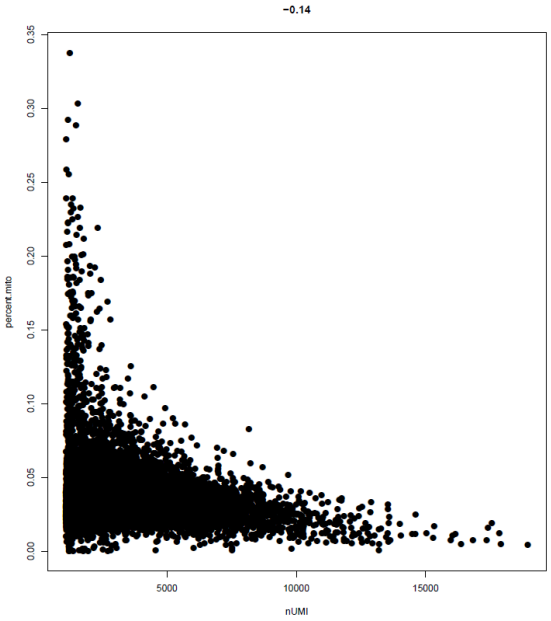
−0.14
percent.mito
nUMI
0.00
0.05
0.10
0.15
0.20
0.25
0.30
0.35
5000
10000
15000

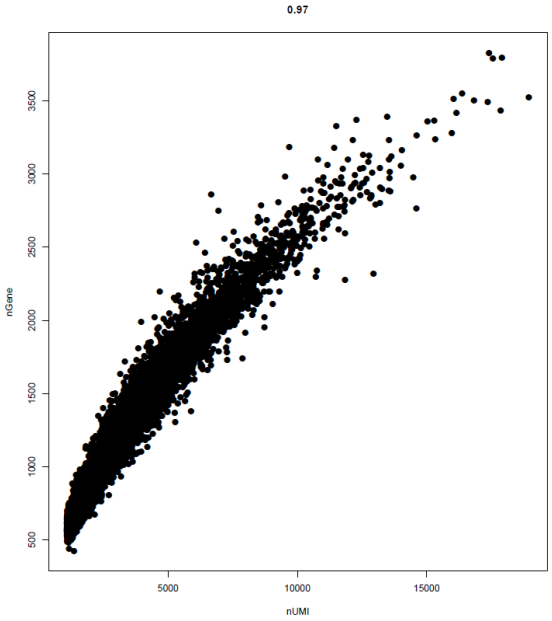
0.97
nGene
nUMI
500
1000
1500
2000
2500
3000
3500
5000
10000
15000

mDN1

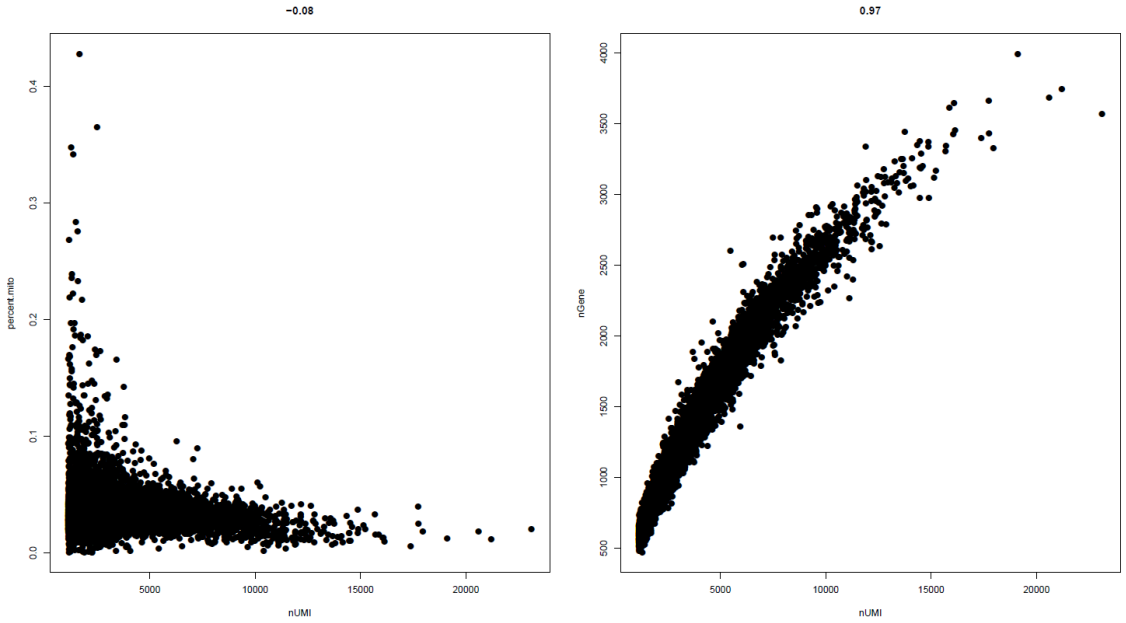

mDN2

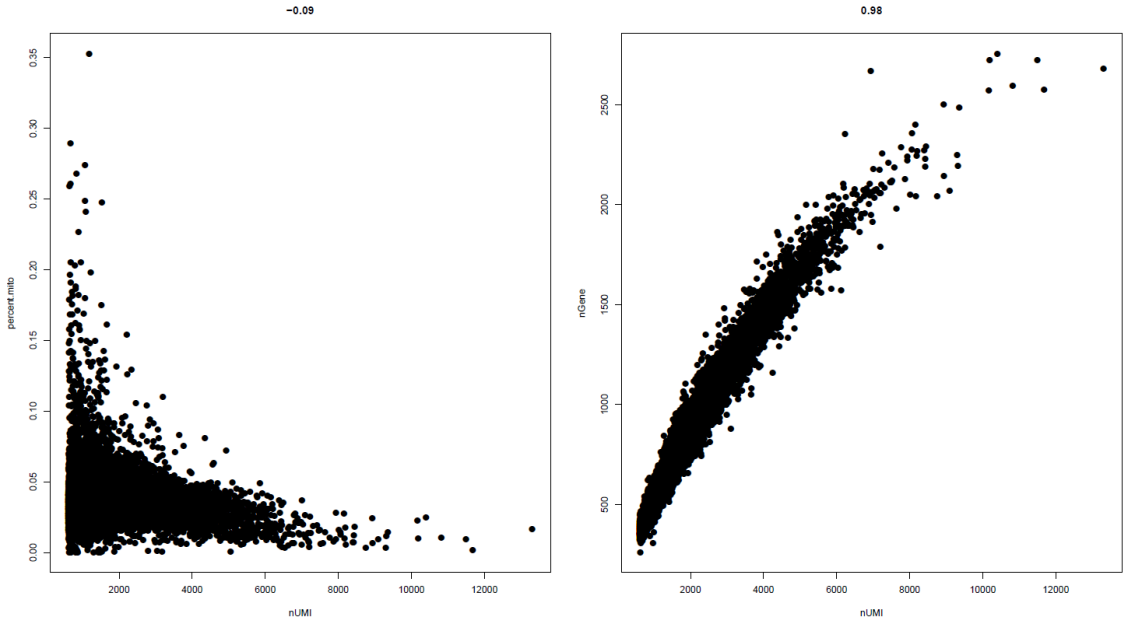

Figure 17. Quality control of cells in shallow scRNA-seq. To exclude dead cells and multiple cells in the same droplet (sharing same UMI), the percentage of mitochondria gene in each cell and the number of genes in each cell was analyzed. For each sample, the left plot is the percentage of mitochondria genes to the cell number (nUMI), and the right plot is the number of genes (nGene) to nUMI. The dead or dying cells express higher mitochondria genes for apoptosis, so the cutoff value was set as 0.1. The higher number of genes in each cell implies that more than one cell was capsulated in the same droplet. Therefore, the cutoff value was set as 4000 genes per cell to include as many cells as possible. GFP1, GFP2: Transduction by Ad-GFP viral vector from different batches; mDN1, mDN2: Transduction by Ad-mdnAkt-GFP viral vector from different batches.

GFP1

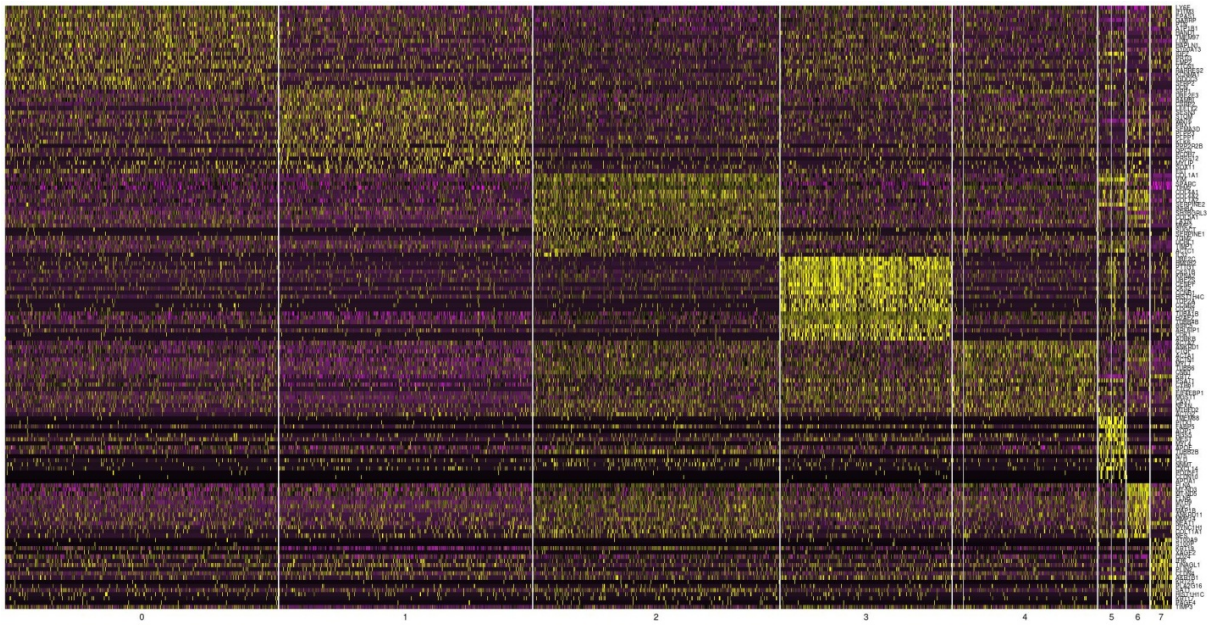

GFP2

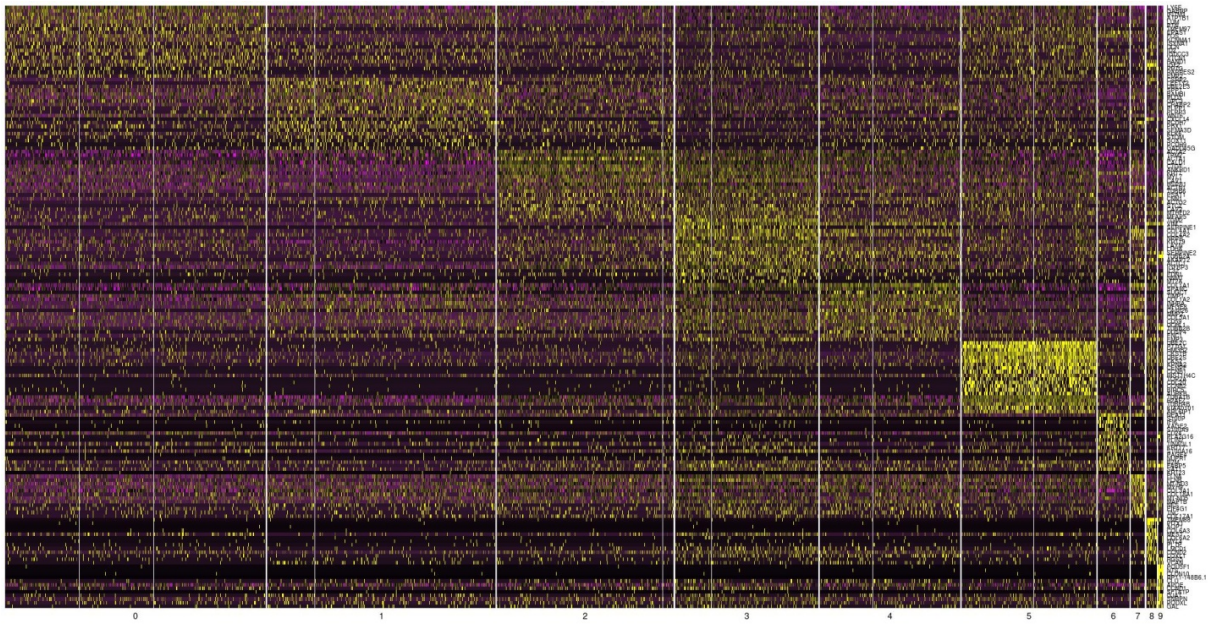

mDN1

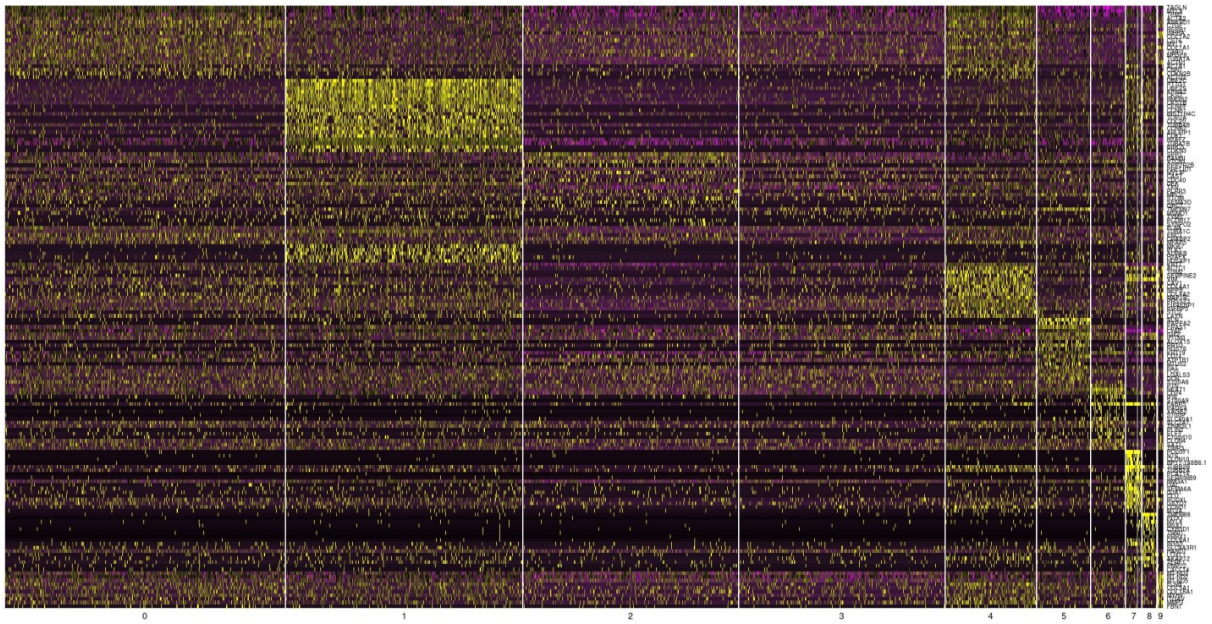

mDN2

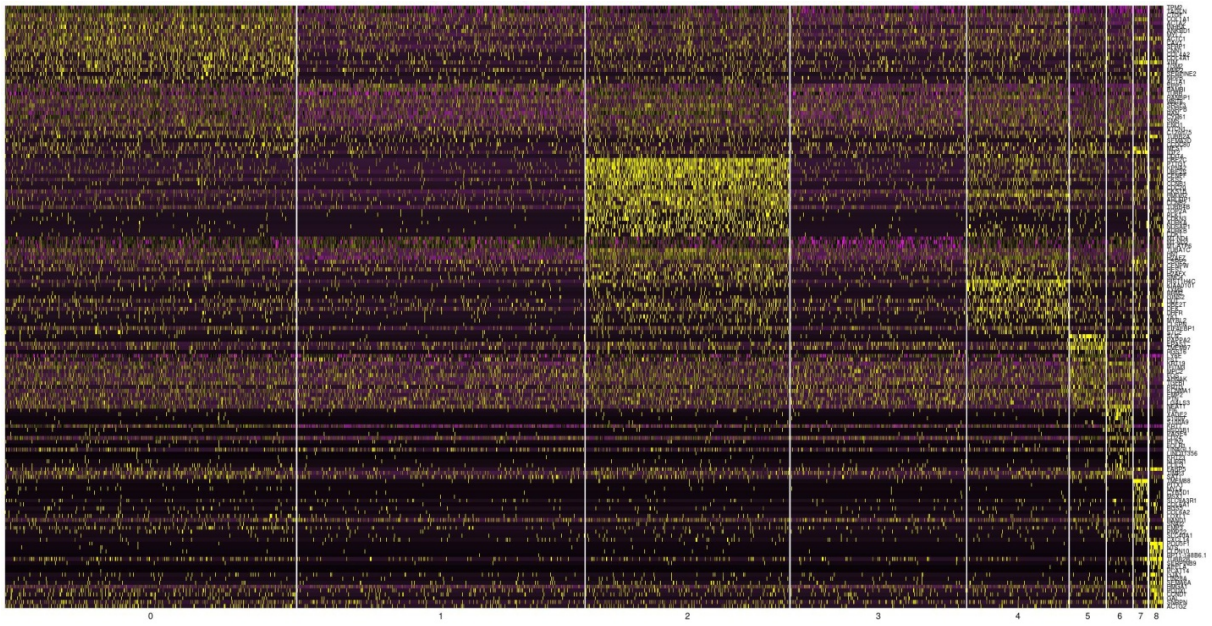

Figure 18. Top20 gene expression HeatMap of each cluster in shallow scRNA-seq. The heatmaps were generated by top20 expressed genes in each cluster. The clusters need to be annotated by downstream analysis, such GO term enrichment analysis. GFP1, GFP2: transduction by Ad-GFP viral vector; mDN1, mDN2: transduction by Ad-mdnAkt-GFP viral vector.

Annotation of clusters

The Biological process of gene ontology enrichment analysis (GO enrichment analysis) and PANTHER classification system[84] was used to annotate clusters by cluster biomarker genes. Deep sequencing data were analyzed by WebGestal GSAT [85-87], Pathway Commons, WikiPathways, and Ingenuity Pathway Analysis (IPA, QIAGEN Inc., https://www.qiagenbioinformatics.com/products/ingenuity-pathway-analysi).

4.3 Shallow Sequencing of scRNA-Seq

In shallow sequencing, the sequencing saturation was around 11% in the GFP group and 10% in mDN group, and all samples showed good quality. Most clusters in the t-SNE plot were closed and overlapped one another. When performing annotation by GO enrichment analysis, it was difficult to get a clear annotation of each cluster either in the GFP group or mDN group (**Figure 19**). Because the cell numbers in each sample were higher than 10,000, the mean gene number per cell was lower, around 600 to 1400 (**Figure 16**). The low gene number per cell was not enough for accurate cluster annotation because of high heterogeneity in these samples. In line with this, mixed cell types were collected in one cluster, and the neighboring clusters were overlapped to each other. Also, the difference in clusters between the GFP and the mDN cells were not clearly defined. For that reason, deep sequencing was done to get higher sequencing saturation for definite clustering.

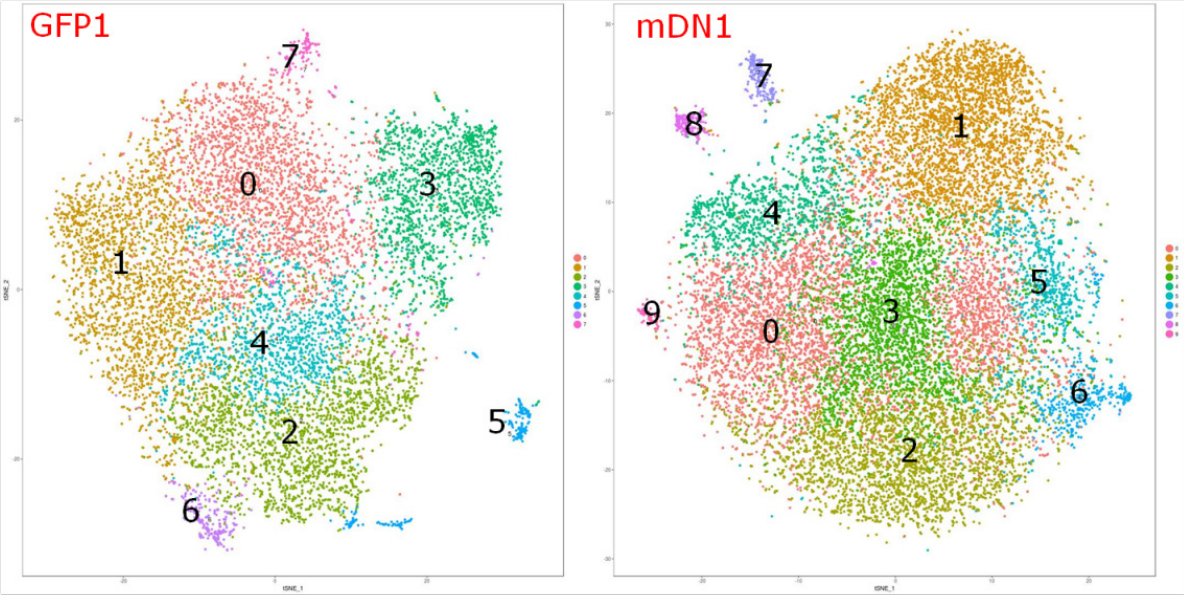

Cluster	GFP1	mDN1
0		Mesenchyme migration
1	Cardiovascular system	Cell cycle
2	Endodermal cell differentiation	Cardiac & striated muscle
3	Cell cycle	Mesenchyme migration
4	Cartilage/heart	Angiogenesis, neurogensis,
5	Endodermal	Vasculacture development, blood vessel morphogenesis
6	Viral transcription	Cardiamyocyte (Troponin-t)
7	Epithelial?	Endothelial cell migration Endoderm differentiation
8	X	Endothelial cell differentiation
9	X	Viral transcription

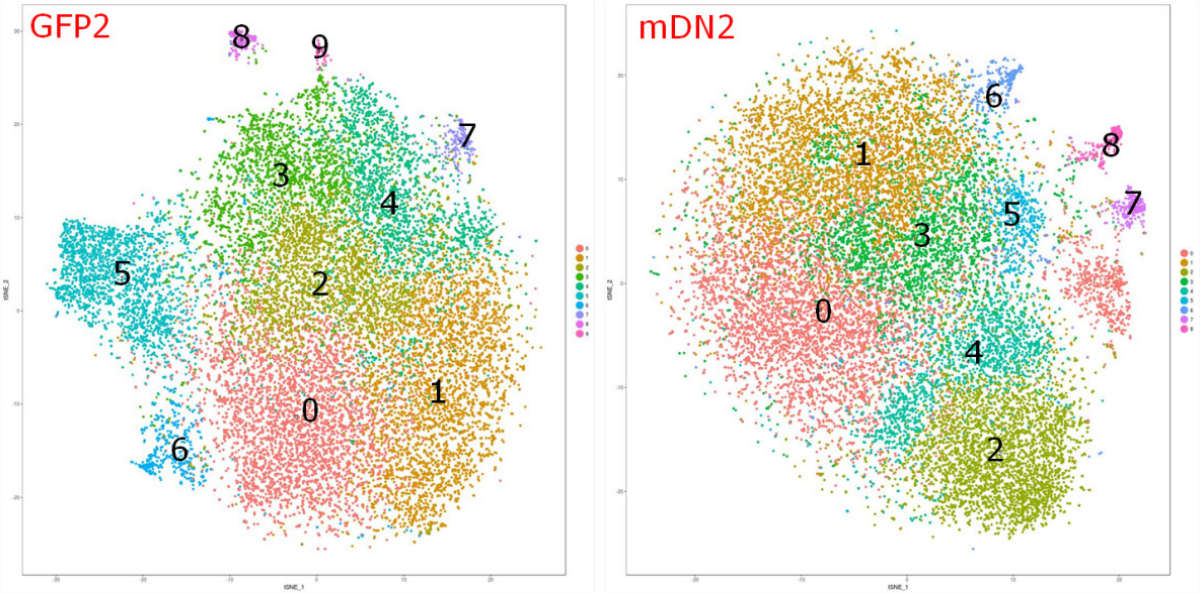

Cluser	GFP2	mDN2
0	Mesenchyme migration	Mesenchyme migration
1	Blood vessel, epithelium differentiation	Muscle development
2	Cartilage, muscle, blood vessel	
3	Epithelium development	
4	Endoderm, epithelium development	
5	Mitotic,	
6	Cardiac ventricle development	
7		Endothelial cell differentiation
8		
9		X

Figure 19. Cluster annotation by GO enrichment analysis in shallow scRNA-seq. Using GO enrichment analysis to annotate clusters with representative genes in each cluster. Some clusters cannot be annotated properly. Cluster numbers and colors in each sample were generated by software automatically. The same cluster number from different samples did not represent the same cell cluster.

4.4 Deep Sequencing of scRNA-Seq

The saturation of deep sequencing was 21.3% in GFP1 and 27.4 % in mDN1. Both were two-folds over shallow sequencing and showed good quality. GFP1 and mDN1 data were analyzed individually or pooled together by Cell Ranger and R package-Seurat. To validate the similar clusters between GFP1 and mDN1, differentially expressed genes of each cluster were analyzed by (1) top5 canonical signaling pathway (**Figure 6**) and physiological system development and function (**Table 8**) analyzed through the use of IPA (**Figure 23**), (2) biological process of GO-Slim enrichment analysis, including trilineage development and system development (**Figure 22** & **Figure 24**); (3) Pathway Commons (**Table 9**); and (4) GO enrichment analysis.

A.

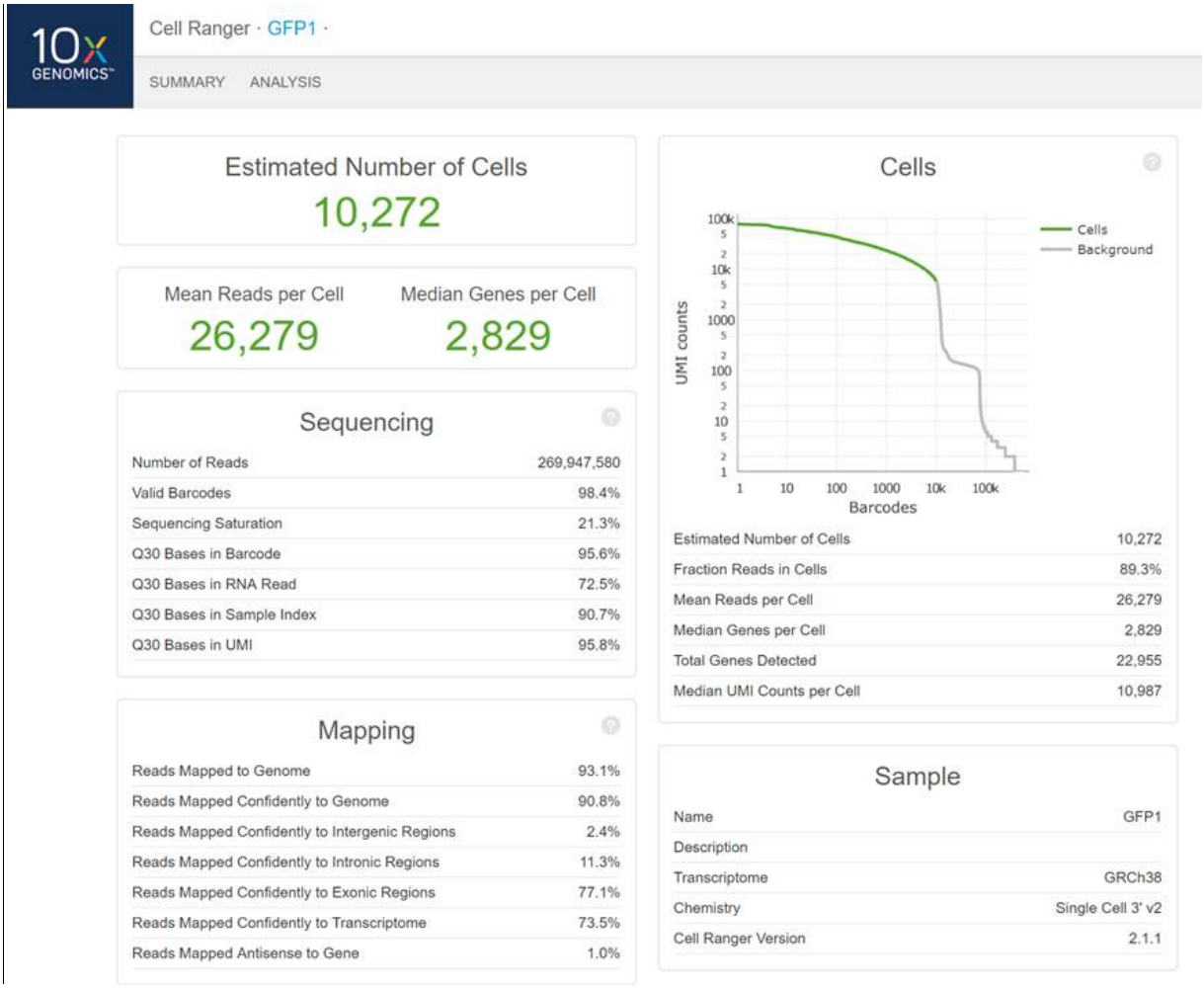
10x GENOMICS
Cell Ranger · GFP1 ·
SUMMARY ANALYSIS
Estimated Number of Cells
10,272
Mean Reads per Cell
26,279
Median Genes per Cell
2,829
Sequencing
Number of Reads 269,947,580
Valid Barcodes 98.4%
Sequencing Saturation 21.3%
Q30 Bases in Barcode 95.6%
Q30 Bases in RNA Read 72.5%
Q30 Bases in Sample Index 90.7%
Q30 Bases in UMI 95.8%
Mapping
Reads Mapped to Genome 93.1%
Reads Mapped Confidently to Genome 90.8%
Reads Mapped Confidently to Intergenic Regions 2.4%
Reads Mapped Confidently to Intronic Regions 11.3%
Reads Mapped Confidently to Exonic Regions 77.1%
Reads Mapped Confidently to Transcriptome 73.5%
Reads Mapped Antisense to Gene 1.0%
Cells
UMI counts
Barcodes
Cells
Background
Estimated Number of Cells 10,272
Fraction Reads in Cells 89.3%
Mean Reads per Cell 26,279
Median Genes per Cell 2,829
Total Genes Detected 22,955
Median UMI Counts per Cell 10,987
Sample
Name GFP1
Description
Transcriptome GRCh38
Chemistry Single Cell 3' v2
Cell Ranger Version 2.1.1

B.

10x GENOMICS™ Cell Ranger · mDN1 ·

SUMMARY ANALYSIS

Estimated Number of Cells
16,049

Mean Reads per Cell
29,106

Median Genes per Cell
2,737

Sequencing

Number of Reads	467,136,522
Valid Barcodes	98.4%
Reads Mapped Confidently to Transcriptome	71.9%
Reads Mapped Confidently to Exonic Regions	75.5%
Reads Mapped Confidently to Intronic Regions	12.4%
Reads Mapped Confidently to Intergenic Regions	2.5%
Reads Mapped Antisense to Gene	5.1%
Sequencing Saturation	27.4%
Q30 Bases in Barcode	95.4%
Q30 Bases in RNA Read	71.1%
Q30 Bases in Sample Index	90.5%
Q30 Bases in UMI	95.6%

Cells

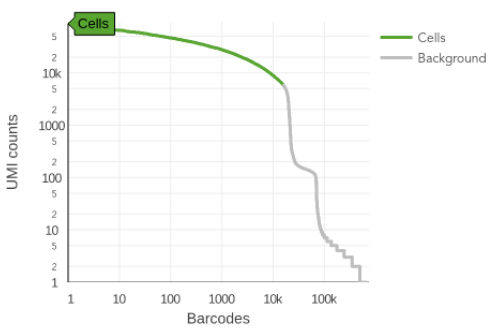

Estimated Number of Cells	16,049
Fraction Reads in Cells	87.7%
Mean Reads per Cell	29,106
Median Genes per Cell	2,737
Total Genes Detected	23,933
Median UMI Counts per Cell	10,463

Sample

Name	mDN1
Description	
Transcriptome	GRCh38
Chemistry	Single Cell 3' v2

C.

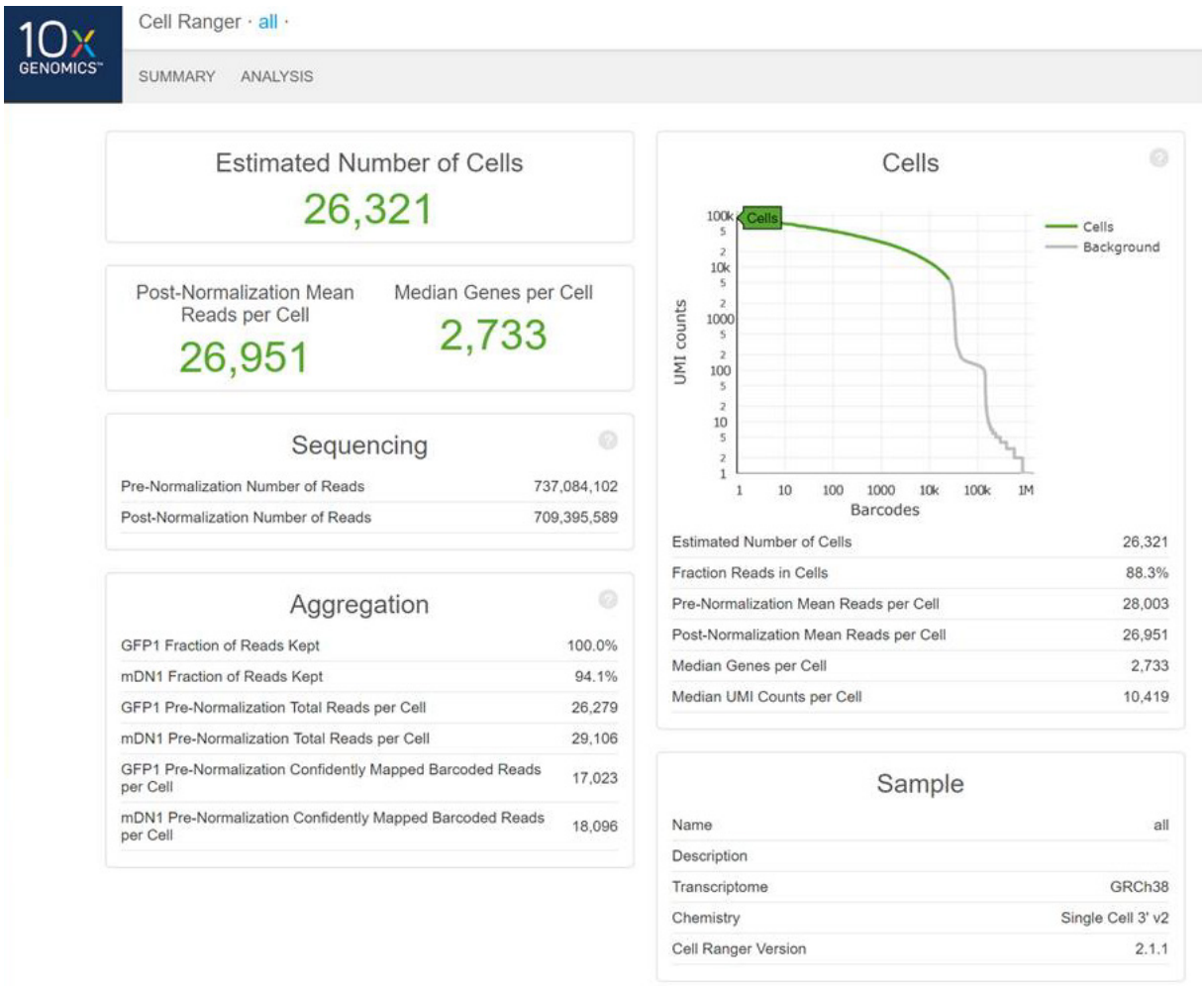

Figure 20. Ranked barcode plot for quality control evaluation in deep scRNA-seq. Qualities of deep sequencing from (A) GFP1, (B) mDN1 and (C) all (pooling of GFP1 and mDN1) were good.

Comparing the identity of each cell cluster in the GFP and mDN group

To explore the effect of mitochondrial Akt1 signaling in differentiation, the first step was to identify similar clusters in GFP1 and mDN1. Comparing the signaling pathways and physiological system development by IPA (**Table 6** & **Table 8**) and Pathway Commons showed that five clusters were similar between GFP1 and mDN1, including cluster 0, 1, 2, 4, 5 of GFP1 *versus* cluster 2, 0, 3, 1, 6 of mDN1 correspondingly (**Figure 23** and **Figure 21**). On the other hand, the cluster 3 and 6 of GFP1 and cluster 4, 5, and 7 of mDN1 were different.

Intriguingly, using different methods to compare similar clusters revealed that they were in fact, distinct. For example, validation of similar clusters with the trilineage development of GO-slim biological process showed that cluster 0 of GFP1 and cluster 2 of mDN1 were different. The cluster 0 of GFP1 was mesoderm, but cluster 2 of mDN1 was not annotated to any lineage (**Figure 24** A). Subsequent validation with system development of GO-slim biological process showed that cluster 4 of GFP1 and cluster 1 of mDN1 were different. The cluster 4 of GFP1 was nervous development, yet no system development was identified in cluster 1 of mDN1 (**Figure 24** B). Furthermore, comparing the signaling pathways of the similar clusters by different methods, showed differences between GFP1 and mDN1 samples (**Table 9**).

Table 6. Top5 canonical pathways generated by IPA

Cluster	GFP1	mDN1
0	Cholesterol Biosynthesis I	Wnt/-catenin Signaling
	Cholesterol Biosynthesis II (via 24,25-dihydrolanosterol)	Human Embryonic Stem Cell Pluripotency
	Cholesterol Biosynthesis III (via Desmosterol)	Glioblastoma Multiforme Signaling
	Superpathway of Cholesterol Biosynthesis	Hepatic Fibrosis / Hepatic Stellate Cell Activation
	Oncostatin M Signaling	PCP pathway
1	Regulation of the Epithelial-Mesenchymal Transition Pathway	Hepatic Fibrosis / Hepatic Stellate Cell Activation
	PCP pathway	ILK Signaling
	Human Embryonic Stem Cell Pluripotency	Caveolar-mediated Endocytosis Signaling
	Tight Junction Signaling	Agranulocyte Adhesion and Diapedesis
	Wnt/-catenin Signaling	Leukocyte Extravasation Signaling
2	ILK Signaling	Cholesterol Biosynthesis I
	Epithelial Adherens Junction Signaling	Cholesterol Biosynthesis II (via 24,25-dihydrolanosterol)
	Remodeling of Epithelial Adherens Junctions	Cholesterol Biosynthesis III (via Desmosterol)
	Integrin Signaling	Superpathway of Cholesterol Biosynthesis
	RhoA Signaling	Epoxysqualene Biosynthesis
3	Glutamate Removal from Folates	ILK Signaling
	Inhibition of Matrix Metalloproteases	Epithelial Adherens Junction Signaling
	Hepatic Fibrosis / Hepatic Stellate Cell Activation	Integrin Signaling
	PCP pathway	Caveolar-mediated Endocytosis Signaling
	Glioma Invasiveness Signaling	RhoA Signaling
4	Germ Cell-Sertoli Cell Junction Signaling	Cdc42 Signaling
	ILK Signaling	OX40 Signaling Pathway
	Caveolar-mediated Endocytosis Signaling	Caveolar-mediated Endocytosis Signaling
	Epithelial Adherens Junction Signaling	Polyamine Regulation in Colon Cancer
	Integrin Signaling	Neuroinflammation Signaling Pathway
5	Mitotic Roles of Polo-Like Kinase	Cell Cycle Control of Chromosomal Replication
	Cell Cycle: G2/M DNA Damage Checkpoint Regulation	Cell Cycle: G2/M DNA Damage Checkpoint Regulation
	ATM Signaling	Pyrimidine Deoxyribonucleotides De Novo Biosynthesis I
	Cell Cycle Control of Chromosomal Replication	Role of CHK Proteins in Cell Cycle Checkpoint Control
	RAN Signaling	Mismatch Repair in Eukaryotes
6	EIF2 Signaling 8	Cell Cycle: G2/M DNA Damage Checkpoint Regulation
	Glycolysis I	Mitotic Roles of Polo-Like Kinase
	Superpathway of Serine and Glycine Biosynthesis I	ATM Signaling
	Sirtuin Signaling Pathway	Oxidized GTP and dGTP Detoxification
	Serine Biosynthesis	RAN Signaling

Table 7. Top5 canonical pathways generated by IPA (Continue)

Cluster	GFP1	mDN1
7		Superpathway of Cholesterol Biosynthesis Hepatic Fibrosis / Hepatic Stellate Cell Activation Superpathway of Geranylgeranyldiphosphate Biosynthesis I (via Mevalonate) EIF2 Signaling ILK Signaling

Table 8. Physiological system development and function by IPA

Cluster	GFP	mDN1
0	Embryonic Development Organ Development Organismal Development Skeletal and Muscular System Development and Function Tissue Development	Digestive System Development and Function Embryonic Development Hair and Skin Development and Function Organ Development Organismal Development
1	Digestive System Development and Function Embryonic Development Hair and Skin Development and Function Organ Development Organismal Development	Cardiovascular System Development and Function Embryonic Development Hair and Skin Development and Function Organ Development Organismal Development
2	Cardiovascular System Development and Function Organismal Development Tissue Development Embryonic Development Hair and Skin Development and Function	Embryonic Development Hair and Skin Development and Function Organ Development Organismal Development Tissue Development
3	Hematological System Development and Function Humoral Immune Response Immune Cell Trafficking Connective Tissue Development and Function Tissue Development	Cardiovascular System Development and Function Organismal Development Tissue Development Skeletal and Muscular System Development and Function Embryonic Development
4	Cardiovascular System Development and Function Organismal Development Connective Tissue Development and Function Hematological System Development and Function Hematopoiesis	Organismal Survival Cardiovascular System Development and Function Organismal Development Skeletal and Muscular System Development and Function Embryonic Development
5		
6	Cardiovascular System Development and Function Organismal Development Tissue Development Embryonic Development Organismal Survival	Lymphoid Tissue Structure and Development Tissue Development Hair and Skin Development and Function
7		Organismal Survival Cardiovascular System Development and Function Organismal Development Tissue Development Connective Tissue Development and Function

Figure 21. Hierarchy heatmap of the canonical pathways in each cluster generated through IPA. Comparing of clusters according to the canonical pathway showed that GFP-1 and mDN-0; GFP-0 and mDN-2; GFP-6 and mDN-7; GFP-5 and mDN-6; and GFP-4 and mDN-1 were similar. GFP-0~6: GFP1-cluster 0~6; mDN-0~7: mDN-cluster 0~7.

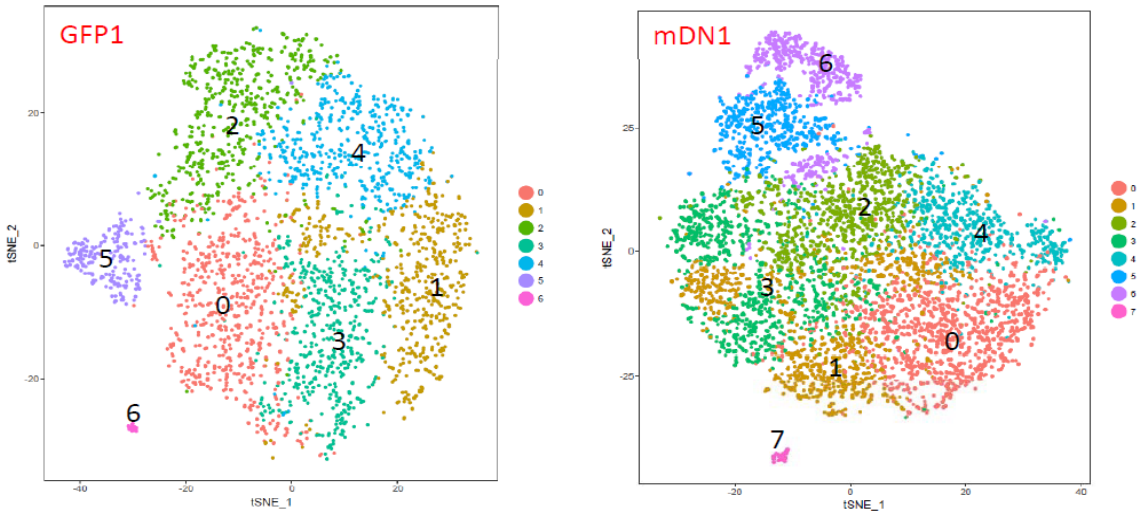

Cluster	GFP1	mDN1
0	Mesoderm System - nervous	Ectoderm, Mesoderm System - nervous
1	Ectoderm, Mesoderm System - Nervous	Ectoderm, Mesoderm
2	Mesoderm System - heart, muscle organ, nervous	System - nervous, skeletal
3	Embryo, Ectoderm, Endoderm System - angiogenesis, nervous	Mesoderm System - muscle organ, nervous
4	Ecoderm, Mesoderm System - nervous	Mesoderm, Digestive system System - angiogenesis, nervous
5	Embryo System - nervous, skeletal	Ectoderm System - nervous
6	Ectoderm, Mesoderm System - angiogenesis, heart, nervous, skeletal	Embryo System - nervous
7		Ecoderm, Mesoderm System - angiogenesis, heart, nervous, skeletal

Figure 22. Cluster annotation of deep scRNA-seq by GO-slim enrichment analysis. All representative genes in each cluster were used for annotation. The biological development process was listed in the table.

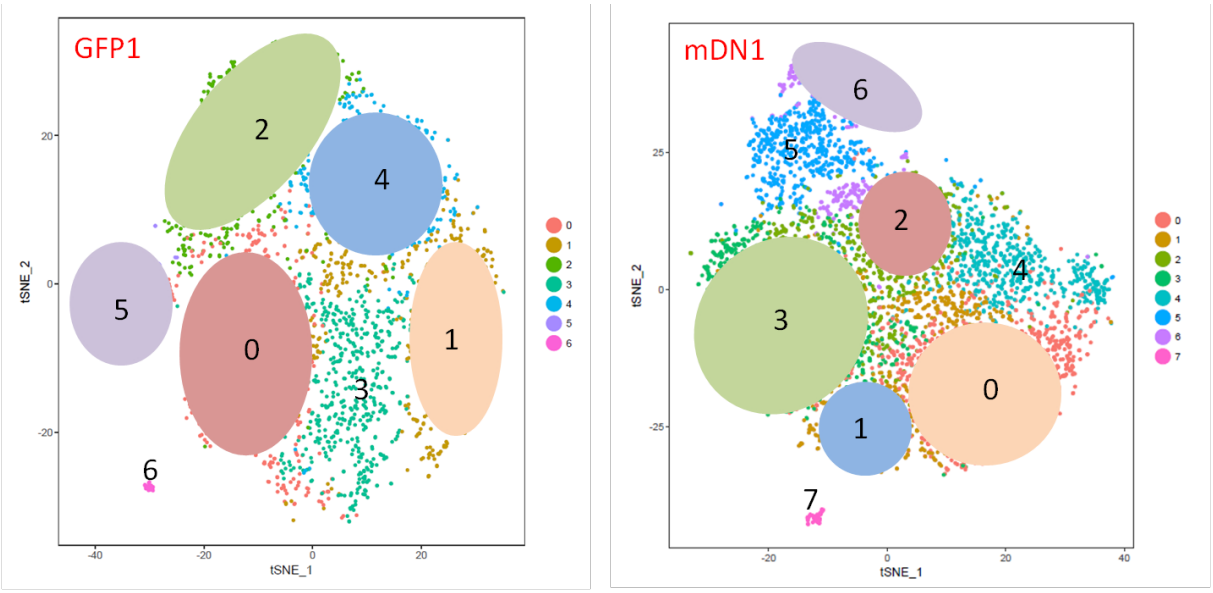

Figure 23. Comparing the identities of cell clusters from deep scRNA-seq. The "top5 canonical pathways" and "physiological system development and function" of each cluster are analyzed by Ingenuity Pathway Analysis (IPA) to locate the same cluster in the GFP and mDN group. Similar cell clusters across two samples are labeled with the same color in this plot.

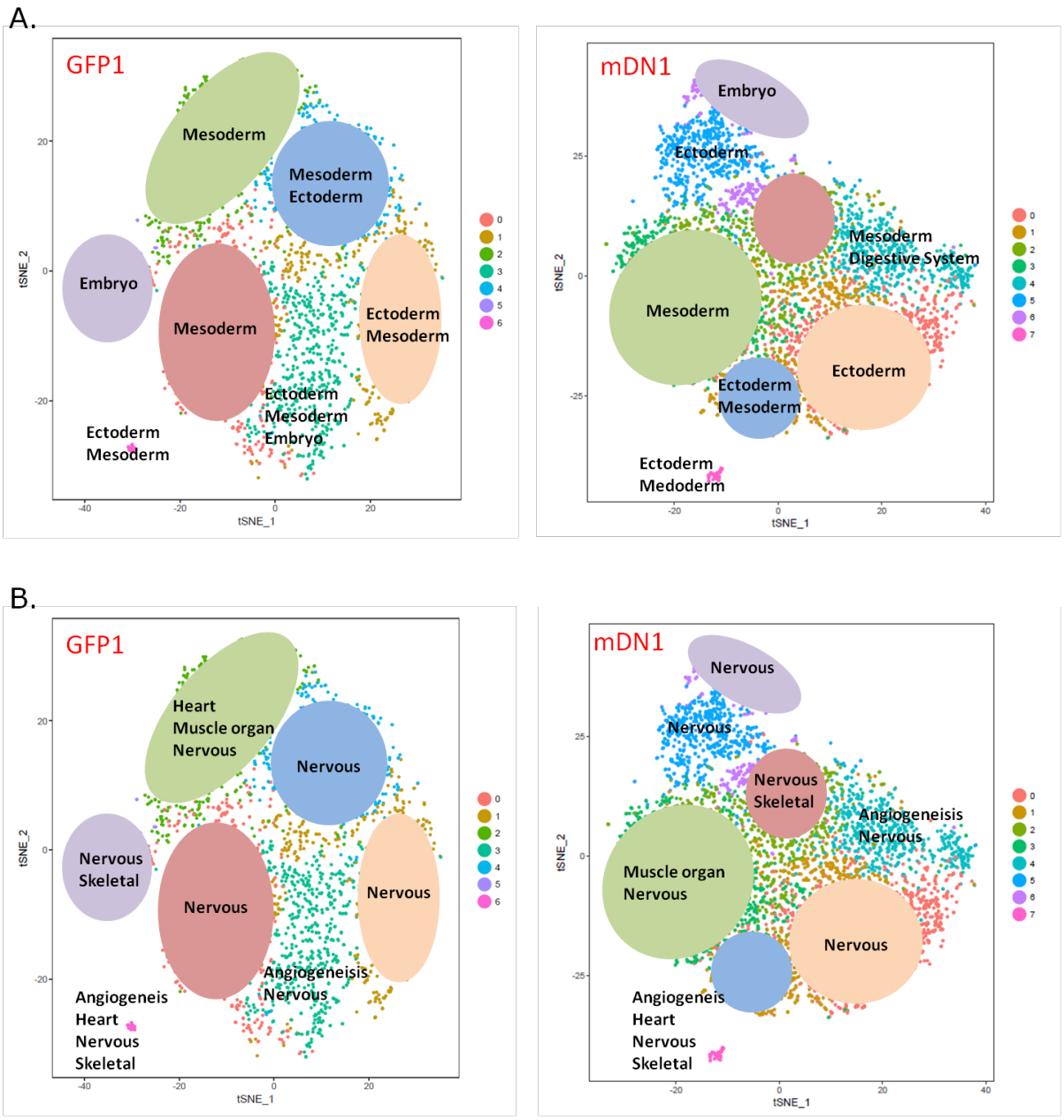

Figure 24. Annotation by GO-Slim enrichment analysis in deep scRNA-seq. The same color represented similar clusters according to IPA. Clusters were named after (A) trilineage development and (B) system development of the development process by GO-Slim biological process.

Table 9. Analysis of similar clusters by different methods

Method	Group Cluster	GFP1 0	mDN1 2
GO-Slim	Trilineage	Mesoderm	No
	System	Nervous	Nervous Skeletal
IPA	Signaling pathway	Cholesterol Biosynthesis I Cholesterol Biosynthesis II (via 24,25-dihydrolanosterol) Cholesterol Biosynthesis III (via Desmosterol) Superpathway of Cholesterol Biosynthesis Oncostatin M Signaling	Cholesterol Biosynthesis I Cholesterol Biosynthesis II (via 24,25-dihydrolanosterol) Cholesterol Biosynthesis III (via Desmosterol) Superpathway of Cholesterol Biosynthesis Epoxysqualene Biosynthesis
	Physiological system development and function	Embryonic Development Organ Development Organismal Development Skeletal and Muscular System Development and Function Tissue Development	Embryonic Development Hair and Skin Development and Function Organ Development Organismal Development Tissue Development
Pathway Commons		cholesterol biosynthesis III (via desmosterol) cholesterol biosynthesis II (via 24,25-dihydrolanosterol) cholesterol biosynthesis I Cholesterol biosynthesis superpathway of cholesterol biosynthesis	cholesterol biosynthesis I cholesterol biosynthesis II (via 24,25-dihydrolanosterol) cholesterol biosynthesis III (via desmosterol) Cholesterol biosynthesis superpathway of cholesterol biosynthesis

Unique lineage and system development modulating by mitochondrial Akt1 signaling

The next step was to use the differentially expressed genes of each cluster to run GO enrichment analysis (**Table 10**). Comparing the results of cluster 3 and 6 of GFP1 to cluster 4, 5, and 7 of mDN1 by GO enrichment analysis, some unique lineages and development were identified in mDN1, including lung and kidney development, middle ear morphogenesis, and smooth muscle cell differentiation. According to IPA, the cluster 5 of mDN1 was unique, and no physiological system development but cell cycle signaling pathway were identified. Specific physiological system development in cluster 3 of GFP1 was hematological and immune cells development which was not found in mDN1 by IPA. Annotation of deep scRNA-seq also supported the results of the restricted PCR array, but scRNA-seq was able to identify new cell lineage types and provided higher resolution of analysis to add new insight into the underlying signaling pathways. Taken together, inhibiting mitochondrial Akt1 signaling in hESC inhibits hematological and immune cells differentiation and increases lung and kidney development, middle ear morphogenesis, and smooth muscle cells differentiation.

Table 10. GO enrichment analysis of unique clusters

Cluster	GFP	Cluster	mDN
3	regulation of multicellular organismal process	**4**	striated muscle tissue development
	system development		lung development
			blood vessel endothelial cell migration, angiogenesis
			positive regulation of T cell proliferation
6	Outflow tract septum morphogenesis (heart)		kidney development
	artery morphogenesis		gland development
	regulation of endothelial cell proliferation		nerve development
	embryonic hindlimb morphogenesis		brain development
	osteoblast differentiation		epithelial cell differentiation
	Endochondral bone growth		
	cartilage morphogenesis	**5**	DNA replication
	skeletal muscle organ development		
	gliogenesis	**7**	lung-associated mesenchyme development
	brain development		forebrain neuroblast division
			middle ear morphogenesis
			regulation of cardiac muscle cell proliferation
			embryonic hindlimb morphogenesis
			cartilage morphogenesis
			chondrocyte development involved in endochondral bone morphogenesis
			endochondral bone growth
			smooth muscle & striated muscle cell differentiation
			positive regulation of osteoblast differentiation
			endothelium development

Pooling deep sequencing data of GFP1 and mDN1 was done by cellranger aggr, and the ranks barcode plot showed that mean gene numbers per cell were 2,733 genes (**Figure 20**). Clustering by t-SNE plot showed a similar distribution of GFP1 and mDN1 in each cluster, which meant that there was no batch effect between samples (**Figure 25**). The proportion of cell numbers in each cluster of the individual group was normalized by total cell numbers in each group (**Table 11**). The proportion of cells in cluster 3 & 4 were higher in the mDN1 group, but cluster 0 was higher in GFP1 group. These differences suggested that these clusters were unique and worthy to do further analysis. Principle component analysis (PCA) plot showed slightly rotation between GFP1 and mDN1 (Plot not shown here). The rotation indicated that the differences between GFP1 and mDN1 were small and only detectable by scRNA-seq. Using GO enrichment analysis to identify cluster 0, 3 and 4 in pooled GFP1 and mDN1 data, cluster 0 was similar to a mixture of cluster 6 in GFP1 and cluster 4 in mDN1; cluster 4 was similar to cluster 5 in mDN1 (**Table 12**). Herein, pooling data analyzed with PCA plot can identify the differences between groups through the 2-D PCA plot and normalized cell number proportion. However, it is still hard to match the clusters in pooled sequencing data to the clusters in GFP1 or mDN1. Because the clusters in pooled one were a mixture of GFP1 and mDN1 and the marker genes for clusters in pooled data were different from these in GFP1 or mDN1 data. By comparing the annotation in pooled data to original data by GO enrichment analysis, the similarity of clusters still can be found. This result was also agreed with the t-SNE plot cluster distribution when the axis was normalized in different samples. Taken together, scRNA-seq provided information across the whole population in a single cell level, which can help us identify unique cell types and signaling pathways.

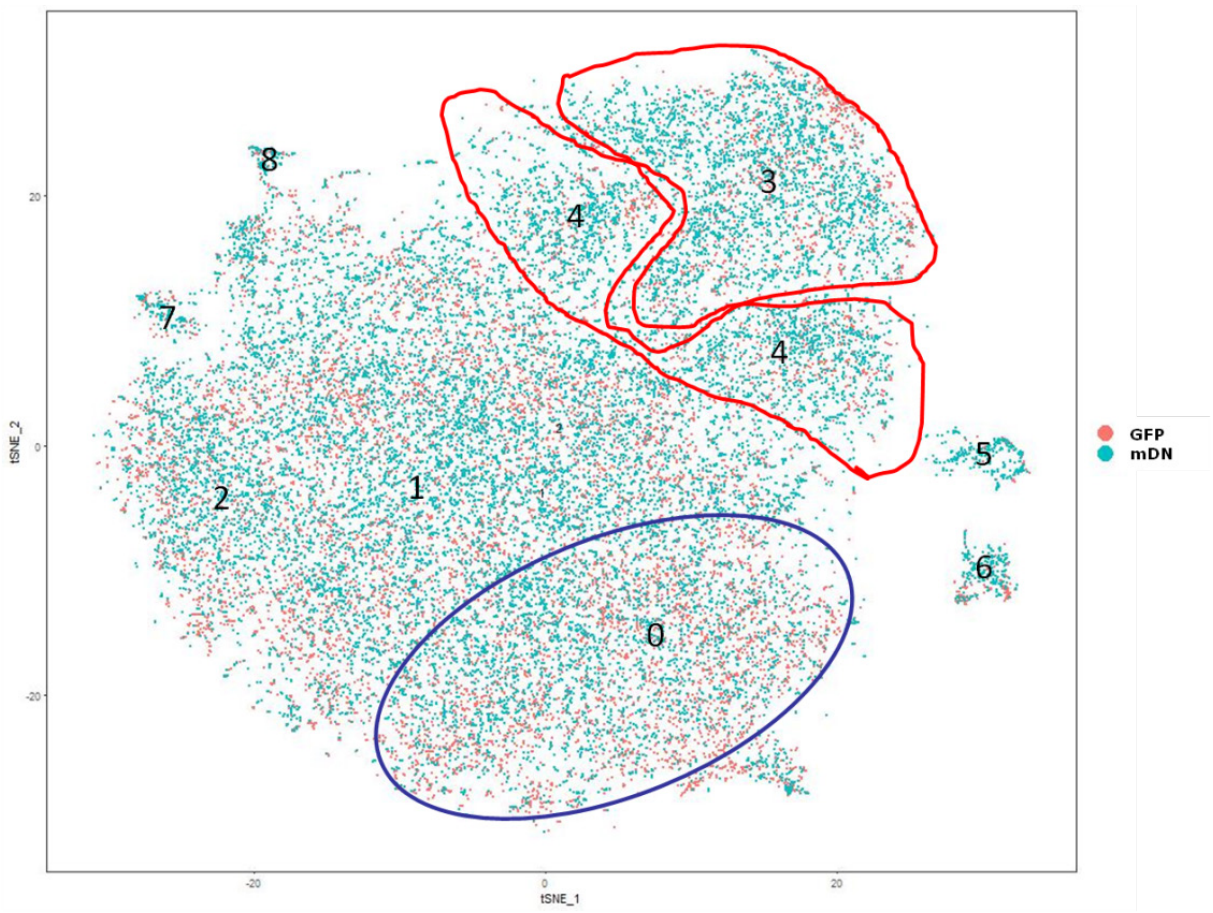

Figure 25. Distribution of GFP and mDN in pooled deep sequencing data. Eight clusters were labeled. After normalization by total cell numbers in each group, calculate the proportion of cell numbers in each cluster of the individual group. The percentage of cells distributed at cluster 3 & 4 were higher in the mDN1 group (red line area), but cluster 0 was higher in the GFP group (blue line area).

Table 11. The proportion of cell numbers in each cluster of GFP1 and mDN1 based on a pooled analysis

Cluster	0	1	2	3	4	5	6	7	8	Total
GFP	3808	2505	1547	1097	663	172	141	94	57	10084
	37.76%	24.84%	15.34%	10.88%	6.57%	1.71%	1.40%	0.93%	0.57%	100%
mDN	4224	4202	2365	2617	1748	323	201	122	95	15897
	26.57%	26.43%	14.88%	16.46%	11.00%	2.03%	1.26%	0.77%	0.60%	100%

Table 12. GO enrichment analysis of clusters in pooled GFP1 and mDN1

Cluster	Biological process
0	negative regulation of B cell differentiation
	mesenchyme migration
	caveola assembly
	dTTP biosynthetic process
	ascending aorta morphogenesis
	intramembranous ossification
	bone trabecula formation
	negative regulation of hematopoietic progenitor cell differentiation
	glomerular mesangium development
	pharyngeal arch artery morphogenesis
	positive regulation of astrocyte differentiation
	membranous septum morphogenesis
	positive regulation of erythrocyte differentiation
	positive regulation of cardiac muscle tissue growth
	embryonic digestive tract development
	positive regulation of heart contraction
	myoblast differentiation
	negative regulation of epithelial cell differentiation
	endodermal cell differentiation
	skeletal muscle tissue development
	cardiac muscle tissue morphogenesis
	striated muscle cell development
	negative regulation of epithelial cell proliferation
	negative regulation of angiogenesis
	positive regulation of smooth muscle cell proliferation
	hematopoietic progenitor cell differentiation
	embryonic placenta development
	cardiocyte differentiation
	regulation of fat cell differentiation
	angiogenesis
	gland development
	regulation of neuron projection development
	brain development
3	mitotic chromosome condensation
	G2/M transition of mitotic cell cycle
	negative regulation of G2/M transition of mitotic cell cycle
4	regulation of transcription involved in G1/S transition of mitotic cell cycle
	positive regulation of chromosome segregation
	mitotic G2/M transition checkpoint
	mitotic anaphase
	positive regulation of mitotic nuclear division
	negative regulation of DNA metabolic process

Chapter 5

Conclusions and Future Direction

5.1. Conclusion

The ability of self-renewal and unlimited potential to differentiate into three germ layers make pluripotent stem cells a key player in regenerative medicine and disease modeling. The more we understand its underlying mechanism of differentiation, the better stem cells can become an effective tool in the future. Recent studies have shown that signaling pathways and metabolism may affect stem fate differentiation. Our previous works also demonstrated that constitutive active mitochondrial Akt1 signaling enhanced somatic cell reprogramming to iPSCs by reducing oxidative stress and improving the efficiency of oxidative phosphorylation [65].

Interestingly, the PSCs in a different stage of pluripotency alter the mitochondrial ultrastructure and metabolism was reported recently. Two-stage of pluripotency, naïve and primed, can be distinguished. Naïve PSCs are highly dependent on both glycolysis and OXPHOS in ATP production. However, high glycolysis and low OXPHOS were observed in primed PSCs, including hESCs and iPSCs. Human ESCs and iPSCs are metabolically similar to mouse epiblast stem cells (mEpiSCs), which are derived from the postimplantation epiblast and represent a more mature stage. On the other hand, naïve human PSCs resemble mESCs, which represent a less mature pluripotent stage. Therefore, to study the

metabolism change in stem cells, it is important to clarify the original spices of PSCs and maintain the stage of PSCs.

Nowadays, there are several different methods to study the regulation of genes and proteins. The first key step is designing proper constructs, such as promoter and gene sequences, and carrying system, such as a virus. The viral vectors are one of the popular cargos. The property of viral vectors such as integrated to the host genome or not, should be taken into consideration according to experiment design. The second step is to evaluate the expression of genes or proteins through RNA by PCR or protein expression by image or western blot. Even though it is easy to detect mutant gene expression through carrying GFP or other fluorescence protein gene at the same time, the design between mutant gene and fluorescence-expressed gene (shared promoter or individual promoter) is important, especially when mutant gene expressed on specific organelle or compartment of the cells. For example, the adenoviral vector in this dissertation carried the mutant gene and GFP with the individual promoter; the GFP expression cannot represent the location of mutant gene expression, further confirmation by western blot of cell component subfractionation must be done.

Finally, the effect of the mutant gene or protein to cell phenotype and the mechanism of mutant gene or protein can be analyzed. In this dissertation, Seahorse XF24 Extracellular Flux Analyzer was used to evaluate the metabolism of stem cells. This platform can evaluate the mitochondrial respiration, glycolytic function, fatty acid oxidative assay and cell energy phenotype of living cells or mitochondria. It is a pretty useful method

to evaluate cell metabolism, but optimizing seeding of cells, including cell number, distribution, and viability, is crucial to get consistent and inclusive data. Based on this data, the more specific target of metabolism can be studied, such as ATP production, mtDNA copy number, ROS production, mitochondria protein complex, or uncoupling protein on mitochondria membrane.

This dissertation provides evidence that serum stimulation promoted translocation of Akt into mitochondria in the hESC and modulated its respiration. Transient inhibition of mitochondrial Akt1 signaling via transduction of mitochondria-targeting dominant negative Akt1 with adenoviral vector modulated hESCs differentiation lineage. Initial screening by cell lineage PCR array showed up-regulation and down-regulation of representative genes from three germ layers, with mesoderm and endoderm terminal differentiation markers up-regulated in the hESC transduced with mitochondria-targeting dominant negative Akt1. This finding supported my hypothesis that embryonic stem cells favored differentiation into mesoderm and endoderm when mitochondrial Akt1 signaling was inhibited during the early stage of embryonic development.

To further explore the unique cells differentiation modulated by mitochondrial Akt1 signaling, scRNA-seq was done by 10X Genomics and Illumina sequencer and analyzed by Seurat package in R to group cells into the cluster. Annotation of scRNA-seq by IPA, GO enrichment analysis, and common pathway demonstrated that inhibiting mitochondrial Akt1 signaling suppressed hematological and immune cells differentiation whereas increased lung and kidney development, middle ear morphogenesis, and smooth muscle

cells differentiation. Compared to the results of restricted PCR array from bulk RNA, scRNA-seq was able to identify new cell lineage types and provided higher resolution of analysis for new insight into underlying signaling pathways and biological processes.

There are several different scRNA-seq platforms can be used, depending on the cell number and purpose of the study. The 10X Genomics platform is an oil-drop microfluidic system which can study large cell numbers with high specificity, low sensitivity, and up to 20% of transcriptomes. Sample quality and subpopulation ratio in samples have a great impact on sequencing results. Therefore, it is important to design a protocol to get a well dispersed and alive single cell samples. With good quality samples and sequencing data, the next step is to computational analysis of the scRNA-seq data. Several public software and data banks can be used to align sequencing and annotate a gene, such as Cell Ranger. The cell-gene matrices can be further analysis by the R package Seurat or other software. Even though this software can statistically list the representative genes of clustering and plot 2-D or 3-D figure to show the relative distance between clusters, the exact annotation of each cluster in a highly diverse cell population, such as spontaneous differentiation cells, is difficult. Therefore, developing alternative strategies to dissect the highly diverse cell population is needed.

5.2. Future Direction

Analysis of scRNA-seq data with alternative methods

As specific cell types were clustered, alternative strategies are needed to explore the data, such as subtracting cells with some lineage or cell-specific markers in the GFP and mDN groups, to reduce the background noise in the dataset and further dissect the scRNA-seq data. After data cleaning by eliminating cells in the early stage of differentiation, specific cell types with late differentiation markers may be identified. We can further verify these cell types through immunostaining with cell-specific antibodies or by flow cytometry to quantify the abundance of specific cell types in the hESC transduced with mitochondria-targeting dominant negative Akt1.

My data support a new hypothesis that transient inhibition of mitochondrial Akt1 signaling at the initial stage of hESC differentiation enhances differentiation into mesendoderm, and lung and kidney development. This finding raises more questions worthy to be explored. How does mitochondrial bioenergetics change the expression of genes that regulated differentiation? Do mitochondria metabolites modulate transcriptomes? To address these questions, hESCs transduced with Ad-mdnAkt1/GFP or control GFP viral vector coupled with ES cells effective promoter, such as EF-1α or CA promoter, in the mTeSR1 medium can be utilized. We can analyze the changes of mitochondria metabolites, including 2-KG (which has been known to modulate gene expression through methylation) [88], and compare to the time course of key mesoderm marker gene expression that has been identified from my scRNA-seq analysis. If the

temporal relationship suggested that specific changes of metabolites correlate with the changes of marker gene expression, we can study direct effect of specific metabolite on hESC and verify its effect on mesoderm lineage by directed differentiation in hESC.

According to the clusters and annotations of scRNA-seq data, the most dominant lineage and physiology development are mesendoderm and cardiovascular system. Therefore, these data suggested that inhibition of mitochondrial Akt1 singling can modulate cardiomyocyte and endothelial cell differentiation or maturation. To test the hypothesis, GFP-positive hESCs with Ad-GFP or Ad-mdnAkt1/GFP can be grown with direct differentiation protocols to direct differentiation into cardiomyocytes[89,90] or endothelial cells [91-93]. With direct differentiation protocol, we can further confirm the effect of mitochondrial Akt1 signaling on stem cell differentiation.

REFERENCE

1 Wanet, A., Arnould, T., Najimi, M. & Renard, P. Connecting Mitochondria, Metabolism, and Stem Cell Fate. *Stem Cells and Development* **24**, 1957-1971, doi:10.1089/scd.2015.0117 (2015).

2 De Los Angeles, A. *et al.* Hallmarks of pluripotency. *Nature* **525**, 469, doi:10.1038/nature15515 https://www.nature.com/articles/nature15515#supplementary-information (2015).

3 Reubinoff, B. E., Pera, M. F., Fong, C.-Y., Trounson, A. & Bongso, A. Embryonic stem cell lines from human blastocysts: somatic differentiation in vitro. *Nat Biotech* **18**, 399-404 (2000).

4 Stevens, L. C. Studies on transplantable testicular teratomas of strain 129 mice. *Journal of the National Cancer Institute* **20**, 1257-1270 (1958).

5 Martin, G. R. Isolation of a pluripotent cell line from early mouse embryos cultured in medium conditioned by teratocarcinoma stem cells. *Proceedings of the National Academy of Sciences of the United States of America* **78**, 7634-7638 (1981).

6 Evans, M. J. & Kaufman, M. H. Establishment in culture of pluripotential cells from mouse embryos. *Nature* **292**, 154, doi:10.1038/292154a0 (1981).

7 Thomson, J. A. & Marshall, V. S. in *Current Topics in Developmental Biology* Vol. 38 (eds Roger A. Pedersen & Gerald P. Schatten) 133-165 (Academic Press, 1997).

8 Thomson, J. A. *et al.* Isolation of a primate embryonic stem cell line. *Proceedings of the National Academy of Sciences of the United States of America* **92**, 7844-7848 (1995).

9 Thomson, J. A. *et al.* Embryonic stem cell lines derived from human blastocysts. *Science* **282**, 1145-1147 (1998).

10 Takahashi, K. & Yamanaka, S. Induction of Pluripotent Stem Cells from Mouse Embryonic and Adult Fibroblast Cultures by Defined Factors. *Cell* **126**, 663-676, doi:http://dx.doi.org/10.1016/j.cell.2006.07.024 (2006).

11 Yu, J. *et al.* Induced Pluripotent Stem Cell Lines Derived from Human Somatic Cells. *Science* **318**, 1917-1920, doi:10.1126/science.1151526 (2007).

12 Takahashi, K. *et al.* Induction of Pluripotent Stem Cells from Adult Human Fibroblasts by Defined Factors. *Cell* **131**, 861-872, doi:http://dx.doi.org/10.1016/j.cell.2007.11.019 (2007).

13 Margineantu, D. H. & Hockenbery, D. M. Mitochondrial functions in stem cells. *Current Opinion in Genetics & Development* **38**, 110-117, doi:https://doi.org/10.1016/j.gde.2016.05.004 (2016).

14 Hu, C. *et al.* Energy Metabolism Plays a Critical Role in Stem Cell Maintenance and Differentiation. *International journal of molecular sciences* **17**, doi:10.3390/ijms17020253 (2016).

15 Heo, H. J. *et al.* Mitochondrial pyruvate dehydrogenase phosphatase 1 regulates the early differentiation of cardiomyocytes from mouse embryonic stem cells. *Experimental & Molecular Medicine* **48**, e254, doi:10.1038/emm.2016.70 (2016).
16 Folmes, C. D. L., Ma, H., Mitalipov, S. & Terzic, A. Mitochondria in pluripotent stem cells: stemness regulators and disease targets. *Current Opinion in Genetics & Development* **38**, 1-7, doi:https://doi.org/10.1016/j.gde.2016.02.001 (2016).
17 Teslaa, T. & Teitell, M. A. Pluripotent stem cell energy metabolism: an update. *The EMBO Journal* **34**, 138-153, doi:10.15252/embj.201490446 (2015).
18 Sart, S., Song, L. & Li, Y. Controlling Redox Status for Stem Cell Survival, Expansion, and Differentiation. *Oxidative Medicine and Cellular Longevity* **2015**, 14, doi:10.1155/2015/105135 (2015).
19 Xu, X. *et al.* Mitochondrial Regulation in Pluripotent Stem Cells. *Cell Metabolism* **18**, 325-332, doi:http://dx.doi.org/10.1016/j.cmet.2013.06.005 (2013).
20 Van Camp, J. K., Beckers, S., Zegers, D. & Van Hul, W. Wnt signaling and the control of human stem cell fate. *Stem cell reviews* **10**, 207-229, doi:10.1007/s12015-013-9486-8 (2014).
21 Nusse, R. Wnt signaling and stem cell control. *Cell research* **18**, 523, doi:10.1038/cr.2008.47 (2008).
22 Onishi, K. & Zandstra, P. W. LIF signaling in stem cells and development. *Development* **142**, 2230-2236, doi:10.1242/dev.117598 (2015).
23 Hirai, H., Karian, P. & Kikyo, N. Regulation of embryonic stem cell self-renewal and pluripotency by leukaemia inhibitory factor. *The Biochemical journal* **438**, 11-23, doi:10.1042/BJ20102152 (2011).
24 Ho, L. *et al.* ELABELA Is an Endogenous Growth Factor that Sustains hESC Self-Renewal via the PI3K/AKT Pathway. *Cell Stem Cell* **17**, 435-447, doi:https://doi.org/10.1016/j.stem.2015.08.010 (2015).
25 Ormsbee Golden, B. D., Wuebben, E. L. & Rizzino, A. Sox2 Expression Is Regulated by a Negative Feedback Loop in Embryonic Stem Cells That Involves AKT Signaling and FoxO1. *PLoS ONE* **8**, e76345, doi:10.1371/journal.pone.0076345 (2013).
26 Zhou, B. P. *et al.* HER-2/neu blocks tumor necrosis factor-induced apoptosis via the Akt/NF-kappaB pathway. *The Journal of biological chemistry* **275**, 8027-8031 (2000).
27 Voskas, D., Ling, L. S. & Woodgett, J. R. Signals Controlling Un-Differentiated States in Embryonic Stem and Cancer Cells: Role of the Phosphatidylinositol 3′ Kinase Pathway. *Journal of Cellular Physiology* **229**, 1312-1322, doi:10.1002/jcp.24603 (2014).
28 Stiles, B. L. PI-3-K and AKT: Onto the mitochondria. *Advanced Drug Delivery Reviews* **61**, 1276-1282, doi:http://dx.doi.org/10.1016/j.addr.2009.07.017 (2009).
29 Bijur, G. N. & Jope, R. S. Rapid accumulation of Akt in mitochondria following phosphatidylinositol 3-kinase activation. *Journal of Neurochemistry* **87**, 1427-1435, doi:10.1046/j.1471-4159.2003.02113.x (2003).
30 Yang, J.-Y., Yeh, H.-Y., Lin, K. & Wang, P. H. Insulin stimulates Akt translocation to mitochondria: Implications on dysregulation of mitochondrial oxidative phosphorylation in diabetic myocardium. *Journal of Molecular and Cellular Cardiology* **46**, 919-926, doi:http://dx.doi.org/10.1016/j.yjmcc.2009.02.015 (2009).
31 Deng, W. *et al.* Protein Kinase B (PKB/AKT1) Formed Signaling Complexes with Mitochondrial Proteins and Prevented Glycolytic Energy Dysfunction in Cultured

Cardiomyocytes During Ischemia-Reperfusion Injury. *Endocrinology* **155**, 1618-1628, doi:10.1210/en.2013-1817 (2014).
32 Chen, Y., Li, X., Eswarakumar, V. P., Seger, R. & Lonai, P. Fibroblast growth factor (FGF) signaling through PI 3-kinase and Akt/PKB is required for embryoid body differentiation. *Oncogene* **19**, 3750-3756, doi:10.1038/sj.onc.1203726 (2000).
33 Takahashi, K., Mitsui, K. & Yamanaka, S. Role of ERas in promoting tumour-like properties in mouse embryonic stem cells. *Nature* **423**, 541-545, doi:http://www.nature.com/nature/journal/v423/n6939/suppinfo/nature01646_S1.html (2003).
34 Watanabe, S. *et al.* Activation of Akt signaling is sufficient to maintain pluripotency in mouse and primate embryonic stem cells. *Oncogene* **25**, 2697-2707, doi:http://www.nature.com/onc/journal/v25/n19/suppinfo/1209307s1.html (2006).
35 Chan, D. C. Mitochondria: dynamic organelles in disease, aging, and development. *Cell* **125**, 1241-1252, doi:10.1016/j.cell.2006.06.010 (2006).
36 Calvo, S. E. & Mootha, V. K. The mitochondrial proteome and human disease. *Annual review of genomics and human genetics* **11**, 25-44, doi:10.1146/annurev-genom-082509-141720 (2010).
37 Leese, H. J. & Barton, A. M. Pyruvate and glucose uptake by mouse ova and preimplantation embryos. *Journal of reproduction and fertility* **72**, 9-13 (1984).
38 Brinster, R. L. & Troike, D. E. Requirements for blastocyst development in vitro. *Journal of animal science* **49 Suppl 2**, 26-34 (1979).
39 Shyh-Chang, N., Daley, G. Q. & Cantley, L. C. Stem cell metabolism in tissue development and aging. *Development* **140**, 2535-2547, doi:10.1242/dev.091777 (2013).
40 Chung, S. *et al.* Mitochondrial oxidative metabolism is required for the cardiac differentiation of stem cells. *Nature clinical practice. Cardiovascular medicine* **4 Suppl 1**, S60-67, doi:10.1038/ncpcardio0766 (2007).
41 Cho, Y. M. *et al.* Dynamic changes in mitochondrial biogenesis and antioxidant enzymes during the spontaneous differentiation of human embryonic stem cells. *Biochem Biophys Res Commun* **348**, 1472-1478, doi:10.1016/j.bbrc.2006.08.020 (2006).
42 Aoki, M., Batista, O., Bellacosa, A., Tsichlis, P. & Vogt, P. K. The Akt kinase: Molecular determinants of oncogenicity. *Proceedings of the National Academy of Sciences* **95**, 14950-14955 (1998).
43 Franke, T. F. PI3K/Akt: getting it right matters. *Oncogene* **27**, 6473-6488 (2008).
44 Kroczynska, B., Kaur, S. & Platanias, L. C. Growth suppressive cytokines and the AKT/mTOR pathway. *Cytokine* **48**, 138-143, doi:http://dx.doi.org/10.1016/j.cyto.2009.07.009 (2009).
45 Bellacosa, A. *et al.* Structure, expression and chromosomal mapping of c-akt: relationship to v-akt and its implications. *Oncogene* **8**, 745-754 (1993).
46 Burgering, B. M. T. & Coffer, P. J. Protein kinase B (c-Akt) in phosphatidylinositol-3-OH kinase signal transduction. *Nature* **376**, 599, doi:10.1038/376599a0 (1995).
47 Osaki, M., Oshimura, M. & Ito, H. PI3K-Akt pathway: Its functions and alterations in human cancer. *Apoptosis* **9**, 667 (2004).

48 Franke, T. F. *et al.* The protein kinase encoded by the Akt proto-oncogene is a target of the PDGF-activated phosphatidylinositol 3-kinase. *Cell* **81**, 727-736 (1995).
49 Hemmings, B. A. & Restuccia, D. F. PI3K-PKB/Akt Pathway. *Cold Spring Harbor Perspectives in Biology* **4**, a011189, doi:10.1101/cshperspect.a011189 (2012).
50 Zhang, J. & Li, L. BMP signaling and stem cell regulation. *Developmental Biology* **284**, 1-11, doi:https://doi.org/10.1016/j.ydbio.2005.05.009 (2005).
51 Varga, A. C. & Wrana, J. L. The disparate role of BMP in stem cell biology. *Oncogene* **24**, 5713, doi:10.1038/sj.onc.1208919 (2005).
52 Mishra, L., Derynck, R. & Mishra, B. Transforming Growth Factor-ß Signaling in Stem Cells and Cancer. *Science* **310**, 68-71, doi:10.1126/science.1118389 (2005).
53 Abruzzese, R. V. & Fekete, R. A. in *T Pluripotent Stem Cells* Vol. 997 *Methods in Molecular Biology* 217-224 (2013).
54 Takahashi, K., Murakami, M. & Yamanaka, S. Role of the phosphoinositide 3-kinase pathway in mouse embryonic stem (ES) cells. *Biochemical Society Transactions* **33**, 1522-1525, doi:10.1042/bst0331522 (2005).
55 Ling, L. S., Voskas, D. & Woodgett, J. R. Activation of PDK-1 maintains mouse embryonic stem cell self-renewal in a PKB-dependent manner. *Oncogene* **32**, 5397-5408, doi:10.1038/onc.2013.44 (2013).
56 Riley, J. K., Carayannopoulos, M. O., Wyman, A. H., Chi, M. & Moley, K. H. Phosphatidylinositol 3-kinase activity is critical for glucose metabolism and embryo survival in murine blastocysts. *The Journal of biological chemistry* **281**, 6010-6019, doi:10.1074/jbc.M506982200 (2006).
57 Riley, J. K. *et al.* The PI3K/Akt pathway is present and functional in the preimplantation mouse embryo. *Developmental Biology* **284**, 377-386, doi:https://doi.org/10.1016/j.ydbio.2005.05.033 (2005).
58 Chen, Y., Li, X., Eswarakumar, V. P., Seger, R. & Lonai, P. Fibroblast growth factor (FGF) signaling through PI 3-kinase and Akt/PKB is required for embryoid body differentiation. *Oncogene* **19**, 3750, doi:10.1038/sj.onc.1203726 (2000).
59 Paling, N. R., Wheadon, H., Bone, H. K. & Welham, M. J. Regulation of embryonic stem cell self-renewal by phosphoinositide 3-kinase-dependent signaling. *The Journal of biological chemistry* **279**, 48063-48070, doi:10.1074/jbc.M406467200 (2004).
60 Armstrong, L. *et al.* The role of PI3K/AKT, MAPK/ERK and NFκβ signalling in the maintenance of human embryonic stem cell pluripotency and viability highlighted by transcriptional profiling and functional analysis. *Human Molecular Genetics* **15**, 1894-1913, doi:10.1093/hmg/ddl112 (2006).
61 Mans, K. A. *Translocation and Function of Akt in the Mitochondria*, University of Alabama at Birmingham, (2010).
62 Barksdale, K. A. & Bijur, G. N. The basal flux of Akt in the mitochondria is mediated by heat shock protein 90. *Journal of Neurochemistry* **108**, 1289-1299, doi:10.1111/j.1471-4159.2009.05878.x (2009).
63 Chen, Kevin G., Mallon, Barbara S., McKay, Ronald D. G. & Robey, Pamela G. Human Pluripotent Stem Cell Culture: Considerations for Maintenance, Expansion, and Therapeutics. *Cell Stem Cell* **14**, 13-26, doi:http://dx.doi.org/10.1016/j.stem.2013.12.005 (2014).
64 Chen, G. *et al.* Chemically defined conditions for human iPSC derivation and culture. *Nat Meth* **8**, 424-429,

doi:http://www.nature.com/nmeth/journal/v8/n5/abs/nmeth.1593.html#supplementary-information (2011).
65 Chen, Y.-H. H. Mitochondrial Akt1 Signaling Enhanced iPSC Reprogramming - Mechanism of Mitochondrial Akt1-PDH E3 subunit Interaction. *University of California, Irvine* (2016).
66 Smith-Arica, J. R. *et al.* Infection efficiency of human and mouse embryonic stem cells using adenoviral and adeno-associated viral vectors. *Cloning and stem cells* **5**, 51-62, doi:10.1089/153623003321512166 (2003).
67 Baer, A. & Kehn-Hall, K. Viral Concentration Determination Through Plaque Assays: Using Traditional and Novel Overlay Systems. *Journal of visualized experiments : JoVE*, e52065-e52065, doi:10.3791/52065 (2014).
68 Parish, J. H. The Biochemistry of viruses: By S. J. Martin. Pp 145. Cambridge University Press, Cambridge and London. 1978. Cambridge texts in chemistry and biochemistry series. £10.45 (hard cover) or £3.95 (paperback). *Biochemical Education* **6**, 68-68, doi:doi:10.1016/0307-4412(78)90084-5 (1978).
69 Kawabata, K., Sakurai, F., Koizumi, N., Hayakawa, T. & Mizuguchi, H. Adenovirus Vector-Mediated Gene Transfer into Stem Cells. *Molecular Pharmaceutics* **3**, 95-103, doi:10.1021/mp0500925 (2006).
70 Brand, Martin D. & Nicholls, David G. Assessing mitochondrial dysfunction in cells. *Biochemical Journal* **435**, 297-312, doi:10.1042/BJ20110162 (2011).
71 Brokhman, I. *et al.* Genetic modification of human embryonic stem cells with adenoviral vectors: differences of infectability between lines and correlation of infectability with expression of the coxsackie and adenovirus receptor. *Stem Cells Dev* **18**, 447-456, doi:10.1089/scd.2008.0127 (2009).
72 Kawabata, K., Sakurai, F., Yamaguchi, T., Hayakawa, T. & Mizuguchi, H. Efficient Gene Transfer into Mouse Embryonic Stem Cells with Adenovirus Vectors. *Mol Ther* **12**, 547-554 (2005).
73 Jastroch, M., Divakaruni, A. S., Mookerjee, S., Treberg, J. R. & Brand, M. D. Mitochondrial proton and electron leaks. *Essays in biochemistry* **47**, 53-67, doi:10.1042/bse0470053 (2010).
74 Brown, D. F. S. R. a. G. C. Cellular energy utilization and molecular origin of standard metabolic rate in mammals. *Physiological Reviews* **77**, 731-758 (1997).
75 Brand, Martin D. *et al.* The basal proton conductance of mitochondria depends on adenine nucleotide translocase content. *Biochemical Journal* **392**, 353-362, doi:10.1042/BJ20050890 (2005).
76 Grün, D. & van Oudenaarden, A. Design and Analysis of Single-Cell Sequencing Experiments. *Cell* **163**, 799-810, doi:https://doi.org/10.1016/j.cell.2015.10.039 (2015).
77 Vladimir Kiselev, T. A., Jennifer Westoby, Davis McCarthy, Maren Büttner and Martin Hember. http://hemberg-lab.github.io/scRNA.seq.course/. (2018).
78 Tang, F. *et al.* Tracing the Derivation of Embryonic Stem Cells from the Inner Cell Mass by Single-Cell RNA-Seq Analysis. *Cell Stem Cell* **6**, 468-478, doi:http://dx.doi.org/10.1016/j.stem.2010.03.015 (2010).
79 Hedlund, E. & Deng, Q. Single-cell RNA sequencing: Technical advancements and biological applications. *Molecular Aspects of Medicine* **59**, 36-46, doi:https://doi.org/10.1016/j.mam.2017.07.003 (2018).

80 Andrew, H. *et al.* sRNA-seq Analysis of Human Embryonic Stem Cells and Definitive Endoderm Reveals Differentially Expressed MicroRNAs and Novel IsomiRs with Distinct Targets. *STEM CELLS* **32**, 2360-2372, doi:doi:10.1002/stem.1739 (2014).
81 Zheng, G. X. Y. *et al.* Massively parallel digital transcriptional profiling of single cells. *Nature Communications* **8**, 14049, doi:10.1038/ncomms14049 https://www.nature.com/articles/ncomms14049#supplementary-information (2017).
82 Butler, A., Hoffman, P., Smibert, P., Papalexi, E. & Satija, R. Integrating single-cell transcriptomic data across different conditions, technologies, and species. *Nature Biotechnology* **36**, 411, doi:10.1038/nbt.4096 https://www.nature.com/articles/nbt.4096#supplementary-information (2018).
83 Macosko, Evan Z. *et al.* Highly Parallel Genome-wide Expression Profiling of Individual Cells Using Nanoliter Droplets. *Cell* **161**, 1202-1214, doi:10.1016/j.cell.2015.05.002 (2015).
84 Mi, H., Muruganujan, A., Casagrande, J. T. & Thomas, P. D. Large-scale gene function analysis with the PANTHER classification system. *Nature Protocols* **8**, 1551, doi:10.1038/nprot.2013.092 https://www.nature.com/articles/nprot.2013.092#supplementary-information (2013).
85 Wang, J., Vasaikar, S., Shi, Z., Greer, M. & Zhang, B. WebGestalt 2017: a more comprehensive, powerful, flexible and interactive gene set enrichment analysis toolkit. *Nucleic Acids Research* **45**, W130-W137, doi:10.1093/nar/gkx356 (2017).
86 Wang, J., Duncan, D., Shi, Z. & Zhang, B. WEB-based GEne SeT AnaLysis Toolkit (WebGestalt): update 2013. *Nucleic Acids Research* **41**, W77-W83, doi:10.1093/nar/gkt439 (2013).
87 Zhang, B., Kirov, S. & Snoddy, J. WebGestalt: an integrated system for exploring gene sets in various biological contexts. *Nucleic Acids Research* **33**, W741-W748, doi:10.1093/nar/gki475 (2005).
88 TeSlaa, T. *et al.* α-Ketoglutarate Accelerates the Initial Differentiation of Primed Human Pluripotent Stem Cells. *Cell Metabolism* **24**, 485-493, doi:https://doi.org/10.1016/j.cmet.2016.07.002 (2016).
89 Breckwoldt, K. *et al.* Differentiation of cardiomyocytes and generation of human engineered heart tissue. *Nat. Protocols* **12**, 1177-1197, doi:10.1038/nprot.2017.033 http://www.nature.com/nprot/journal/v12/n6/abs/nprot.2017.033.html#supplementary-information (2017).
90 Batalov, I. & Feinberg, A. W. Differentiation of Cardiomyocytes from Human Pluripotent Stem Cells Using Monolayer Culture. *Biomarker Insights* **10**, 71-76, doi:10.4137/BMI.S20050 (2015).
91 Marcelo, K. L., Goldie, L. C. & Hirschi, K. K. Regulation of Endothelial Cell Differentiation and Specification. *Circulation research* **112**, 1272-1287, doi:10.1161/CIRCRESAHA.113.300506 (2013).
92 Silva, G. V. *et al.* Mesenchymal Stem Cells Differentiate into an Endothelial Phenotype, Enhance Vascular Density, and Improve Heart Function in a Canine Chronic Ischemia Model. *Circulation* **111**, 150-156, doi:10.1161/01.cir.0000151812.86142.45 (2005).
93 Oswald, J. *et al.* Mesenchymal Stem Cells Can Be Differentiated Into Endothelial Cells In Vitro. *STEM CELLS* **22**, 377-384, doi:10.1634/stemcells.22-3-377 (2004).